NASA Reference Publication 1316

1993

Nimbus-7 Earth Radiation Budget Calibration History--Part I: The Solar Channels

H. Lee Kyle
Goddard Space Flight Center
Greenbelt, Maryland

Douglas V. Hoyt
Brenda J. Vallette
Research and Data Systems Corporation
Greenbelt, Maryland

John R. Hickey
The Eppley Laboratories
Newport, Rhode Island

Robert H. Maschhoff
Gulton Industries
Albuquerque, New Mexico

National Aeronautics and Space Administration

Scientific and Technical Information Branch

ACRONYMS AND ABBREVIATIONS

ACRIM	Active Cavity Radiometer Irradiance Monitor
A/D	analog to digital convertor
APEX	Advanced Photovoltaic Experiment
CZCS	Coastal Zone Color Scanner
DSAS	Digital Solar Aspect Sensor
ERB	Earth Radiation Budget
ERBS	Earth Radiation Budget Satellite
FOV	field of view
H-F	Hickey-Frieden Cavity Radiometer
IPS	International Pyrheliometric Standard
JPL	Jet Propulsion Laboratory
LDEF	Long Duration Exposure Facility
LIMS	Limb Infrared Monitor of the Stratosphere
NASA	National Aeronautics and Space Administration
NIP	Normal Incidence Pyrheliometer
NSSDC	National Space Science Data Center
PEERBEC	Passive Exposure Earth Radiation Budget Experiment Components
ppm	parts per million
RSM	reference sensor model
SEFDT	Solar Earth Flux Data Tapes
SMM	Solar Maximum Mission
SMMR	Scanning Multichannel Microwave Radiometer
UARS	Upper Atmosphere Research Satellite
UV	ultraviolet
WRR	World Radiometric Reference

TABLE OF CONTENTS

1. INTRODUCTION

The Earth's climate and biosphere receives its necessary energy from the Sun. The 14 years of Nimbus-7 solar measurements demonstrate that year-to-year variations in the solar energy output did slightly affect the Earth's climate during this period (Ardanuy et al., 1992). In the future, longer term solar measurement sets may well show much stronger Sun/climate interactions (Friis-Christensen and Lassen, 1991). However, for such studies to be valid, great care must be taken with the long-term calibration of the solar sensors. The present report describes the calibration procedures used to keep the Nimbus-7 sensor stable to an estimated ± 0.03 percent or better over a 14-year period. During this period, the year-to-year range in the mean solar irradiance was 0.15 percent.

The Earth Radiation Budget (ERB) experiment on the Nimbus-7 spacecraft has 10 solar and 12 Earth flux channels. The solar channels were designed to measure the total, extraterrestrial solar irradiance, plus several spectral bands (Table 1). The self-calibrating cavity radiometer (channel 10c) has provided a very important 14-year record of the total solar irradiance. The spectral channels 4-9 lacked adequate in-flight calibration adjustment procedures and, hence, these measurements have received little attention. Channels 1-3 all measure the total solar irradiance; they are similar in type to the Earth flux channels 12 and 13. They could be calibrated by comparison with channel 10c, but it would be redundant to do so. The 12 Earth flux channels also took important measurements, and their calibration will be reviewed in Part II of this history.

Table 1. Characteristics of ERB Solar Channels

Channel	Wavelength Limits (μm)	Filter	Noise Equivalent Irradiance ($W \cdot m^{-2}$)
1*	0.2 to 3.8	Suprasil W	1.77×10^{-2}
2*	0.2 to 3.8	Suprasil W	1.77×10^{-2}
3	(0.2 to) 50	None	1.43×10^{-2}
4	0.536 to 2.8	OG530	1.94×10^{-2}
5	0.698 to 2.8	RG695	1.91×10^{-2}
6	0.398 to 0.508	Interference Filter	3.58×10^{-2}
7	0.344 to 0.460	Interference Filter	5.73×10^{-2}
8	0.300 to 0.410	Interference Filter	7.55×10^{-2}
9	0.275 to 0.360	Interference Filter	0.94×10^{-2}
10c†	(0.2 to) 50	None	2.39×10^{-2}

The unencumbered field of view for all channels is 10°; the maximum field is 26° for channels 1 through 8 and 10c. The maximum FOV for channel 9 is 28°. All are types of Eppley wire-bound thermopiles.

* Channels 1 and 2 are redundant; Channel 1 is normally shuttered. Its shutter, when opened for comparison measurements, covers channel 3.

† Channel 10c is a self-calibrating cavity channel added to Nimbus-7 and replacing a UV channel (0.246 to 0.312 μm) on Nimbus-6.

All of the sensors were carefully calibrated before the satellite was launched into orbit on October 24, 1978 (Hickey and Karoli, 1974; Jacobowitz et al., 1984). This established the basic calibration equations.

However, differences in the satellite and laboratory environment, instrument changes, and other factors have required major in-flight calibration adjustments. Here we will concentrate on the postlaunch adjustments and will only briefly summarize the prelaunch procedures. The cavity radiometer, its calibration equation, and its prelaunch calibration are discussed in Section 2. Section 3 examines pointing problems and the sensor's angular response function while lesser calibration adjustments are described in Section 4. Comparisons with other, contemporary solar measurements are given in Section 5. Section 6 contains discussion and conclusions.

Additional details are contained in the Appendices. Of particular interest are Appendix A which discusses solar channels 1-9 and Appendix B which describes the examination of similar sensors which were recovered after 6 years in space on the Long Duration Exposure Facility (LDEF) satellite.

2. THE HICKEY-FRIEDEN (H-F) CAVITY RADIOMETER

2.1 The Radiometer

The channel 10c cavity sensor is one of a family of thermopile-based radiometers, commonly referred to as Hickey-Frieden (H-F) type (Hickey et al., 1977). The specifics of this unit (channel 10c) were given in Hickey et al. (1980) and are reviewed here. A side view cross-section is shown in Figure 1. The basic sensing element of the radiometer is a toroidal-plated thermopile to which a cavity receiver is affixed. The cavity is composed of an inverted cone within a cylinder, the interior of which is coated with a specularly reflecting Z302 black paint. The baffles are coated with Z306 black paint. Chemglaze paints are used throughout since they have been shown to present minimum outgassing and weight-loss problems under normal orbital conditions. A calibration heater is wound mostly on the cone (about 94 percent) and partially on the lower cylinder (about 6 percent). This distribution is to achieve the best match to where radiation heating will occur for direct beam measurements. A precision aperture of 0.5 cm^2 is mounted in front of the cavity. The cavity has a larger diameter than the aperture so that all of the direct beam energy falls on the cone. This radiometer differs from most other H-F pyrheliometers in that the Nimbus sensor has a flat silver plate as compensator attached to the cold junctions. The available space would not allow for a matching rear cavity since this was a retrofit operation on an existing flight spare instrument from Nimbus-6.

The radiometer has a 10° field of view which allows the Sun to fully irradiate the cavity for about 3 minutes of each 104-minute orbit. The angular response is similar to a cosine function. This is examined in detail in Section 3. The off-axis angle is sensed by the Digital Solar Aspect Sensor, which is part of the satellite's attitude control system. It was planned to make the measurements with off-axis angles of less than 0.5°. However, various problems resulted in prolonged periods when the off-axis angles were 1° or larger during the measurement period.

Nimbus-7 is a polar-orbiting satellite. The ERB experiment is on the leading surface of the satellite. Thus, solar measurements are possible only as the satellite traverses the terminator near the southern extension of the orbit, about every 104 minutes. The Sun is in the field of view for about 3 minutes. The remainder of the time the sensor views deep space allowing for an accurate assessment of the offset, or radiation reference. Each solar sensor is sampled once per second, with an integration period of 0.8 s. The data system allows for digital output of $\pm$2,047 counts. The gain of channel 10c was set to measure in the range from 1,700 to 1,850 counts. When viewing space, it measures negative as would be expected for a thermopile instrument which is radiating to cold space. The device is electrically calibrated, and the heater is energized periodically while the sensor views space. Because of the operating schedule of the satellite (not ERB), these calibrations are performed once every 12 days. Because channel 10c was an "add-on" to the Nimbus-7 ERB, there was no place in the data stream to conveniently handle the

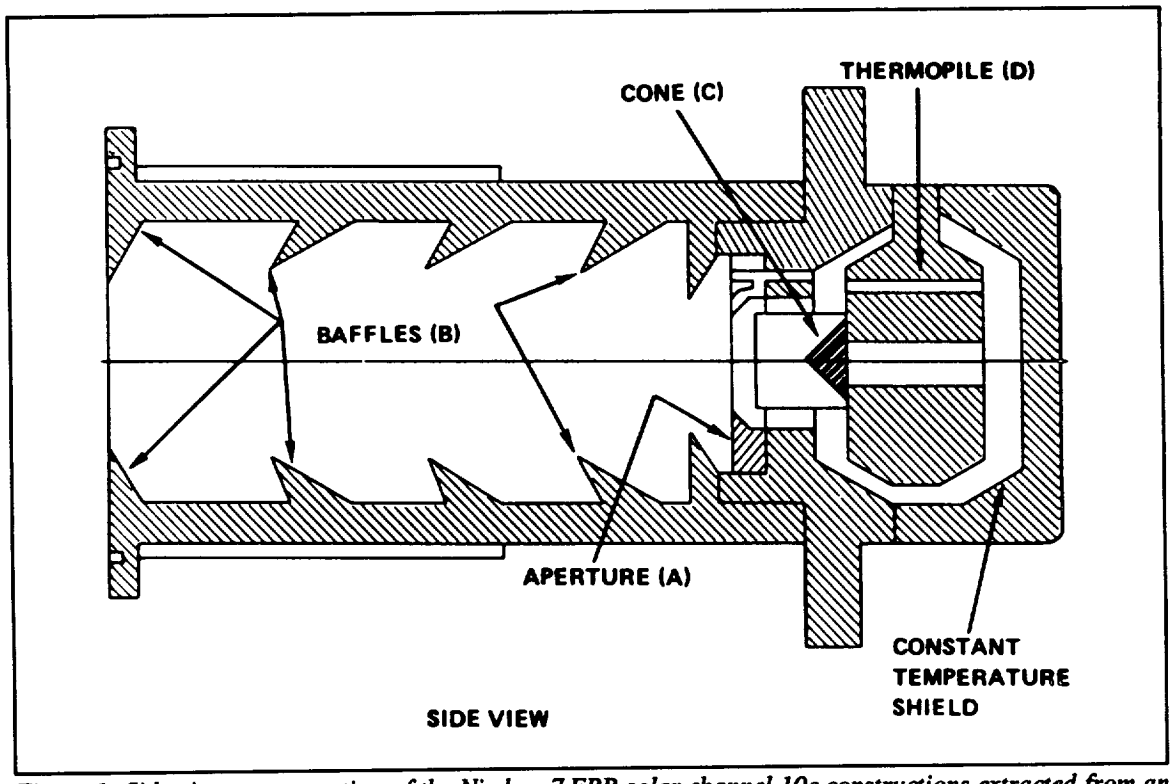

Figure 1. Side view, cross-section of the Nimbus-7 ERB solar channel 10c constructions extracted from an Eppley Laboratory blueprint.

calibration data. To accommodate the measurement of the three required parameters, thermopile signal, heater current and heater voltage, a submultiplexing scheme was devised which inserts the calibration data in the channel 10c data stream when the "go/no-go" heater command is exercised. That command is one which is used to energize the heater and which was originally intended as a prelaunch check capability for the solar channels when not illuminated (Hickey and Karoli, 1974). It was anticipated that there might be a need for correction to the responsiveness of the cavity thermopile with time, but aside from one small, apparent change in 1987 (see Section 4), the sensor has not changed. This electrical calibration procedure monitors the stability of the voltage reference and the data system, at least for nearly constant temperature, to the resolution for each parameter which amounts to 1 count in 1776 for the thermopile, which is equivalent to on-Sun values.

2.2 Preflight Calibration

Preflight calibration of the solar channels consisted of a number of comparisons and transfer operations. The reference for the absolute calibrations was the new World Radiometric Reference (WRR) scale, which is embodied in a number of self-calibrating cavity radiometers. Channel 10c of the Nimbus-7 ERB is itself such a device. This scale can be referenced to previous scales such as the International Pyrheliometric Scale (IPS 1956). The four major solar channels (1, 2, 3, and 10c) have been directly compared with self-calibrating cavity instruments.

For transfer operations a solar simulator as used as a source, and a normal incidence pyrheliometer (NIP) was employed. Both of these are also traceable to the WRR. When calibrating the filtered channels (4, 5, 6, 7, 8, and 9), the NIP was fitted with a filter wheel containing filters matching the flight set. The incident irradiance is calculated by using the measured irradiance and the appropriate filter factor for the

particular filter. The spectral response of all channels was recorded. A solar simulator was used to measure the off-axis response of each channel.

The ERB reference sensor model (RSM), which is a duplicate of the flight instruments relative to the solar channels, has been employed as a transfer and checking device throughout the Nimbus-6 and -7 calibration programs (Hickey and Karoli, 1974). All vacuum calibrations of the Nimbus-6 and -7 ERB solar channels were referenced through the RSM, as were many of the calibrations performed at atmospheric pressure.

The solar channels were not calibrated during thermal vacuum testing of the spacecraft. Their calibrations were checked during an ambient test after the thermal vacuum testing. Final calibration values for the solar channels were expressed in units of counts/Watt/meter^2 (c/W/m^2), relating the on-Sun signal output to the incident extraterrestrial solar irradiance in the pertinent spectral band of the channel.

In retrospect, some problems existed which were partially imposed by cost and engineering constraints. Nimbus data handling constraints kept the signal digitization range to $\pm 2{,}047$ bits where a range of $\pm 8{,}191$ bits would have been preferable for channel 10c. In addition, the solar simulator used to measure the off-axis response of the channels was only stable to about 0.5 percent. Thus, the off-axis response measured for channel 10c was of little practical use (see Section 3).

2.3 The Radiometer Calibration Equation

The calibration equation used to convert counts to solar total irradiance (S_o) is:

$$S_0 = \frac{k_{ref}}{k_{cal}} r^2 \frac{(C_{sun} - C_{space})}{\cos(G)} \frac{1}{[1. + A(T-22)]} \qquad (1)$$

where K_{cal} is the calibration constant with a value of 1.3013 counts/Watt/meter^2. k_{ref} is a dimensionless correction constant to account for spurious reflections from the baffles into the cavity and is taken to equal 0.998 because the signal jumps up 0.2 percent as the Sun enters the unrestricted field-of-view and down by 0.2 percent as it leaves it. In between the signal behaves normally. The jumps were interpreted as due to the presence of spurious reflections. Since k_{ref} is a constant, it has no influence on the relative accuracy of the measurements. The Earth-Sun distance is r, C_{sun} is the mean on-Sun counts, C_{space} is the mean space-look counts, A ($°C^{-1}$) is the coefficient for the temperature sensitivity of the radiometer, T is the temperature of the radiometer in degrees Celsius, and G is the offset angle between the normal vector to radiometer cavity and the vector to the Sun. This equation is an attempt to remove the portions of the counts signal which arise from the instrument and geometry effects so only a pure signal arising from solar behavior remains. The equation becomes less accurate in non-thermal equilibrium conditions when the temperature (T) is changing rapidly, as will be discussed in Section 4.4.3 (see also Smith et al., 1983 and Appendices C and E).

The form of this equation has remained unchanged over the years, but from time to time improved coefficients have been introduced. In 1990, improved estimates of the off-axis pointing angle (G), the calibration coefficient (k_{cal}), the Earth-Sun distance (r), the temperature coefficient (A), and the space-look offset counts (C_{space}) were introduced and the earlier measurements were reprocessed to produce a consistent dataset. Other equations are possible which can model the radiometer. For example, instead of a linear temperature correction, the fourth power of the temperature could be used. Hickey et al. (1987) investigated an alternative calibration equation of this form and found it provided some additional insight concerning the sensor's behavior, but did not change the final results.

The cavity radiometer is electrically calibrated. A measured input of electrical heat and measured thermopile output allows the calibration coefficient k_{cal} to be measured. These measurements, repeated once every 12 days, have shown no systematic variation in the calibration coefficient in 14 years with perhaps one exception in 1987, which is discussed in Section 4.4.2. The electrical calibration is a method for monitoring changes in instrument sensitivity from all causes except changes in the optical properties of the black paint of the cavity, which is a problem reviewed in Section 4.5.

Nimbus-7 orbits the Earth about 5049 times per year. Thus, there are a potential for this many solar measurements per year. However, for the first few years the ERB instrument was on a 3-day-on/one-day-off schedule in order to share with the experiments the available spacecraft power. In later years, several of the other instruments failed. Eventually, this allowed the ERB to remain on all the time. However, end-of-life procedures for two of the other instruments forced the ERB into special schedules for parts of 1986 and 1987. The ERB operations schedule is reviewed in Appendix C. In addition, some measurements were obviously noisy and were deleted from further analysis (see Appendix E). Most of the noisy data are associated with thermal transients which occur for a period after the instrument is switched on. Channel 10c started making measurements November 16, 1978 and since that time about 61,722 good solar observations have been made.

3. OFF-AXIS POINTING

3.1 Pointing Problems

Analysis started in 1989 indicated that uncorrected telescope pointing problems were introducing errors of the order of 0.06 percent into the Nimbus-7 total solar irradiance products. Mean 11-year total irradiance variations during sunspot cycles 21 and 22 are only of the order 0.1 percent to 0.2 percent. Thus errors of the order of 0.06 percent seriously degrade long-term trend analysis. This section documents the errors found and the corrections made in the processing algorithms. The reprocessed Nimbus-7 total solar irradiance products have less short-term noise and better long-term trends than did the original solar products.

The study found that two unanticipated problems existed. First the γ-angle scale on the ERB telescope slipped twice during the experiment. The γ-angle indicates the direction in which solar telescope is pointing. As a result of these slippages, incorrect telescope pointing angles were transmitted to Nimbus operations after July 20, 1980. Based on the geometry of the cavity radiometer and on inconclusive initial tests, it was assumed that the ERB channel 10c sensor had a simple cosine response function centered on the telescope axis. This cosine correction was made when the Sun was thought not to pass through the center of the field of view. However, in the original algorithm these cosine corrections failed to improve the results. Our analysis shows that along the telescopes γ-angle axis, the sensors response function is asymmetric with a peak response at -2.4° rather than at the origin.

The ERB solar telescope is mounted looking forward on the leading face of the satellite. It views the Sun for a few minutes once per orbit as the satellite passes near the south pole. Relative to the satellite orbit, the Sun makes a seasonal progression back and forth across the orbit. The satellite Operations center periodically changes the pointing of the telescope to follow the Sun. A geared drive wheel allows the telescope to move only in 1° angular steps around its so-called γ-axis. The actual position of the Sun relative to the spacecraft is measured by the Digital Solar Aspect Sensor (DSAS) which is also mounted on the front of the satellite. Figure 2 shows how the position of the solar transit relative to the axis of the telescope is determined during the measurement period. The DSAS measures the solar β-angle, while the ERB instrument records the telescope γ-angle. The desired off-axis angle is given by:

$$g = \gamma - \beta \tag{2}$$

Sensor readings are taken every second. The Sun is in the unrestricted sensor field of view for about 3 minutes out of each 104-minute orbit. Somewhat arbitrarily, a mean orbital reading is normally taken to be the average of the 40 largest, continuous measurements. This measurement region is designated as "m" in Figure 2.

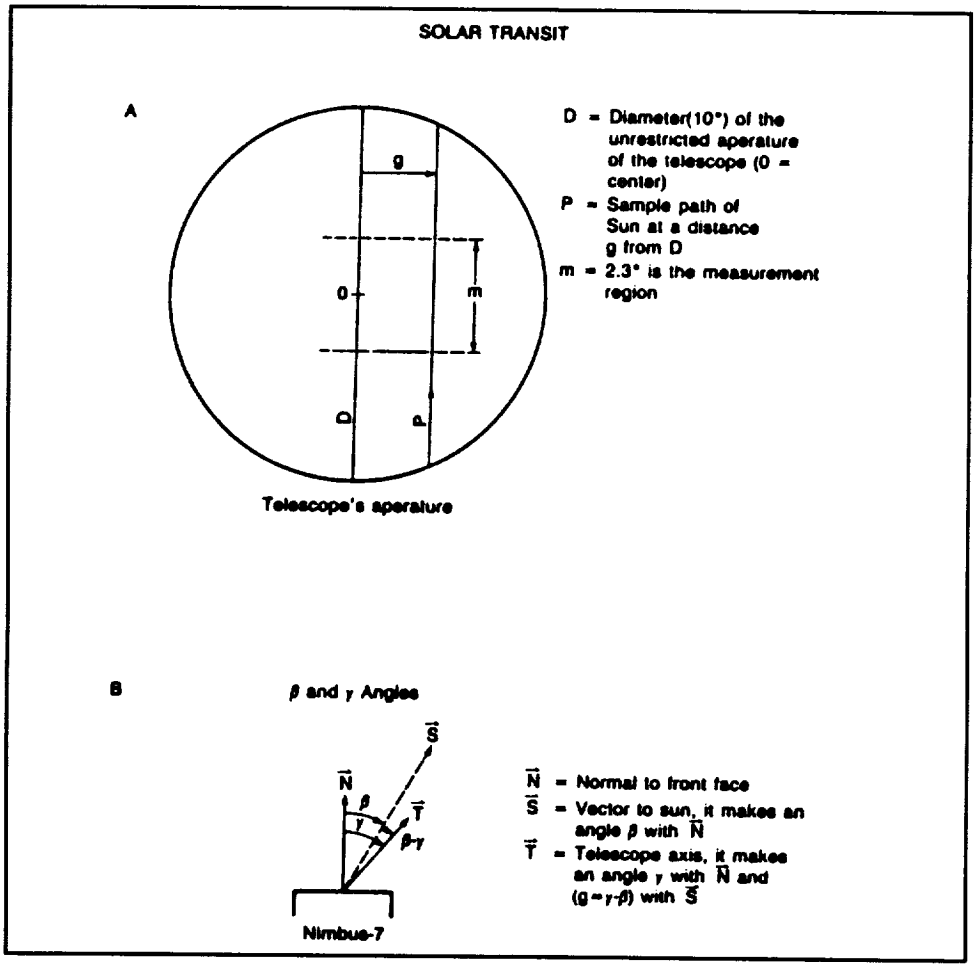

Figure 2. The geometry of the solar measurement is illustrated in (a) and (b). The transit of the Sun across the telescope is diagrammed in (a). The transit cord, P, is an angular distance (g) from diameter D. Only the maximum 40 contiguous measurements, Region m, are used in the calculation. The measured solar and telescope angles, β and γ, respectively, are shown in (b). As planned, the off-axis angle was supposed to be $g=(\gamma-\beta)$; however, an error developed in the measured γ-angle (see text).

As planned the solar transit would normally pass within 0.5° of the telescope center. Since the sensor was thought to have a cos (g) response function, moving the telescope pointing from g = +0.5° to g = -0.5° should have had no effect on the measured signal. During any one year, the beta and γ-angles vary predictably over a range of about 10° to 12°. The ERB solar telescope is directed to follow the beta angle changes by successive 1° changes in the γ-angle. Figure 3 provides an illustration of how the beta and γ-angles vary for a typical year (1987). The measured difference between the two angles is normally small and usually does not exceed 1°, although in Figure 3 a period around day 318 occurs when

incorrect γ-angle settings were commanded and the difference exceeded 1°. Between November 1978 and July 1989, the γ-angle of the satellite was changed 236 times. If the originally calculated off-axis angle and assumed sensor response function had been correct, the γ-angle shift should have had a negligible effect on the derived solar irradiances. In fact, it was found that each γ-angle change caused a discontinuity in the derived solar irradiance values and these discontinuities followed a repeatable annual cycle. This observation told us that some problem existed with the original assumptions.

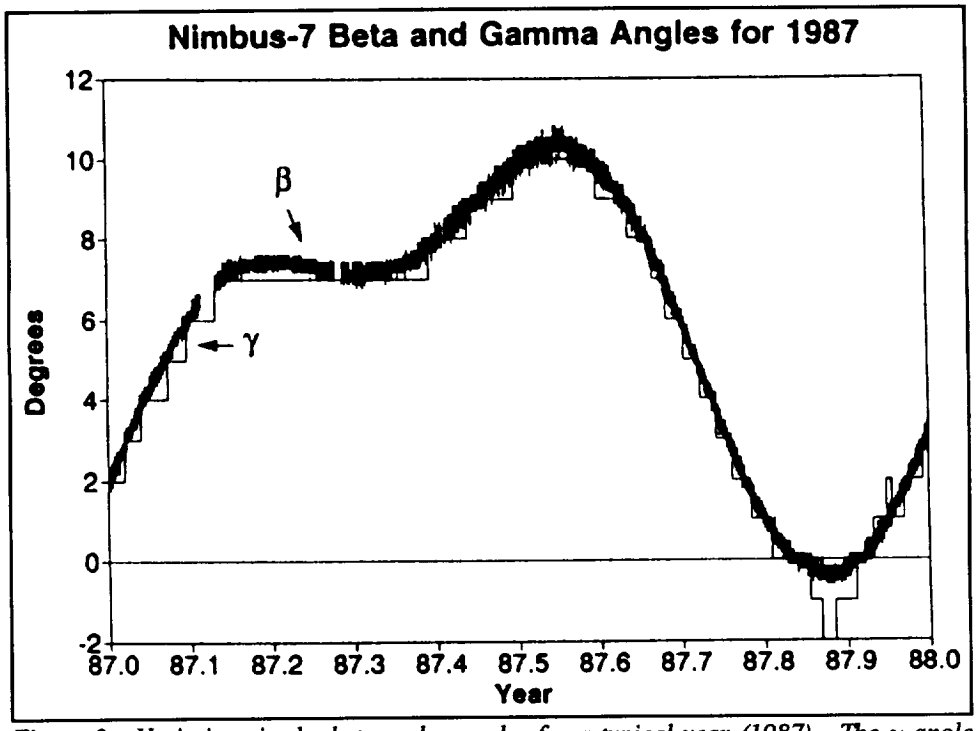

Figure 3. Variations in the beta and γ-angles for a typical year (1987). The γ-angle varies in a step-like fashion to match the predicted mean beta angles. The beta angle measured by the DSAS is shown. Around day 318 the two curves drift apart and in fact the sun came closest to drifting across the response center for channel 10c at this time.

Two procedures were used to analyze the problem. The first study analyzed the changes in the solar measurements at each operational γ angle change to determine past errors in the telescope pointing at the time of each change. There was considerable uncertainty with each individual change, but an interesting pattern appeared when a large number were analyzed. In the second procedure, the γ angle was deliberately changed from orbit to orbit to observe how the measurements changed at various recorded off-axis angles. The operational analysis is discussed in Section 3.2, while the experimental γ angle tests are analyzed in Section 3.3. A brief summary and discussion is given in Section 3.4.

3.2 Analysis of the Operational γ-Angle Changes

The discontinuities observed in the channel 10c signal when the telescope pointing (γ) angle is changed indicates that there is a problem with the measured off-axis angle g (Figure 2). To derive what the off-axis angle really is, it is assumed that both the solar irradiance and the radiometer properties remain stable just before and just after the γ-angle change and that the radiometer has a cosine response. It follows then that the ratio of the counts, corrected to one astronomical unit, will equal the ratio of the cosine of the off-axis angle before the change to the cosine of that angle plus one degree after the change. The only unknown is the off-axis angle, G, which can be solved for, using the following equation:

$$G = atan\left[\frac{-\frac{C_1}{C_2} + \cos(1)}{\sin(1)}\right] \quad (3)$$

where C_1 is the mean on-Sun counts before the γ-angle change and C_2 is the mean on-Sun count after the γ-angle change. In practice because of noise in the observations, groups of 5, 6, 7, 8, or 9 orbits before and after the angle change are used to form the two means of the counts. These five determinations are averaged together to derive an average off-axis angle. In effect, the observations closest to the γ-angle changes are more heavily weighted. The angle G measures the distance from the center of maximum response and depends on the sensor response function as well as the sensor/Sun geometry. For channel 10c, the angles g and G proved to be different (see Section 3.3).

Figure 4 shows the final mean calculated value for the apparent systematic errors in the off-axis angle. An 81-point running mean, representing about 4 years of individual measurements, is used to derive the slowly varying component of the off-axis angle. This procedure reduces scatter in the raw values and is justified since any individual off-axis angle is uncertain due to 1) the limited resolution of the A/D converter, 2) possible variations in the solar irradiance during each determination, and 3) some small changes in radiometer temperature. The radiometer's γ-angle appears to have been systematically too high by about 2.4° early in the measurement period, but more recently it appears off by about 1.4°. In between it was off by about 1.9° for several years. This is indicated by the step function in the figure. The actual γ-angle read out comes from a shaft angle encoder geared to the telescope axis. Lubricant evaporation is expected to increase the friction inside the encoder which could cause the encoder scale to slip in 0.5° steps (see Appendix D). Thus, the oscillations in the running mean do not represent a real variation in the radiometer pointing, but arise from the limited number of data points we have and the limited resolution of these data points.

This step function model for the systematic off-axis pointing is used to correct the pointing error. The dates for the 0.5° angle shifts are uncertain, but two plausible dates present themselves: July 20, 1980 when the radiometer noise was reduced (see Section 4 and Hoyt et al., 1992) and June 23, 1986 at the end of the special operations period. On July 20, 1980, the radiometer noise was reduced when the ERB scanner was turned off. If no pointing change is assumed to occur at this time, the derived solar irradiances would show a small upward jump in their values even if care is taken to handle the zero offsets. Introducing a 0.5° shift in pointing on this date removes most of this apparent upward jump and leaves a smoother varying curve.

On this basis, July 20 is chosen as the date for the change in pointing from 2.4° to 1.9°. The second date, June 23, 1986 is also uncertain, but reasonable. If no shift in off-axis angle is assumed for this date, the derived solar irradiances would appear to jump upwards by several tenths of a watt per square meter when the Sun is quiet. To avoid this discontinuity, June 23 is chosen as the date for the 0.5° off-axis change. One alternative date for a change in pointing exists, namely September 26, 1987 when the irradiance appeared to increase by 0.029 percent which is equivalent to an improved pointing of 0.2°. However, at present we are attributing this discontinuity to a gain change because a 0.2° change is not mechanically possible and the electrical calibrations support the gain change hypothesis (see Section 4 and Hoyt et al., 1992). Using the step function model for changes in the off-axis pointing and the measured DSAS beta angle and γ-angle, the history of the pointing of the instrument can be reconstructed, as illustrated in Figure 5. The values of the systematic errors nonetheless are uncertain by about $\pm 0.1°$, which translates into an uncertainty in solar irradiance of about ± 0.08 W/m^2.

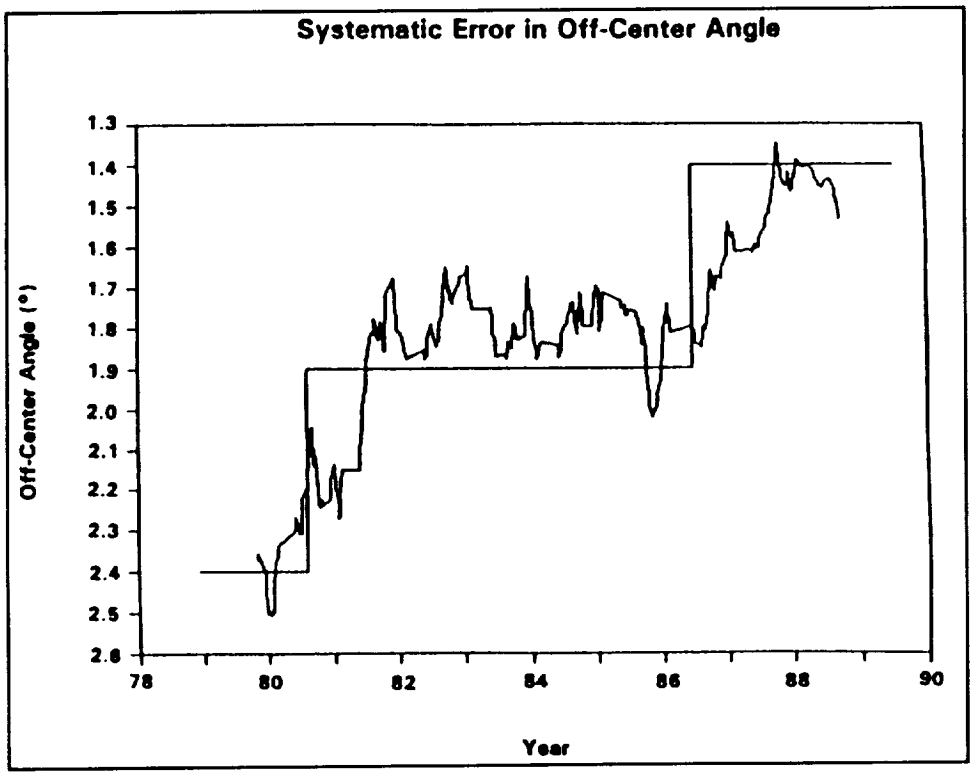

Figure 4. The slowly varying component of the off-center angle, G, is illustrated. The slowly varying curve is an 81-point running mean through the individual determinations. The step function is the model used for systematic error in the off-axis pointing. It follows the expected mechanical behavior of the system. Using the step function model rather than the running mean model avoids the possibility of introducing spurious oscillations in the derived irradiance values. The channel 10c, off-center angle G, is about 2.4° in the early years, then changes to 1.9° in July 1980 and to 1.4° in June 1986.

The off-axis pointing error deduced from Eq.(2) was tested by initiating some new tests. Both the general validity of Eq.(2) and the pointing errors deduced from it were verified by these tests which are described in Section 3.3.

3.3 The Channel 10c Response Function

The off-axis pointing error deduced from Eq.(2) was checked by reviewing old and initiating new tests. In the so-called γ-angle tests, the telescope pointing is moved in geared 1° steps. The tests yield information on how the signal varies with the off-axis angle, g, illustrated in Figure 2. This is termed the γ-angle response function. The tests also yield the solar transit time interval, Δt, and the position of the field-of-view limiter relative to the γ-angle scale. Seven tests have been made; one pre-flight test and six in-orbit tests. The in-orbit tests occurred in November 1978, December 1989, March and September 1990, February 1991, and November 1991. The tests showed two things: 1) the γ-angle recording scale slipped one degree between November 1978 and December 1989 and 2) the γ-angle response function is asymmetric with a peak response at $g = -2.4°$. Both the pre-launch test and the November 1978 test showed that the γ-angle scale was reading correctly whereas the December 1989 and later γ-angle tests indicate that the γ-angle scale had slipped by 1°. Both the transit time data and the positions of the field-of-view limiters verified the change.

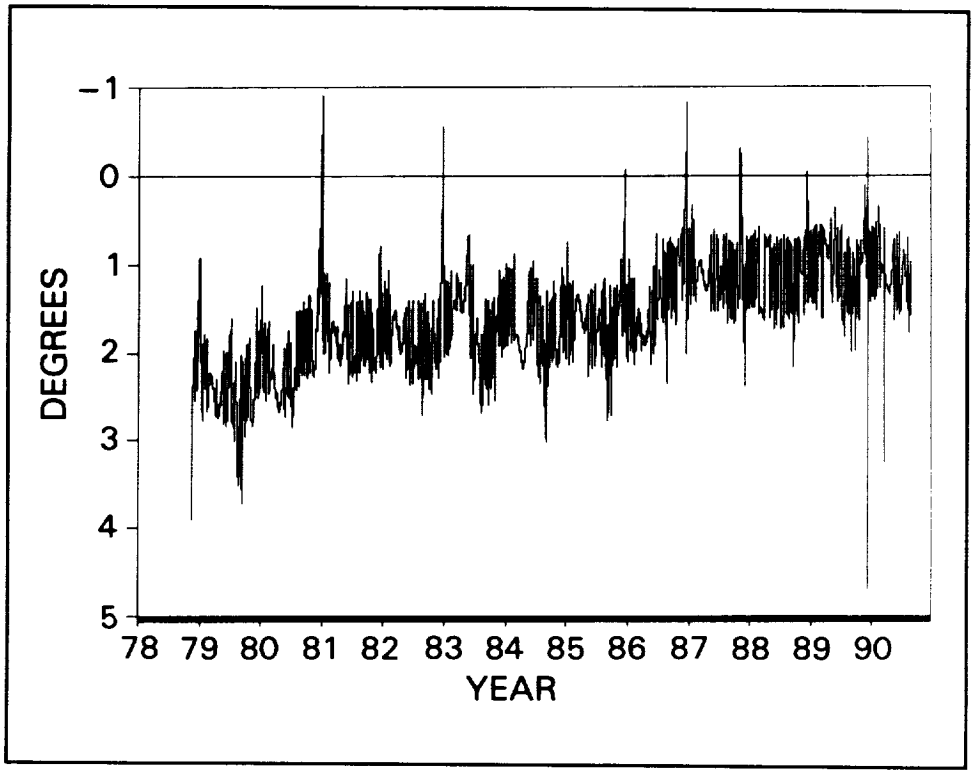

Figure 5. The combined slow component of the off-axis variations from Figure 3 and the rapid component given by the DSAS measurements. These are the off-axis angles used in the solar irradiance determinations. In the original analyses, the slow component was taken to equal zero.

It was originally assumed that the sensor's angular response function was a cosine centered on the telescope axis and this was thought to hold for both the solar transit axis and the perpendicular γ-angle axis. In fact, along the solar transit axis, the response function does closely follow a cosine response centered at the telescope axis. However, the maxima generally occur about one-half degree before the center and the signal rises a little faster than it falls. This asymmetry in the rise and fall of the radiometer response probably is caused by the finite instrumental time response, causing the radiometer to cool slower than it is heated up. The slightly asymmetric transit response is illustrated in Figure 6 which shows the trace of a typical solar transit. (See Appendix D for additional curves.) In practice, the maximum 40 contiguous, one second measurements are averaged to obtain the solar irradiance. No response function enters into this average. The pre-launch test did not definitively show the γ-axis asymmetry because the solar simulator used was only stable to 0.5 percent.

Figure 7 shows the γ-angle response functions derived from the first three inflight tests (November 1978, December 1989, and March 1990). A cosine response, centered at $g = -2.4°$ is also shown. The preflight, Gulton test (not shown) also indicated a non-cosine response on the left-hand (+) side. But, this was not considered significant because of the instablity of the solar simulator. All six of the inflight tests agree on a cosine responses on the right-hand (-) side centered at $g = -2.4°$. Only the first three tests are illustrated in Figure 7, but all are discussed in Appendix D.

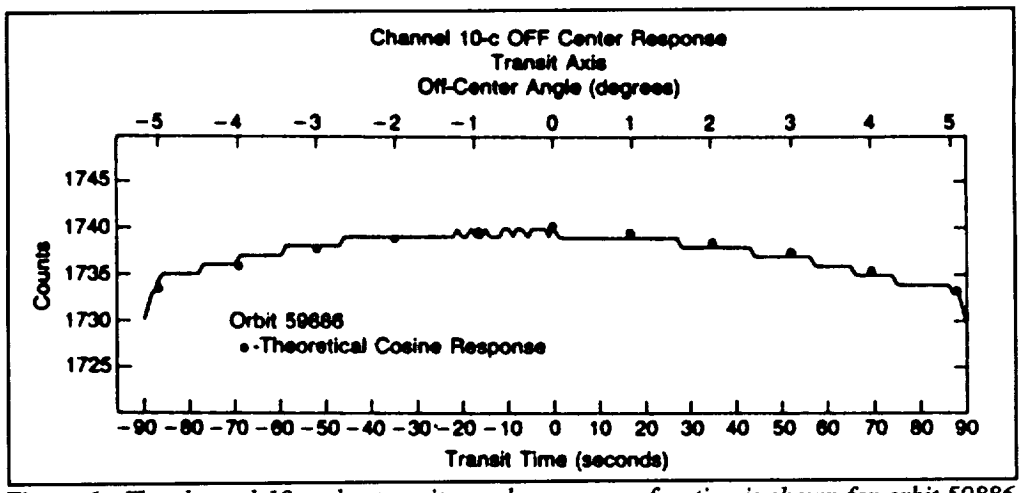

Figure 6. The channel 10c solar transit angular response function is shown for orbit 59886, September 1990. The response function is a step function which can be closely modeled by a cosine centered at the origin (see text).

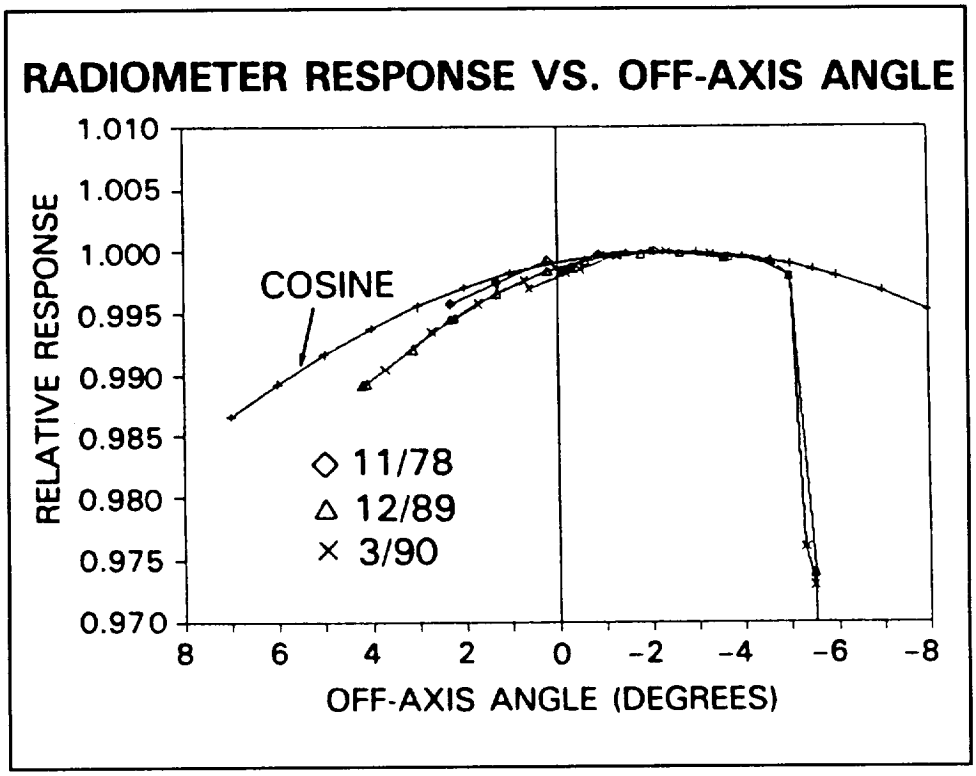

Figure 7. The γ-axis channel 10c angular response function is shown for the first three inflight tests (November 1978, December 1989, and March 1990). Also shown is cos(g + 2.4°) where g is the off-axis angle.

A combined analysis of all six inflight tests is summarized in Table 2 and Figure 8. This analysis justifies the use of the γ-angle response function $\cos(g+2.4°)$. The angle $G = g + 2.4°$ is similar to that calculated in Eq.(2). A cosine response function is valid for most of the measurements, but it is not applicable for transits on the far right hand (positive) side of the field-of-view. The difference between a theoretical response function cos(G) and the measured γ-axis response function, R, is given in Figure 8. The normalized response function, R, is the mean of the results of the six in-orbit tests. For individual tests, R is the ratio of the signal at a given off-center angle, g, to the signal at the point of maximum response ($g = -2.4°$). During a given test the actual solar irradiance appeared to vary by no more than 0.06 percent. This variation could be accounted for down to or below 0.03 percent. The range between the individual tests is indicated by the uncertainty bars. The points on the left had a standard deviation too small to show up at this scale. These results indicate a cosine response function is accurate to within 0.1 to 0.3 W/m^2 on most of the left-hand, minus, side of center, where virtually all the irradiance measurements are made. On the right-hand, positive, side of center a simple cosine function progressively underestimates the true solar irradiance. The underestimation increases from about 0.7 W/m^2 at the nominal center ($g = 0°$) to about 6.0 W/m^2 at $g = +4°$. Since only three of the six tests extended beyond $g = +2.3°$, the uncertainties increase beyond this angle. The cause of the asymmetry along the γ-axis is unknown. Radiation reflected from the open telescope cover door might be the cause. However, reflected light was guarded against in the Gulton preflight test. If reflected light causes the asymmetry in flight, then the dip in the Gulton results from $g = +2°$ to $+5°$ of about 0.5 percent has to be assigned solely to the solar simulator. The actual cause of the non-cosine response cannot be verified.

The γ-angle tests indicate that good channel 10c measurements can be obtained for off-axis angles, $g \geq -4.7°$. However, when the telescope angle is $\gamma = 20°$, the telescope starts to enter its housing. Refer to Figure 2 for definition of the angles. At $\gamma = 19°$, channel 10c is shaded by the telescope door. Thus, observations can only be made for $\gamma \leq 18°$. In the summer of 1992, the Sun angle increased to $\beta = 23.65°$ (July 27) but the telescope angle was held at $\gamma = 18°$. At this extreme telescope angle, the edge of the sensor aperture was apparently shaded. As shown in Figure 9, the Sun exited the unobstructed field of view at the off-axis angle, $g = -4.4°$, instead of at $g = -4.8°$ as expected from Figure 7 and Appendix D.

In January 1992, a temporary jam occurred in the telescope's γ angle drive blocking forward motion beyond $\gamma = 13°$. Exercising the telescope back and forth up to this point cleared the blockage in a few days. One hypothesis held that some originally tied cables had come loose and had temporarily blocked the forward motion until the telescope exercises worked them out of the way. Under this hypothesis, it was thought that excessive motion of the telescope might cause a new jam. It was, therefore, decided to conduct no additional γ-angle tests.

The γ-angle tests verify that the γ-encoder scale slipped 1° between tests in November 1978 and December 1989. This can be told both from analysis of the length of time the Sun takes to pass across the sensor field of view, and by determining at what γ-angle the sensor just misses a direct view of the Sun. The signal falls rapidly once the Sun passes out of the direct field of view (see Figures 7, 8, and Table 2). Both the Gulton test (Figure 7) and the postlaunch, November 1978, test showed that the γ-angle scale was registering correctly. Figure 10 shows the solar in-view times as a function of the measured off center angle ($g = \gamma - \beta$). The curves A, B, and C refer, respectively, to the tests in November 1978, December 1989, and March 1990. Curve D is theoretical and based on a point moving about the orbit in 104 minutes. The point moves 1° in 17.33 seconds. Thus it takes 173.3 seconds to cross the diameter of channel 10c's unrestricted field of view.

The actual Sun in-view times for a particular observation is approximated as:

$$\Delta t = No.\ of\ readings\ T \geq (T_{(MAX)} - 10) \quad (4)$$

Table 2. Subjective Analysis of γ-Angle Tests
Error in cosine response function for channel 10c.

			T_o/T_s - cos G = Δ		Assume I_s = 1371 W/m² Δ x 1371	
g_o (°)	G_o (°)	T_o/T_s	Estimated Value x 10^3	σ x 10^3	Mean (W/m²)	σ (W/m²)
Out-of-Field Measurements						
-6.0	-4.2	0.8893	-108	±6.9	-148	±6.9
-5.5	-3.1	0.9555	-43	±3	-59	±4
-5.3	-2.9	0.9747	-24	±3	-33	±4
In-Field Measurements						
-4.6	-2.2	0.99913	-0.13	±0.06	-0.18	±0.08
-4.2	-1.8	0.99931	-0.2	±0.06	-0.27	±0.08
-3.6	-1.2	0.99964	-0.11	±0.06	-0.15	±0.08
-3.3	-0.9	0.99979	-0.11	±0.06	-0.15	±0.08
-2.7	-0.3	1.0001	+0.023	±0.05	+0.032	±0.07
-2.4	0	0.99998	-0.016	±0.04	-0.022	±0.05
-2.0	+0.04	0.99999	+0.016	±0.04	+0.022	±0.05
-1.6	+0.8	0.99991	+0.004	±0.04	+0.005	±0.05
-1.3	+1.1	0.99970	-0.12	±0.06	-0.16	±0.08
-1.0	+1.4	0.99960	-0.1	±0.06	-0.14	±0.08
-0.6	+1.8	0.99921	-0.3	±0.1	-0.41	±0.14
-0.3	+2.1	0.99946	-0.53	±0.2	-0.73	±0.27
0	+2.4	0.99863	-0.49	±0.2	-0.672	±0.27
+0.5	+2.9	0.99796	-0.6	±0.3	-1.04	±0.4
+1.0	+3.4	0.99730	-0.94	±0.3	-1.29	±0.4
1.3	3.7	0.99672	-1.2	±0.3	-1.65	±0.4
1.7	4.1	0.99574	-1.7	±0.6	-2.33	±0.82
2.2	4.6	0.99478	-2.0	±0.6	-2.74	±0.82
2.6	5.0	0.99359	-2.6	±0.6	-3.56	±0.82
3.2	5.6	0.99203	-3.2	±0.6	-4.39	±0.82
3.7	6.1	0.99024	-4.1	±1.0	-5.62	±1.37
4.2	6.6	0.98877	-4.6	±1.0	-6.31	±1.37
4.8	7.2	0.98701	-5.1	±1.0	-7.0	±1.37
Out-of-Field Measurements						
5.8	8.2	0.8993	-90.5	±3.0	-124.1	±4.0

g_o = off-axis angle = γ-β
G_o = 2.4° + g_o = off maximum angle
T_o = Signal at angle G
T_s = Signal at G=0
I_s = solar irradiance

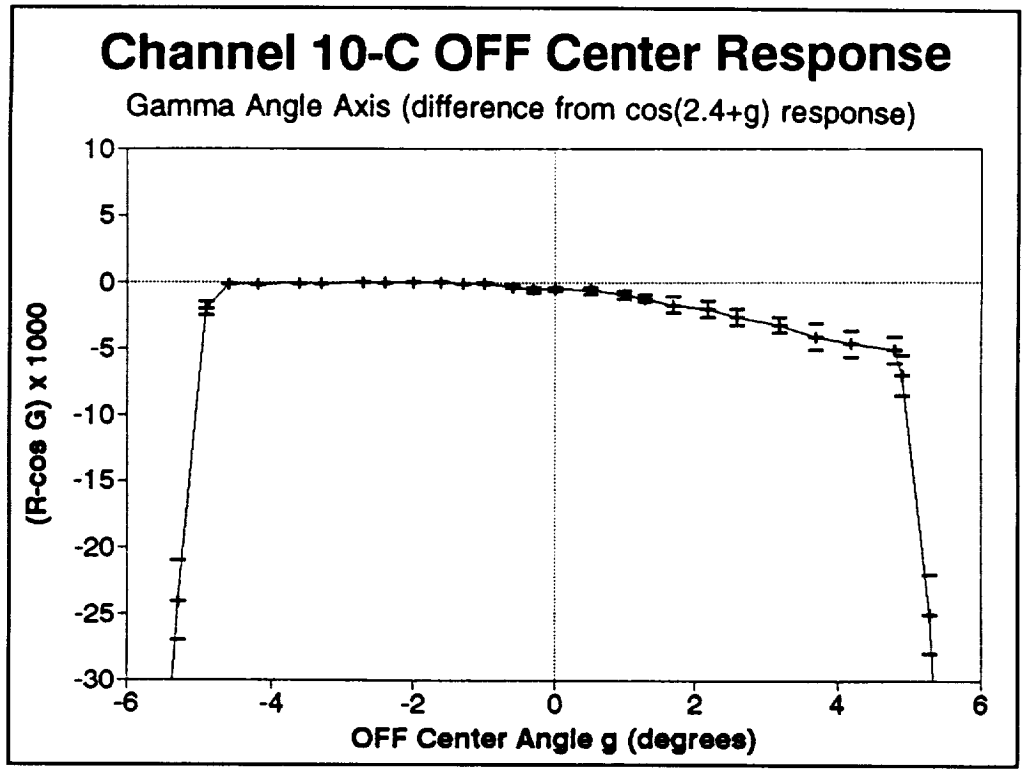

Figure 8. The mean channel 10c γ-angle response function. The results of six inflight γ-angle tests are used to determine for channel 10c the difference [measured response function R - cos(g + 2.4°)]. The difference is small on the left where most of the normal measurements occurred. The lines above and below the crosses indicate the measurement error bars. On the left, the errors were quite small.

One measurement, T, is taken every second and $T_{(MAX)}$ is the maximum value during a particular observation. The Δt thus defined is slightly larger than the true Sun in-view time. Note in Figure 10 that the maximum in November 1978 (Curve A) appears about at (γ-β=0) while by December 1989 and March 1990 (Curves B and C) the maximum had moved to (γ-β=+1°). In these latter two experiments, the γ-angle was swept over a 12° arc in December and an 11° arc in March in an attempt to make out-of-view readings on both sides of the aperture. Because of uncertainties in the anticipated sensor Sun geometry both picked up out-of-view readings only on the left-hand side. Only the November 1992 test picked up out-of-view readings on both sides. However, the out-of-view readings on the left were sufficient to confirm that the γ-angle scale was 1° off center as of December 1989. Additional information on the γ-angle tests is given in Appendix D.

3.4 Conclusions

The analysis given in Sections 3.2 and 3.3 shows that the measurement center was (g=0, normal incidence) at launch, then shifted off-axis to (g = -0.5°) in July 1980 and to (g = -1.0°) in June 1986. For most measurements, the angle g is within 0.5° of the measurement center (see Figure 3). It was also shown that the channel 10c sensor's off-axis response function is different for the solar transit and the perpendicular γ-angle axes. In the solar transit direction, the response function can be closely approximated by a cosine curve centered at the origin (see Figure 6). In the actual processing, the mean of the 40 maximum contiguous readings is taken. No response function is used in the solar transit direction. However, in the γ-angle direction, a response function, cos(g+2.4°) is used in the processing.

Here g is the off-axis angle shown in Figure 2. Table 2 and Figure 7 indicate that the use of this cosine function may cause the 1979 calculated solar irradiances to be about 0.6 W/m^2 too small.

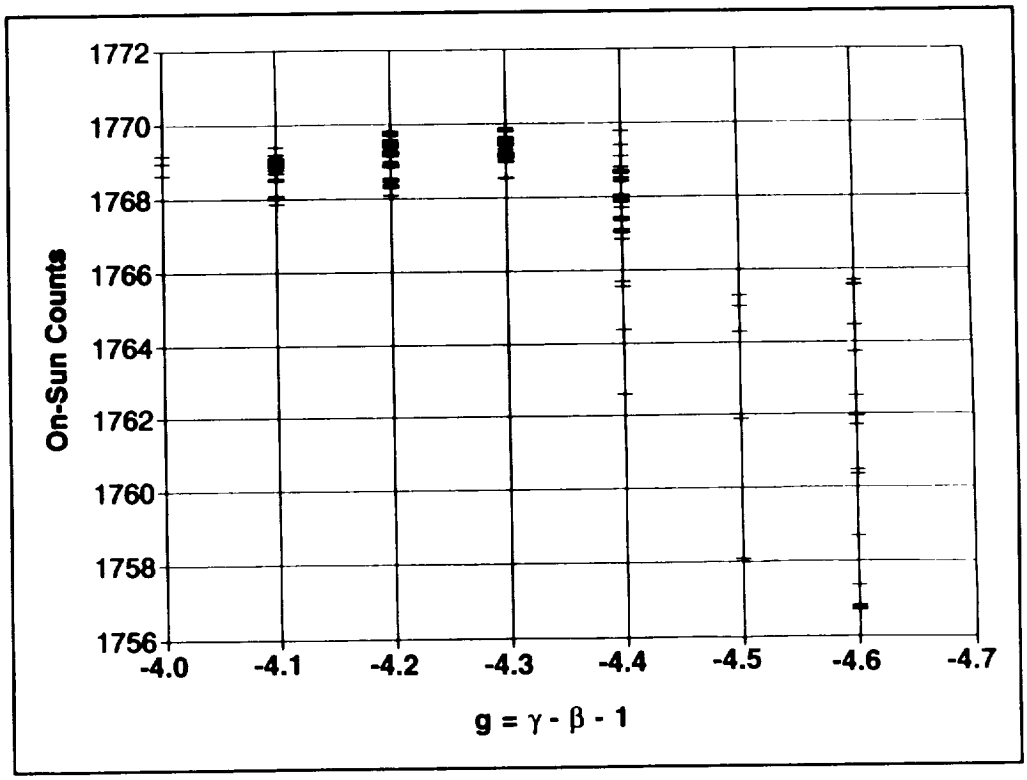

Figure 9. Plot of channel 10c counts versus the γ-axis off center angle (g = γ-β-1) in June 1992 as the Sun slowly moved out of the unrestricted field of view of the sensor. Each dash represents one orbital viewing and the counts are normalized to the mean Earth/Sun distance. This is not a true time plot; because the spacecraft yaws a bit, the readings at a given angle may come from two or three days.

However, by itself, the November 1978 test (Figure 7 and Appendix D) showed the cosine response to be accurate to within 0.1 W/m^2 at (g = 0). This test was brief and somewhat noisy; thus, it is uncertain if any physical change in the response function actually occurred between November 1978 and December 1989. In summary, the present cosine response function should adequately adjust the data from July 20, 1980 onwards with an uncertainty of less than 0.2 W/m^2. From launch up to July 20, 1980 the measurements were centered around (g = 0) and the uncertainty in the cosine response function increases a little.

The results of the γ-angle tests for solar channels 1-9 have not been examined in detail. It appears that their response functions were correctly centered. However, these channels are also sensitive to off-axis pointing. Thus, the 1° shift in the γ-angle scale is expected to have a noticeable effect on their signals. A number of these channels have local minima at the on-Sun position. These appear to be chiefly due to increased reflection from the anodized baffles on these channels when the pointing is off-axis. The 1° shift in the γ-angle scale will probably, therefore, tend to increase the signal from these channels (see Appendix D). All of these first nine channels have suffered noticeable degradation. Thus, their measurement history is harder to analyze than is that of channel 10c.

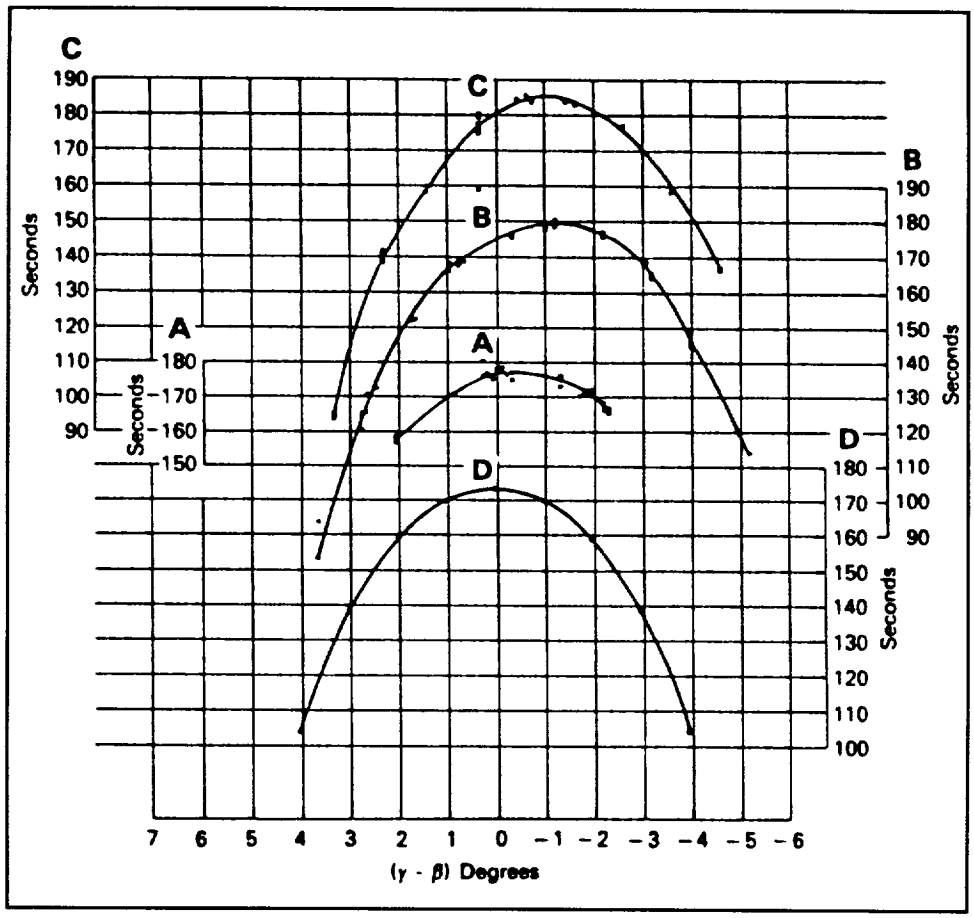

Figure 10. The channel 10c time of passage results for three in-flight tests. A, B, and C represent, respectively, the tests of November 1978, December 1989, and March 1990. D represents a theoretical time of passage.

4. ANALYSIS OF THE INSTRUMENT BEHAVIOR (1978 THROUGH JANUARY 1993)

This section discusses our present understanding of the various terms in the calibration Eq.(1) for channel 10c. The terms discussed include the temperature sensitivity coefficient (A), the zero offset (Z_{space}) of the radiometer, calculation of the Earth-Sun distance (r), a possible change in the sensitivity constant (k_{cal}), "special operations" periods, and possible undetected sensor degradation. The sensor's angular response function, cos(G), was discussed in Section 3. As described in Hoyt et al. (1992), the processing algorithm was revised in 1990 by modifying a number of these terms. The reasons for these modifications are described here.

4.1 Radiometer Temperature Sensitivity

The radiometer is sensitive to temperature since the cavity sees the field-of-view limiters which have different temperatures for each solar irradiance measurement. This problem has previously been examined by Smith et al. (1983) and Hickey et al. (1987). The temperature coefficient (A) is examined by four techniques:

1. If the solar irradiance is taken to be a constant, Eq.(1) can be solved for the temperature coefficient. In reality, of course, the solar irradiance is not a constant but varies by a few tenths of a percent over time. This technique for finding (A) works because the solar variability is

sufficiently small so that the mean of many such determinations gives a reasonable value for (A). For this method to work, temperatures close to 22°C must be avoided so that a division by zero does not occur. Measurements more than 7°C from 22°C were used.

2. If the space-look observations are taken to be a function of the radiometer temperature, a least squares fit can be used to find the temperature coefficient. This technique gives noisy results since the analog to digital (A/D) convertor resolution is low and the space-look observations tend to be pinned to one value.

3. If all other instrumental effects such as off-axis pointing problems are removed, a temperature coefficient can be chosen such that the correlation between the derived solar irradiances and temperatures is reduced to a minimum. An error estimate cannot be derived for this technique.

4. Using the electrical calibration data, including temperature, the radiometer response can be used to derive its temperature coefficient. A few measurements from 1987 to 1989 were used for this last method.

Table 3 summarizes the final results and it is encouraging that three of the four techniques cluster about 0.0003 $°C^{-1}$, which is the value adopted in this analysis. The original Nimbus-7 solar irradiance measurements used a value of 0.000524 $°C^{-1}$ based upon a few determinations in 1978 and 1979.

Table 3. Summary of the Results of Four Techniques Used to Derive the Radiometer Temperature Sensitivity (A)

Technique	Mean	Standard Deviation
Reverse solution of the calibration equation	0.000309	0.000005
Using the space-look observations	0.000196	0.000039
Reducing the irradiance and temperature correlation to a minimum	0.000300	N/A
Using the electrical calibration data	0.000295	0.000023

The temperature coefficient derived from the third technique is used in the revised algorithm. Units are $°C^{-1}$.

4.2 The Zero Offset of the Radiometer

When not viewing the Sun, the radiometer looks at space. In the portion of the data set extracted for further analysis, 32 space-look measurements are collected, along with the radiometer temperature, both 13 minutes before and after each view of the Sun. The mean counts and its standard deviation are calculated and stored for additional processing. The objective of these measurements is to provide a zero level for the measurements by measuring the instrument offset.

In the original calculations of the solar irradiance, the mean for each orbit using all 64 space-look measurements determines the offset.

Two changes are made in the new algorithm. First the zero offset measurements taken 13 minutes after the on-Sun look are discarded because the temperature is about one degree higher than its temperature during the on-Sun look. The radiometer temperatures taken on-Sun and thirteen minutes before on-Sun are within a tenth of a degree of each other. In addition, for various reasons the offset measurements

taken 13 minutes after the on-Sun look are often missing so by discarding these values the use of fill values is avoided. The new offset averages are close to -18.7 counts compared to about -17.5 counts in previous analyses. The 1.2 count difference will increase the calculated solar irradiance by nearly 1 watt per square meter compared to the earlier values.

The second major change is to use yearly mean values of the offset rather than the individual orbital means for the offset. The reason for this procedure is that the individual orbital means have too few observations to provide a reliable mean. The signal from space and the surrounding view limiters is very steady from measurement to measurement compared to the 0.7 watt per square meter resolution of the A/D convertor. Hence, for any small sample, most of the measurements will cluster on one count value. To get a true mean with the poor irradiance resolution requires many observations. If one year of observations is used to form a mean offset, approximately 102,000 to 158,000 individual measurements are used instead of 32.

The mean annual temperature of the radiometer drifts slowly over time, so by splitting the data into one year groups secular changes in the offset caused by temperature drifts are removed. Using all the data to calculate the offset would introduce an artificial trend in the solar irradiance. Choosing a one year blocking of the offset (Table 4), is a compromise between reducing the noise introduced by taking 32 measurements from one orbit and preventing spurious trends from arising. For 1980, the yearly mean is broken into the portion before July 20 and after July 20 when the noise level of the instrument changed (see Section 4.4.1). In 1986 and 1987, the offsets for the special operations periods are separated from the other measurements and their offsets are calculated. The use of these mean offsets does assume that the sensor is in a stable operating condition when the measurements are taken. Procedures for weeding out unstable periods, when the present calibration Eq.(1) is inadequate are discussed in Appendix E.

Table 4. Mean Radiometer Offset 13 Minutes Before a Solar Observation for Each Year

Year	Offset	Year	Offset
1978	-18.508	1986	-18.805
1979	-18.862	1986	-14.082 (special operations)
1980	-19.175 (days 1 to 202)	1987	-18.961
1980	-18.331 (days 203 to 366)	1987	-18.699 (special operations)
1981	-18.462	1988	-18.877
1982	-18.447	1989	-18.819
1983	-18.562	1990	-19.033
1984	-18.609	1991	-19.018
1985	-18.742	1992	-19.192

The daily mean solar irradiance values have their one standard deviation uncertainty reduced by one half using these long-term averages for the offsets. The offset values for blocks of data, usually one year, normally differ by less than 0.1 counts, although changes of a few tenths of a count do occur. Thus, small discontinuities in the irradiance of the order of 0.1 W/m^2 occur between adjacent years. The average changes in solar irradiance from the end of one to the beginning of the next are, however,

smaller than would be expected if the change in offset were causing them and have only a 0.013 correlation with the offset induced changes.

4.3 Earth-Sun Distance Calculations

The originally published values of the solar irradiance used values of the Earth-Sun distance derived by an algorithm used in the routine Nimbus-7 processing. This algorithm was designed to be computationally fast, so an approximation method was used. In the approximation the distance from the Earth-Moon barycentre to the center of the Sun is calculated. This value approximates the true Earth-Sun distance rather well for most applications, but it will introduce spurious 29 day and 1 year oscillations in the solar irradiance of the order of 0.002 percent and 0.01 percent, respectively. These approximate Earth-Sun distances are used in calculating the solar irradiance values which are on the Solar and Earth Flux Data Tapes (SEFDT) distributed by the National Space Science Data Center (NSSDC).

Later an improved Earth-Sun distance was used to revise the SEFDT solar irradiance values which have been distributed by NSSDC on floppy disk. These improved Earth-Sun distances were calculated for noon GMT each day, using a Chebyshev polynomial expansion of 20 terms. If a full day's observation was not available, then the noon value was not used but an appropriate interpolation was made. These Earth-Sun distances are accurate to one part per million (ppm), so derived solar irradiances are affected by up to 2 ppm using this approximation.

For the algorithm presented in this paper, the Earth-Sun distances were re-calculated for each orbital measurement using the Jet Propulsion Laboratory (JPL) subroutines. These subroutines are identical to the ones used by The Astronomical Almanac. The Earth-Sun distance was calculated for each measurement or once per orbit with an accuracy of better than 0.1 ppm based upon checks against the published Almanac values. The differences in this technique compared to using the Chebyshev polynomial technique are generally less than 2 ppm. For the present algorithm, the errors in the derived solar irradiances are less than 0.2 ppm due to Earth-Sun distance uncertainties.

4.4 Special Events During the Life of the Radiometer

Two problems associated with the electronics were found during the analysis of the radiometer. One problem is a sudden change in the noise level of the digitized on-Sun counts after July 20, 1980. The second event was an apparent change in the radiometer gain on September 26, 1987. Two so-called "special operations" periods of 1986 and 1987 have also caused problems with the interpretation of the measurements. These events, and how they were handled in the analysis, are described in the next three sub-sections.

4.4.1 A Change in the Radiometer Noise Level on July 20, 1980

On July 20, 1980, after nearly two years of operation, the Earth Radiation Budget (ERB) scanner was turned off. Previously it was assumed that this event did not affect the channel 10c radiometer measurements. Hoyt and Kyle (1990), however, did notice a change in the observations and tentatively attributed the problem to a change in the A/D convertor, but this explanation is no longer held to be correct.

Turning off the ERB scanner apparently reduced the electronic noise environment in which channel 10c was operating. The offset zeros for 1980 therefore were split into two groups before and after July 20, 1980. In the present analysis 40 samples are made when the Sun crosses the field of view. The average of these counts is used in the derivation of the solar irradiance. The standard deviation of this sample of

40 can be used to monitor the noise environment of the radiometer. In Figure 11, the standard deviation of the orbital on-Sun counts through 1990 are shown. Other than the change on July 20, 1980, no other permanent change is apparent. The noise level does drop to its lowest values in the two special operations in 1986 and 1987. The low temperature of the radiometer accounts for the low noise at these times. Although the 1980 change had only a small influence on the solar irradiance determinations, it is important to identify and explain such changes.

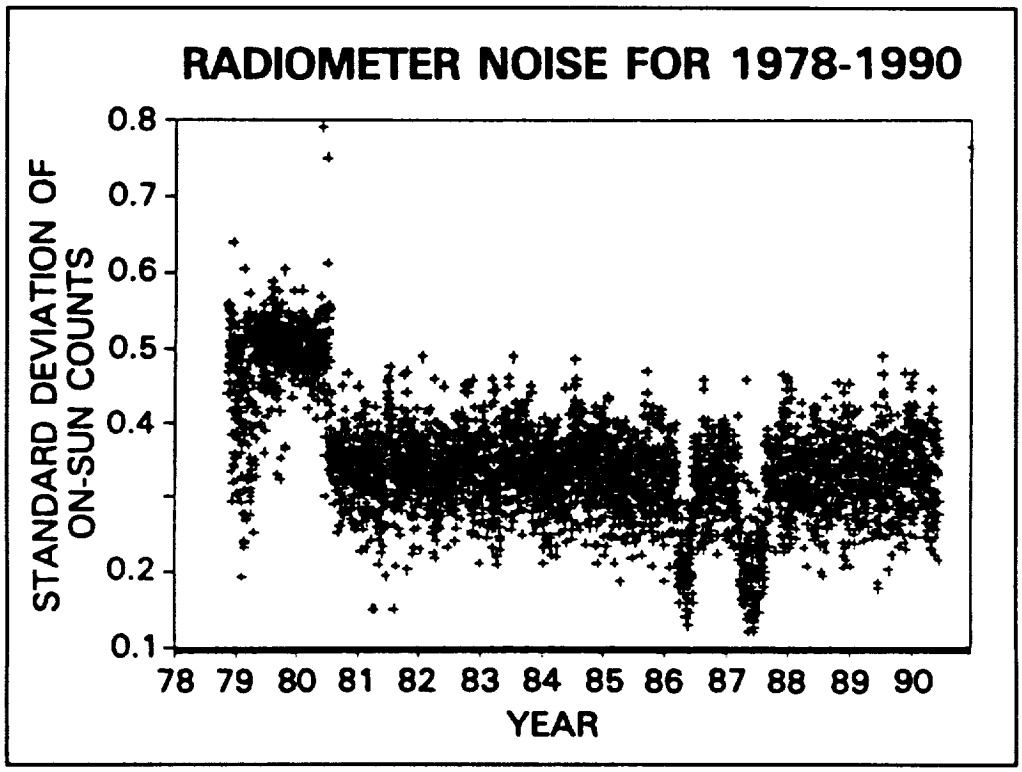

Figure 11. The standard deviation of the on-Sun counts for 1978 to 1990. In addition to the change in 1980, the two special operations periods in 1986 and 1987 are evident by their low radiometer noise levels (Hoyt et al., 1992).

4.4.2 The Apparent Calibration Change of September 26, 1987

Assuming the calibration constant (k_{cal}) of channel 10c remained unchanged throughout the mission, the calculated solar irradiance varies smoothly except one upward step function like discontinuity in irradiance of about 0.029 percent on September 26, 1987 between orbits 45069 and 45070. A change in the calibration coefficient appears to be the cause. The discontinuity in solar irradiance, equal to 0.029 percent of its value or 0.4 W/m^2, is unique in the record and does not appear like a solar phenomena since the step function change occurs over one orbit and persists. Electrical calibrations were made on September 16 and September 28, 1987 (Table 5) and they indicate an increase in sensitivity of 0.031 percent. The radiometer had the same temperature on both days so a temperature effect cannot explain these results. A time history of the calibration coefficients is given in Figure 12. The measured coefficients, corrected to 22°C, and the adopted value (solid line) are given in Figure 12a. The measurements plus estimated error limits (top and bottom curves) are shown in Figure 12b. The error limits were estimated by adding the standard deviations of the voltage and current measurements. For clarity, a number of points present in Figure 12a were omitted in Figure 12b. The measurements are noisy but do indicate a slight downward trend with time. The step function we use is reasonable, but it is, of course, guided by the jump in the solar irradiance on September 26.

Table 5. Electrical Calibration Information Just Before and Just After September 26, 1987					
	Date				
	09/04/87	9/16/87	9/28/87	10/10/87	10/22/87
Temperature	21.5	21.2	21.2	21.2	21.0
Thermal Counts	1756.4	1755.9	1757.0	1756.9	1756.8
Sigma (T)	0.81	0.66	0.71	0.63	0.63
No. of T Obs.	59	67	66	65	58
V Counts	1959.3	1959.1	1960.0	1959.9	1959.8
Sigma (V)	0.66	0.43	0.73	0.59	0.28
No. of V Obs.	38	33	37	36	40
I Counts	-1928.0	-1928.0	-1928.9	-1928.9	-1928.9
Sigma (I)	0.00	0.00	0.29	0.28	0.28
No. of I Obs.	34	31	34	37	37
Resistance	154.96	154.94	154.94	154.93	154.93
Current	0.021003	0.021003	0.021013	0.021013	0.021013
Voltage	3.25472	3.25472	3.25431	3.25580	3.25561
Power	68.35966	68.35091	68.41444	68.41087	68.40872
Cal. Const.	1.2988	1.2986	1.2982	1.2982	1.2981

Notes: Therm. = thermocouple counts; V = voltage counts; I = current counts. One standard deviation uncertainties (sigma) and number of observations are given below each mean. The heater resistance is in ohms, the final current value is in amperes, the final voltage is in volts, the power is in milliwatts, and the calibration coefficient is counts per watt per square meter. The correction factor for the aperture area of the radiometer and nonequivalency of heating effects is 0.5055 square centimeters. A number of quantities are rounded off, but the calculations were done in double precision arithmetic.

The calibration constants (Table 5 and Eq.(1)) are calculated by

$$k_{cal} = C\ (\text{thermal})/P/(Ap) \qquad (4)$$

C(thermal) = sensor counts during calibration minus space reading

Power(P) = $IV = I^2R$, square of current times the resistance

Ap = effective area of the sensor aperture = 0.5055 cm^2.

Now the sensor reading, C, the calibration current (I), and voltage (V) are multiplexed through the same circuitry. Notice (Table 5) that after September 26, 1987, both the reported thermal counts and the calibration current slightly increase. Thus, by Eq.(4), the "measured" calibration constants will slightly decrease due to the change in the system. In reality, of course, the true calibration constant has to increase to offset the system-caused jump in the measured signal.

Observing calibration coefficients for periods well before and well after September 26 indicate a persistent change in sensitivity, although the noise in the electrical calibrations and relative spareness reduces the

certainty of this statement. The initial post-launch calibration coefficient was 1.3013. To correct for a change of 0.029 percent, the calibration coefficient is reduced to 1.30168 after September 26, 1987. If the change were assumed to be in the Sun and not in the instrument, all values of irradiance published here would be increased by 0.4 W/m^2 after September 26, 1987. The change in calibration may be arising from some change in a component of the electronics, such a change in a resistor value.

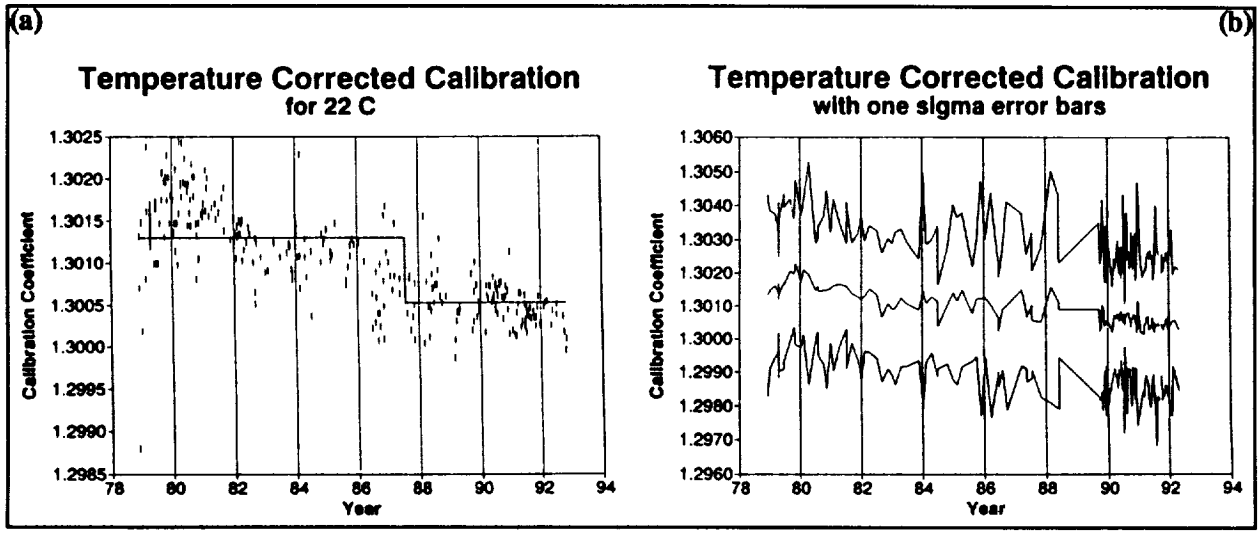

Figure 12. (a) Plot of electrical calibrations corrected to 22°C for the period November 1978 through 1992. The solid line indicates the calibration (sensitivity) coefficient (kcal) actually used in the calibration equation (1) (see text); (b) The electric calibrations are plotted again as the middle curve. The top and bottom curves indicate the one sigma uncertainties in determining the individual points.

Other hypotheses, such as change in off-axis pointing, were investigated, but without success. There is no evidence for a sudden change in temperature, zero offset, A/D convertor properties, or any other aspect of the sensor which is being monitored. Using the radiometer counts and temperature to derive a temperature coefficient for the radiometer by solving the calibration equation for the coefficient, the temperature coefficient shows a sudden jump to negative values in September 1987. Since negative values are impossible, this test provides further evidence for some change in the electronics of the radiometer.

Finally, the SMM/ACRIM observations show no sudden increase in solar irradiance during September. Other measurements, made by the Earth Radiation Budget Experiment, actually show a decrease in irradiance for the days bracketing September 26 (Lee et al., 1988).

4.4.3 The Two "Special Operations" Periods

Between days 100 and 174 of 1986 and days 91 and 233 of 1987, the Nimbus-7 satellite was put in what is known as a special operations mode. In the 1986 operations period, the ERB was on only for 20 minutes per orbit for the solar irradiance measurement. During these periods, the temperature of the radiometer dropped to about 14 or 15°C compared to its normal operation near 20°C. The offset counts rose from -19 to -14, equivalent to about 3.8 W/m^2. In parts of May and June of 1986, some orbits were skipped when the Scanning Multichannel Microwave Radiometer (SMMR) was on to conserve power which caused the radiometer temperature to drop even lower.

In the 1987 special operations period, the ERB was fully on for one day and partly on (i.e., 20 to 30 minutes per orbit) for alternative days. The alternate turning on and off the radiometer meant that the radiometer was seldom in a stable conditions.

Applying the normal algorithm to these periods gives solar irradiance values which are offset from the measurements before and after the special operations periods. This occurs even though these periods have their own space offset values (Table 4). For 1986, the solar irradiance values are offset upwards by 2.5 W/m^2. For 1987, the solar irradiance are offset upwards by 0.2 W/m^2. These offsets are probably explained by the radiometer not being in a full thermal equilibrium state. In the algorithm the irradiance offset values are added to the determined values so the variation in irradiance appears smooth and no discontinuities occur. In addition, in the 1987 period all of the days with 20- or 30-minute measurement periods were rejected in the processing as being too noisy. Figure 13 shows the 1987 measurements with no rejections. The calculated irradiances on the 30-minute power on periods are all offset upwards by 0.5 to 1.5 W/m^2. In the original dataset (see Section 4.6, Figure 14), an effort was made to include these measurements. However, we now conclude that the sensor is still not well enough characterized to produce accurate irradiance values from these readings. Although these corrections and deletions produce a smooth measurement set, we are not entirely satisfied as to why they are necessary. It may be that something other than the radiometer alone, perhaps its associated electronics, is temperature sensitive. Alternatively, because of the rapid temperature fluctuations, the radiometer and its electronics probably never reached equilibrium during the special operations periods. Thus, the calibration equation will not adequately describe the physics of the radiometer. Additional information on the data rejection criteria is given in Appendix E while the general sensor temperature history is discussed in Appendix C.

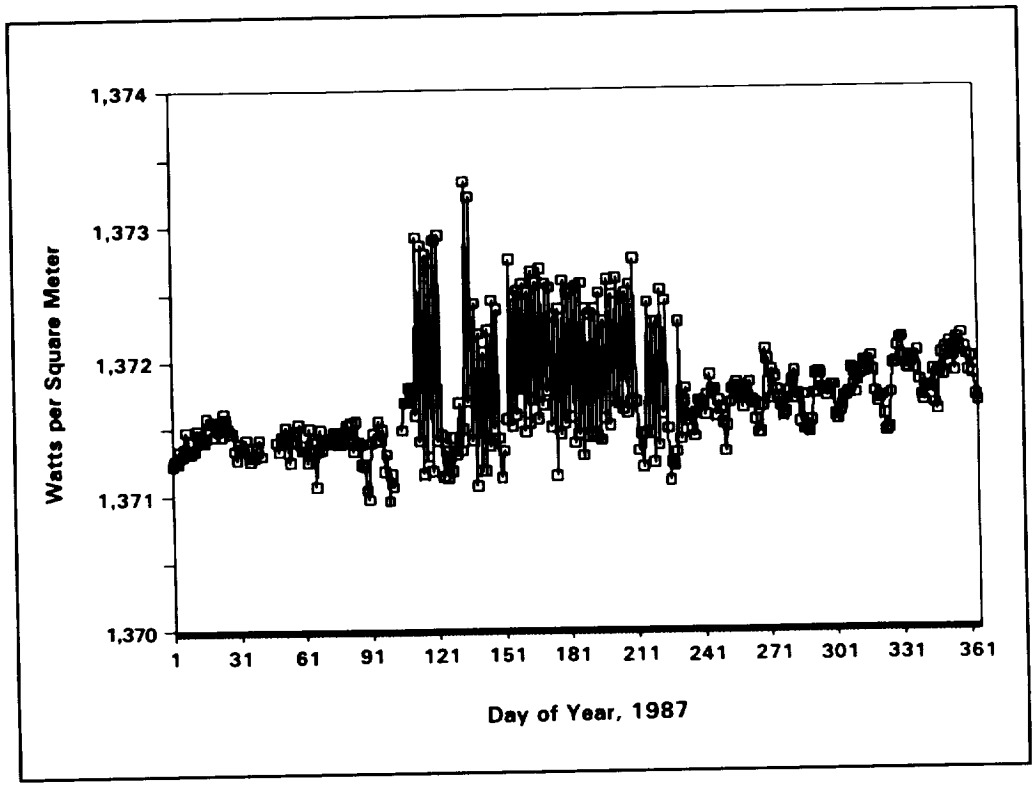

Figure 13. The calibration equation (1) was used to calculate solar irradiances for all of the measurements in 1987. During the special operations period in the spring and summer, much of the data proved too noisy to be properly interpreted by our present equation. Such noisy data were therefore rejected (see text).

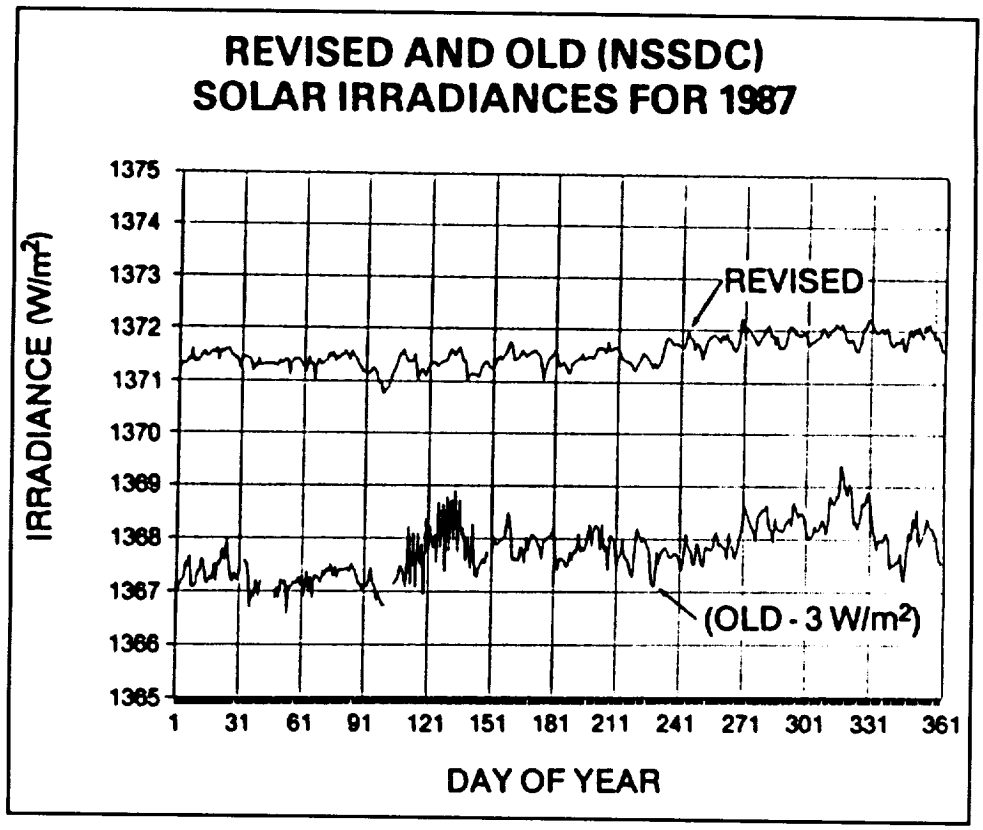

Figure 14. The solar irradiance variations in 1987 using the present revised algorithm (upper curve) and the old NSSDC values (lower curve). The NSSDC solar irradiance values are reduced by 3 Wm^{-2} to separate the two curves for plotting. The rapid oscillations apparent in the NSSDC values which are particularly evident early in the year and late in the year arise from a failure to consider the systematic error in the off-axis pointing. Correcting for this systematic pointing results in a smoother and flatter curve (upper curve). Note how in the lower curve there is an upward peak around day 318 caused by an inadvertent improvement in the pointing. The oscillations in the lower curve around days 100 to 140 are caused by unresolved problems during the first part of the April to August 1 day on, 1 day off duty cycle period (Hoyt et al., 1992).

4.5 Sensor Degradation

Cavity radiometers, such as SMM/ACRIM, have lost sensitivity over time (Willson et al., 1986). It is plausible to postulate that the Nimbus-7 cavity radiometer has degraded and lost sensitivity after long exposure to the space environment. The Nimbus-7 radiometer by itself does not allow any degradation to be monitored, so the problem can only be resolved by identifying the sources of degradation and assessing their impacts, or by comparison to other sensors such as SMM/ACRIM.

During its 9.5 year lifetime, the SMM radiometer decreased in sensitivity by about 600 parts per million (Willson and Hudson, 1991). About 150 parts per million (ppm) of the degradation occurred in the first few months (Willson et al., 1986). The source of degradation is not clear, but several causes are possible. If the degradation is caused by free atomic oxygen, which is combining with the cavity paint and changing its absorptivity, the Nimbus-7 satellite will be affected much less than SMM. Nimbus-7 orbits at 955 kilometers compared to 300 to 400 kilometers for SMM. At 955 km. atomic oxygen is one tenth to one millionth of the density (U. S. Standard Atmosphere, 1976) that it is at 350 km. and is a function of solar activity. If free oxygen is a cause for sensor degradation, the Nimbus-7 would have been

expected to degrade by about 50 ppm. This amount of degradation would have induced a total decrease in solar irradiance of 0.07 W/m^2 over 10 years. Such a small trend (less than 0.001 percent/year) would be very difficult to notice.

Another hypothesis attributes sensor degradation to ultraviolet radiation exposure. SMM/ACRIM was exposed directly to the sun for about 33 minutes per orbit. Nimbus-7 is exposed directly to the sun about 2 to 3 minutes per orbit. Assuming the rate of degradation is proportional to the solar UV exposure, the Nimbus-7 would degrade at a rate of 6 percent to 9 percent of SMM or about 35 to 55 ppm over 10 years. This trend is less than that for the free oxygen degradation hypothesis.

Yet another hypothesis attributes sensor degradation to out-gassing of the cavity paint to the vacuum of space. The rate of out-gassing will be a function of the type of paint used and its pre-treatment before launch. Because of these differences, there is no reason to expect that the sensor degradation experienced by SMM/ACRIM will be a good model for sensor degradation by Nimbus-7.

A similar Hickey-Frieden cavity radiometer was on the Long Duration Exposure Facility (LDEF) satellite from April 1984 to January 1990 (5 years and 10 months). This sensor was exposed to atmospheric conditions similar to those encountered by the SMM/ACRIM, but for a shorter period. Both the LDEF and Nimbus-7 sensors were mounted in the forward looking (ram) orientation which markedly increases the interaction with the atmosphere. The LDEF sensor also had a larger aperture than did the Nimbus-7 sensor. Since the January 1990 recovery of the LDEF satellite, this sensor has been undergoing various tests. Preliminary results indicate that any degradation suffered by the LDEF sensor was below, and possibly significantly below, 0.05 percent. Recent laser reflectivity tests at the World Radiation Center in Davos, Switzerland indicated no change in cavity reflectivity down to the 80 ppm level. More details on the LDEF sensor are given by Hickey et al. (1991) and Appendix B.

4.6 Comparison With Previously Used Algorithms

The calibration adjustments described in this report were derived in 1990 and the old measurements were then reprocessed to produce a consistent dataset. However, many scientists had already received the original products up through 1989. The derived solar irradiances using the algorithm developed here and the algorithm previously used differ on both short and long time scales. These differences arise primarily from (1) the use of different off-axis angles G, (2) a new value for the temperature sensitivity A, (3) a different treatment of the space-look counts C_{space}, and (4) the use of 40 observations of the Sun as it drifts across the radiometer field of view versus 42 observations in previous analyses. The use of fewer observations per orbit changes the mean on-Sun count by less than 0.05 or changes the calculated solar irradiance by less than 0.035 Wm^{-2}. The differences in derived total solar irradiances using the two algorithms are most easily seen by comparison of daily mean values for the short-term variations and by comparison of monthly means for long-term variations.

The differences between the two algorithms are most easily seen in plots. Figure 14 shows the daily means for the moderately active year of 1987 using the old and new algorithms. The new algorithm gives higher irradiance values since the off-axis angle correction in the new algorithm averages about 1.4° off the Sun and hence raises all of the derived values. The old algorithm assumes that the average pointing is on-Sun.

In the new algorithm, the 1987 range of values is about 1 Wm^{-2} compared to about 2.5 Wm^{-2} for the old algorithm. In the old algorithm, some of the solar variations are well correlated with changes in the gamma angle of the satellite. For example, the sharp downward drop in solar irradiance on day 35 corresponds to the change in gamma angle from -5° to -6° (see Figure 1). There is no discontinuity at

this time in the new algorithm. Sharp downward changes in apparent solar irradiance using the old algorithm also occur on days 143, 161, and 181 coincident with changes in the gamma angle. These discontinuous variations are not apparent with the new algorithm. When the gamma angle changes in the opposite direction, the apparent solar irradiance using the old algorithm discontinuously jumps in the opposite direction such as on days 219, 232, 243, and so forth. With the new algorithm these jumps are not apparent. The old algorithm has the solar irradiance exhibiting a downward staircase trend at the end of the year. The downward jumps on days 322, 332, 340, and 346 occur as the gamma angle steps from 2° to 1° to 0° to -1° to -2°, respectively. The new algorithm again does not exhibit this high correlation with the gamma angle changes.

Another obvious difference between the two algorithms is the special operations period around days 100 to 140. With the old algorithm, the apparent solar irradiance values bulge upward and become noisy. The increased noise arises from the one day on followed by the one day off cycle. On the off days, the instrument was turned on about 20 to 30 minutes in most orbits to take solar measurements. On these days the counts are usually high, which causes spikes in the derived irradiances if they were processed by the same method used when the radiometer is on full time. In the new algorithm, these off days in 1987 are not analyzed because the radiometer and its associated electronics are not in thermal equilibrium and Eq.(1) therefore does not apply. The cause of the upward bulge in the previous analysis is not known but appears to arise from thermal conditions which make (1) inappropriate.

Figure 15 provides a long-term plot of a 27-day running means of the solar irradiances using the revised algorithm and using the old algorithm. The old algorithm indicates a much quicker rise in irradiance in the last 3 years than does the new algorithm. Previously, the peak of cycle 21 was about equal to that of cycle 22, but the new algorithm gives a stronger peak for cycle 21. In between, from 1981 to 1987 the two algorithms paralleled each other to within ± 0.5 Wm^{-2}. Since 1987, the old algorithm values rise rapidly to equal and even exceed the values that the new algorithm calculates. The improved treatment in the new algorithm of off-axis pointing seems to be the major but not the sole contributor to these different interpretations of solar behavior. Without careful consideration of off-axis pointing errors, the long-term trends in solar irradiance are distorted. Figures 14 and 15 show that the daily changes were strongly affected by the gamma angle changes in the old algorithm. The new algorithm removes most of the daily discontinuities and in so doing alters the long-term trends.

5. COMPARISON WITH INDEPENDENT SATELLITE MEASUREMENTS

5.1 The Nimbus-7, SMM, and ERBS Experiments

Independent, mean daily, solar irradiance measurements from the Nimbus-7, Solar Maximum Mission (SMM; Willson and Hudson, 1988) and the Earth Radiation Budget Satellite (ERBS; Lee et al., 1991) are shown in Figure 16. The Nimbus-7 data extend from November 1978 through January 1993, the SMM data from February 1980 into July 1989. The ERBS measurements started in late October 1984 and are still continuing. The vertical displacements between the three curves is due to differences in the absolute calibration of the sensors. The claimed accuracy of the absolute calibrations were: Nimbus-7 (± 0.5 percent, i.e., ± 7 W/m^2), ERBS (± 0.2 percent), and SMM (± 0.1 to ± 0.2 percent). However, the mean stability of the sensors is at least 10 times better than this. The general qualitative and quantitative agreement of the three measurement sets re-enforces the claim that we are observing true solar changes. The observed measurement differences indicate deficiencies in the instruments and of our understanding of how they operate.

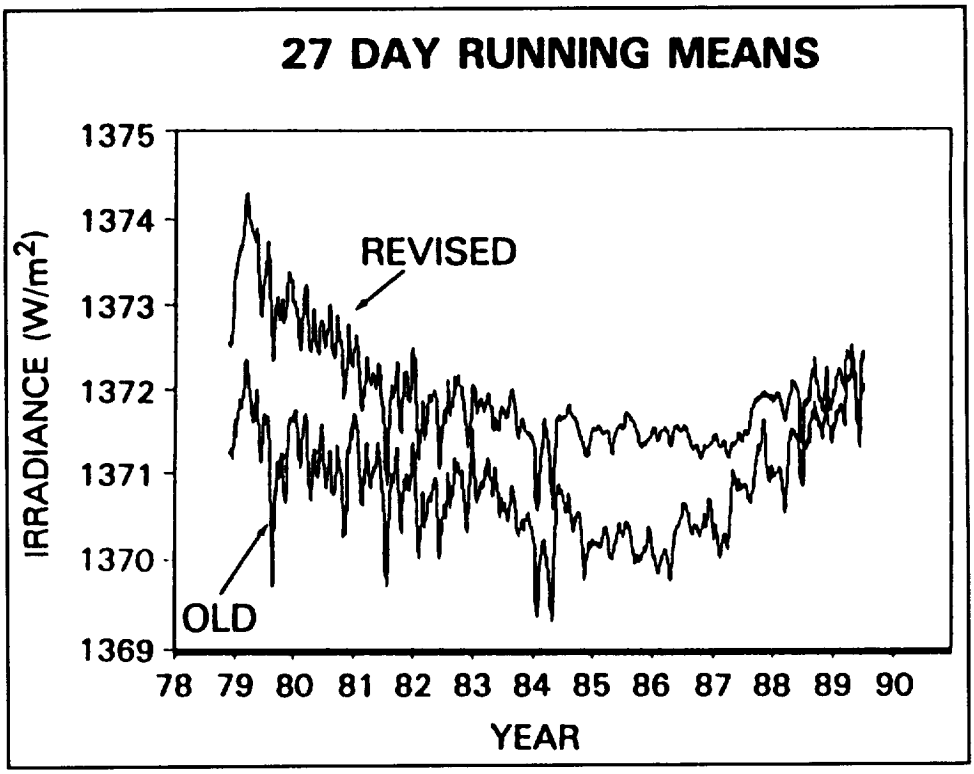

Figure 15. The solar irradiance values after being smoothed by a 27-day running mean from 1978 to 1989 using the old algorithm (lower curve) and the new algorithm (upper curve) (Hoyt et al., 1992).

All three sensors were electrically self-calibrating cavity radiometers but with some design and operational differences. For instance, the ERBS and SMM sensors were of active cavity design which used electrical heating to balance the absorbed radiant energy, while the Nimbus-7 sensor operated in a passive mode. The Nimbus-7 and ERBS measurements were made by allowing the Sun to drift across the sensor field of view, but in the normal operation of the SMM sensor the Sun was actively tracked. The active cavity sensors measured the Sun for a period and then, for reference, observed the sensor shutter for an equal period. The time for each period was 65 seconds for the SMM and 32 seconds for the ERBS. As reference, the Nimbus-7 sensor used a cold space observation 13 minutes before the Sun drifted into the field of view. The number of observations is of particular significance. Because of the ERBS operating schedule, its solar sensor could take only about two measurements once every 2 weeks. The Nimbus-7 sensor saw the Sun for about 3 minutes once per orbit or about 14 times a day. Finally, the SMM could obtain up to 28 shutter cycles per orbit or several hundred in a day. Because of the deficiency of ERBS measurements, this section deals chiefly with the Nimbus-7 and SMM comparisons.

5.2 Nimbus-7 and SMM Daily Values

Differences in the daily averaged readings (Nimbus-7 minus SMM) are shown in Figure 17. Only days when both sensors were active are included. The SMM measurements started on February 16, 1980 and the ones we have end in July 1989. The SMM fell into the Indian Ocean on December 2, 1989. On day 348, December 13, 1980, the solar-pointing system on the SMM failed and the spacecraft was placed in a spin-stabilized mode until its repair in April 1984, by the crew of a NASA space shuttle. In November 1983, the tape recorder became defective and after this only a few solar readings were obtained until after the repair work. During the spin-stabilized period, the shutter of the sensor was opened at orbit sunrise and closed at orbit sunset. About 100 solar observations were made per day, but few were recorded

between November 1983 and February 1984. No data have been released for March, and only 1 day of data for April; however, the regular measurement program resumed in May 1984.

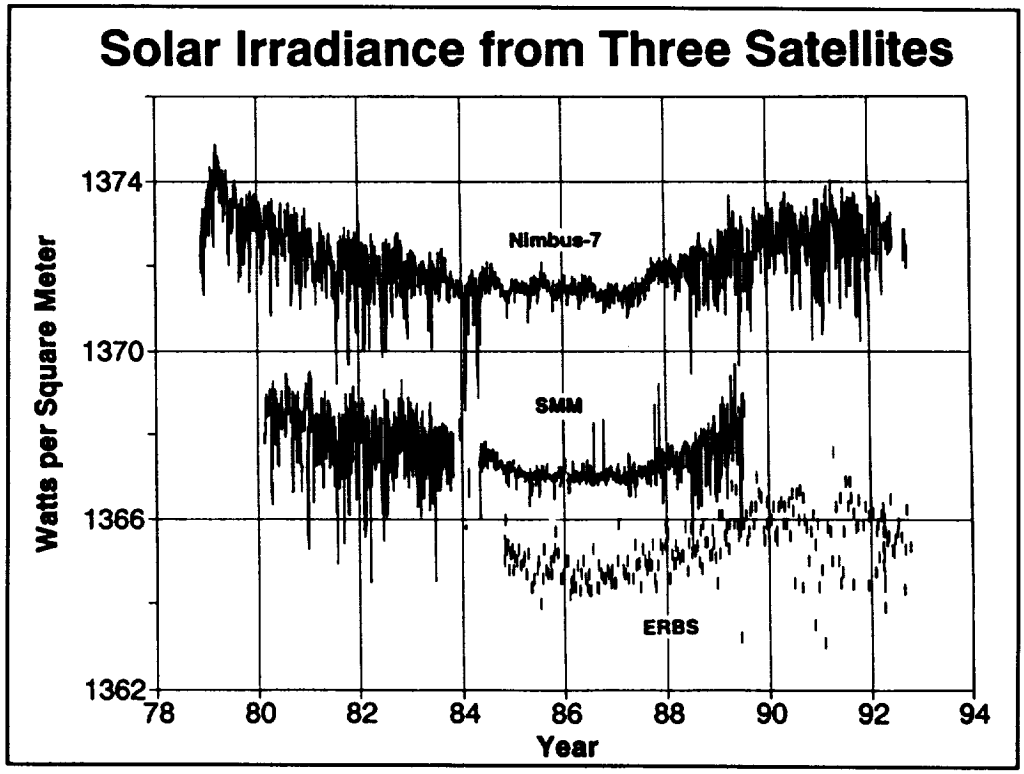

Figure 16. Daily averaged irradiances are plotted for three independent satellite sensors: the Nimbus-7 ERB (November 1978 to September 1992), SMM ACRIM (February 1980 to June 1989), and ERBS solar sensor (October 1984 to October 1992). The vertical gaps between the measurements are caused by uncertainties in the three absolute calibration determinations.

During the spin-stabilization period, measurements were made as the Sun passed through the sensors field of view near its optical axis. Differences in solar exposure time and the sensors thermal response to off-axis irradiance produced a systematic bias compared to the solar pointing measurements. This bias was estimated to be (0.12 $\pm$ 0.02 percent) and the released data included a 0.12 percent adjustment (Willson et al., 1986). The measurements were also noisier during the spin mode period.

The yearly values of the correlations of Nimbus-7 with SMM ACRIM are given in Table 6. The new algorithm in all years correlates better with the SMM values than does the old algorithm. In 1986 and again in 1987, there are two upward spikes in the SMM measurements which degrade the correlation between the two satellites. Removing these spikes increases the correlations to 0.266 and 0.711, respectively, but the overall correlation only increases from 0.832 to 0.836. Figure 17 indicates that daily differences can suddenly shift by up to 0.2 percent in the SMM spin scan period and up to 0.1 percent in the SMM normal operation periods. However, these perturbations tend to be short lived. High correlations occur in 1980 and 1988 when both instruments are operating without problems and solar activity is high. The highest correlation occurs in 1984 and is caused by both sensors detecting a large sunspot group early in the year, which dominates the correlation for this year. From 1981 to 1983, the correlation is reduced by the SMM spin mode operation and the SMM tape recorder problems which caused gaps in the SMM data in 1983. Since Nimbus-7 has more low-frequency noise in the quiet years 1985 and 1987, the correlations between the sensors are reduced. Over the entire 9-year period, the

correlation is 0.832, compared to 0.617 before the Nimbus-7 calibration coefficients were modified in 1990. Thus, 69 percent of the daily variance is in common now, compared to 38 percent previously.

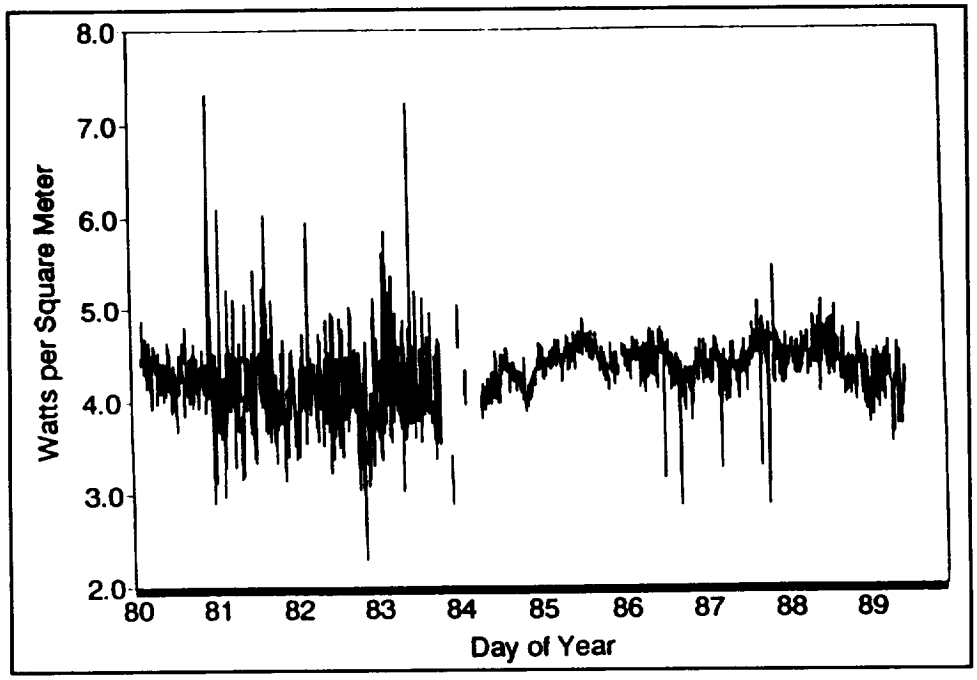

Figure 17. Differences (Nimbus-7 minus SMM) in the daily averaged solar irradiances on the days when both satellites were recording measurements.

Table 6. Correlation of Daily Nimbus-7 Solar Irradiance Measurements, Determined in This Study and as Previously Released to NSSDC, to SMM ACRIM Measurements for Each Year From 1980 to 1988

Year	This Study	Old NSSDC Values
1980	0.881	0.793
1981	0.823	0.771
1982	0.848	0.792
1983	0.522	0.386
1984	0.935	0.854
1985	0.441	0.255
1986	0.168	0.090
1987	0.660	0.586
1988	0.916	0.768
All	0.832	0.617

Figures 18a and 18b compare a quiet Sun year, 1985, with a more active Sun year, 1988, to illustrate why the correlation varies with solar activity. In 1985, there is only a little true solar variability, and the system "noise" on the Nimbus-7 is quite apparent. However, in 1988, active solar variations dominate the low level- system noises. During the quiet Sun period, the SMM data (Figure 17a) are smoother than the Nimbus values. This is primarily because of the smaller number of Nimbus-7 measurements each day and the lower A/D resolution compared to the SMM.

The period December 1980 through February 1984 is interesting because the differences between the two measurement sets are much more variable (Figure 17). It seems probable that the pointing problems of the SMM satellite account for this anomaly. Overall the newly derived Nimbus-7 irradiances agree with SMM measurements better than previous values, which increases our confidence that the new algorithm is providing a reasonable interpretation of the radiometer performance and the true solar behavior is being tracked.

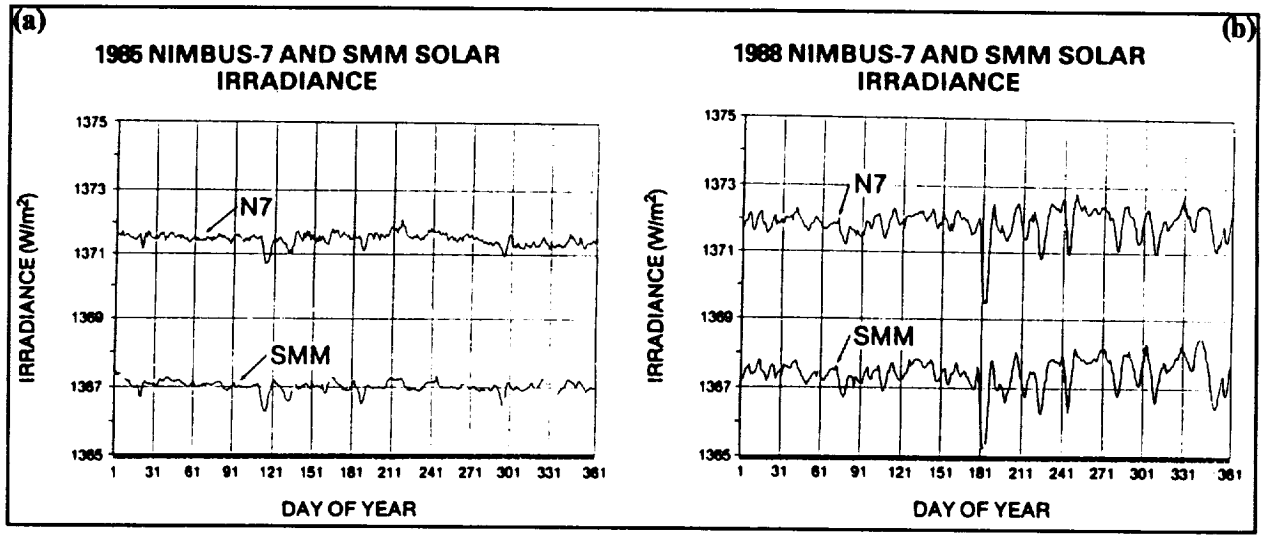

Figure 18. Yearly plots of the Nimbus-7 and SMM ACRIM solar irradiance values for the years (a) 1985 and (b) 1988 both drawn to the same scale (Hoyt et al., 1992).

5.3 Monthly and Yearly Means

Figure 19 provides a plot of the differences in the monthly means calculated using days when both satellites made observations. The SMM spin scan years, 1981 through 1983, are clearly delineated here with values about 0.4 Wm^{-2} (0.03 percent) closer to the Nimbus-7 values than in the solar pointing years (1980 and 1984-1988).

Another way to look at the differences between the two satellite measurements is through an examination of the percent differences between them. The mean difference is 0.3120 percent with small fluctuations about this value. For 1980, the difference is 0.3155 percent and for May, 1984 to December, 1988, it is 0.3204 percent, for a difference between these two differences of 0.0049 percent. During the spin mode operation of the SMM, 1981-1983, the difference is 0.2970 percent or 0.0185 percent to 0.0274 percent less then the other periods. During the spin mode period, the SMM analysis raised the measured values by 0.12 percent. If this percentage had been 0.09 percent or 0.10 percent, there would have been virtually no year-to-year change in the difference between the two satellites. In any case it appears the trends in solar irradiance are the same to a precision of 0.005 percent over the nine year period of common measurements.

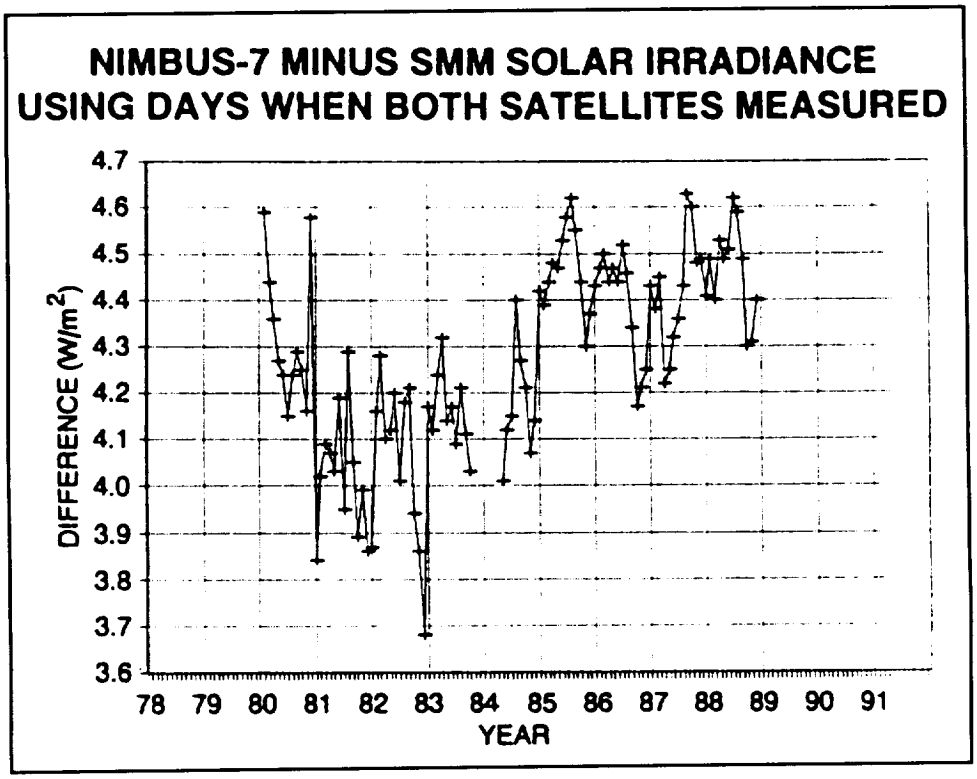

Figure 19. The Nimbus-7 monthly mean solar irradiance minus the monthly mean SMM solar irradiance using only days when both satellites observed. Only months with 10 or more days of observations are used. Most differences are between 4 and 5 Wm^{-2}, and the mean difference is about 0.32% (Hoyt et al., 1992).

Using only those months for which both satellites have more than 10 days of observations, the correlation of the monthly means is 0.908 for 1980 to 1984 and 0.806 for 1985-88. The higher correlation in the early years arises from the greater variability of the Sun whereas in 1985-86, the solar irradiance values cluster about a constant quiet Sun value reducing the correlation for the 1985-88 period. For the entire 1980-88 period, the correlation is 0.897 using monthly means for which both satellites have at least 10 daily measurements.

Both Figures 17 and 19 show indications of an annual cycle in the differences. This annual cycle is somewhat obscured by shorter term fluctuations and by the spin scan perturbations. It is clearest in Figure 17 during the quiet Sun period (1984 to 1987). Because of this annual cycle, the annual mean differences for the years (1980 and 1985 to 1980) vary only by ± 0.07 W/m^2. The plot of the annual mean differences, Figure 20, shows this as does Table 7 which also gives the annual means and standard deviations for the SMM and Nimbus-7. The exact cause of the annual cycle in the differences is not well understood. However, it is probably due to the varying stress on the sensor systems caused by the annual cycle in the solar heating. The small eccentricity of the Earth's orbit causes the mean irradiance at the Earth to vary by 6.7 percent from January to July. Differences in the SMM and Nimbus-7 procedures for compensating for the variations in the solar heating are thought to cause the observed annual cycle. The shorter term fluctuations may be due to unknown internal instrument and satellite system perturbations.

The annual differences (Nimbus-7 minus ERBS) are also shown in Figure 20. The unexplained year-to-year variations are considerably larger than in the (Nimbus-7 minus SMM) case. However, some of this increased variability must be assigned to the paucity of ERBS measurements.

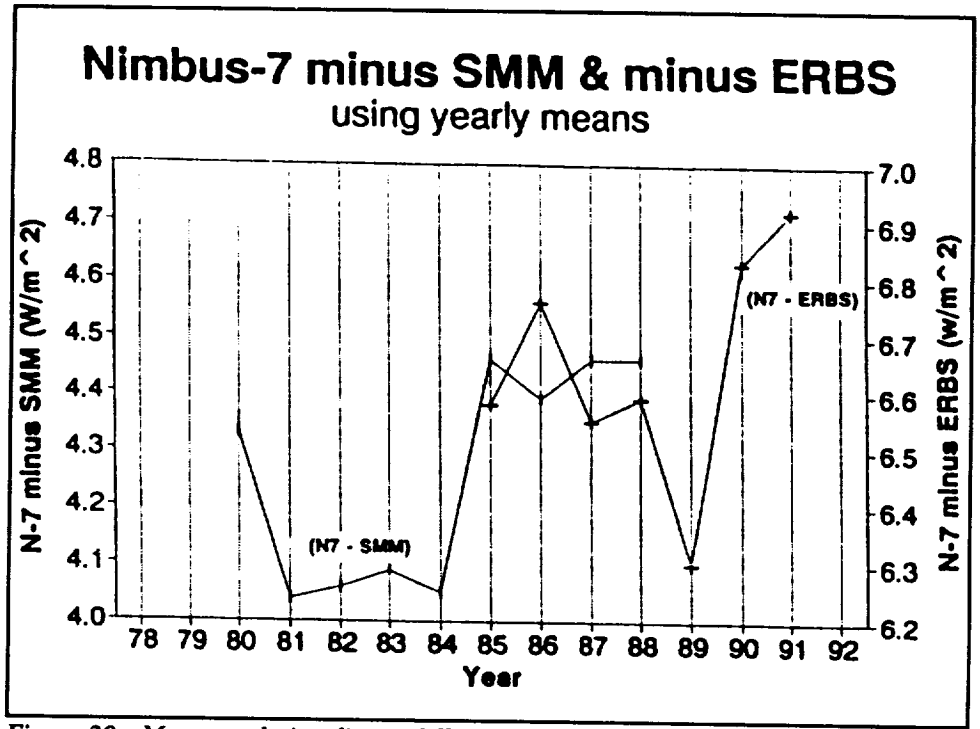

Figure 20. Mean yearly irradiance differences (Nimbus-7 minus SMM) and (Nimbus-7 minus ERBS).

The comparison of the Nimbus, SMM, and ERBS measurement sets qualitatively confirms the Nimbus-7 finding that the Sun was about 0.1 percent brighter in the excited Sun periods 1979 to 1980 and 1990 to 1991 compared to the quiet Sun years of 1985 to 1986. Quantitatively, the Nimbus-7 and SMM comparison indicates that the Nimbus measured trends may be accurate to ± 0.07 W/m^2 for the period 1980 through 1988. We know of no reasons why the Nimbus values should be considered less accurate in its other years (1979 and 1989-1992). However, it would be useful to know the cause of the 0.45 Wm^{-2} jump in the (Nimbus-7 minus ERBS) mean difference from 1989 to 1990. Figure 20 does strongly illustrate the importance of multiple independent solar measurement programs.

6. SUMMARY AND CONCLUSIONS

This document emphasizes the calibration theory and history of the Nimbus-7 ERB Channel 10c which measured the total solar irradiance. This sensor not only made the first accurate measurements of variations in the mean irradiance, but also continued the measurements for over 14 years, from November 16, 1978 into 1993. In 1990, an intensive review of Channel 10c calibration procedures produced improvements at and below the 0.1 percent accuracy level (Hoyt et al., 1992). This is important since multiyear solar variations with amplitudes similar to 0.1 percent are being examined.

The experiment was also designed to measure the broadband spectral components of the solar irradiance using Channels 4-9 (Table 1). All of these channels were protected by Suprasil-W windows which suffered time-dependent fogging due to outgassed chemicals from the instrument and the satellite. This plus lesser problems has made the measurements from these channels very difficult to interpret. A brief discussion of this spectral dataset is given in Appendix A.

Table 7. Yearly Mean and Standard Deviations of Solar Total Irradiances for Nimbus-7 and SMM					
	Nimbus-7		SMM ACRIM		
Year	N	Irradiance	N	Irradiance	Difference
1978	37	1372.66 ± 0.60			
1979	270	1373.33 ± 0.67			
1980	276	1372.60 ± 0.58	297	1368.27 ± 0.67	4.33
1981	285	1371.95 ± 0.67	338	1367.90 ± 0.70	4.04
1982	277	1371.72 ± 0.66	356	1367.66 ± 0.73	4.06
1983	307	1371.65 ± 0.35	290	1367.56 ± 0.52	4.09
1984	319	1371.32 ± 0.55	238	1367.27 ± 0.34	4.05
1985	365	1371.46 ± 0.19	348	1366.99 ± 0.16	4.46
1986	362	1371.38 ± 0.18	340	1366.99 ± 0.16	4.39
1987	310	1371.55 ± 0.30	343	1367.09 ± 0.27	4.46
1988	366	1371.85 ± 0.45	362	1367.40 ± 0.46	4.46
1989	362	1372.21 ± 0.65			
1990	365	1372.62 ± 0.56			
1991	212	1372.76 ± 0.75			
For 1980 and 1985-1988, the differences between the two satellites cluster about 4.4 Wm^{-2}. For 1981-1984, when the SMM is in the spin mode, the differences cluster about 4.07 Wm^{-2}. N is the number of observation days.					

The calibration procedures for Channel 10c derived the solar irradiance form the Nimbus-7 raw counts data. The algorithm includes the basic sensitivity factor (counts per Wm^{-2}) and considers adjustments for (1) off-axis angles G, (2) the temperature sensitivity coefficient A, (3) the zero offset C_{space}, and (4) the Earth-Sun distance. The 1990 review touched on all these points. A revision in the data rejection criteria also removed some additional measurements of questionable validity. Using new off-axis angles has removed discontinuities in the solar irradiance of the order of 0.06 percent which would otherwise occur. The new method for treating the zero offset reduces the daily standard deviation in solar irradiance by about one half or about 0.02 percent of the solar irradiance. Improved earth-Sun distance calculations and the new temperature coefficient have smaller effects on the day to day variations. The net effect of these changes are smoother day to day solar irradiance variations then previous analyses.

Although some of the problems with the Nimbus-7 measurements are removed in this analysis, like all experiments, insufficient information exists to remove all the instrumental influences. In particular, the off-axis angle corrections remove much of the apparent noise in the measurements, but because of the limited number of off-axis determinations and their limited resolution, it is not possible to be certain that all the off-axis effects have been completely removed. This source of error alone makes the monthly means uncertain to ± 0.08 W/m^2 and makes the trend in the measurements uncertain by about ± 0.08 W/m^2 or ± 0.006 percent of the mean solar irradiance over the past 12 years. Errors in the temperature

coefficient (A) of the order of ± 0.00001 will cause errors in the trend of ± 0.005 percent over 12 years, because the radiometer's temperature drifted by about 1°C over this time. The change in gain (k_{cal}) of 0.029 percent on September 26, 1987 is also a potential uncertainty in the long-term trend. Errors in the zero offset (C_{space}) and earth-Sun distance (r) have negligible effects on the long-term trends. The net error in the trend over the last 12 years, in the worst case, equals the sum of the individual uncertainties or about ± 0.04 percent. The root-mean square uncertainty in the trend is ± 0.03 percent. Over the years 1980 to 1988 the Nimbus-7 measurements drifted relative to SMM/ACRIM by the order of 0.13 W/m^2 or 0.01 percent (see Table 4), which indicates the tracking of long-term trends may be better than the estimate given by the above error analysis.

The improved agreement between the Nimbus-7 and SMM satellites increases our confidence that they are both measuring a real solar signal. Despite nearly equal levels of solar activity for the last two solar cycles based upon Wolf sunspot numbers, the solar irradiance for the two cycles are not equal (see Figure 21). For solar cycle 21, the maximum monthly mean was 1374.3 W/m^2 in March 1979, and for cycle 22 the corresponding maximum observed so far is 1373.39 W/m^2 in April 1991.

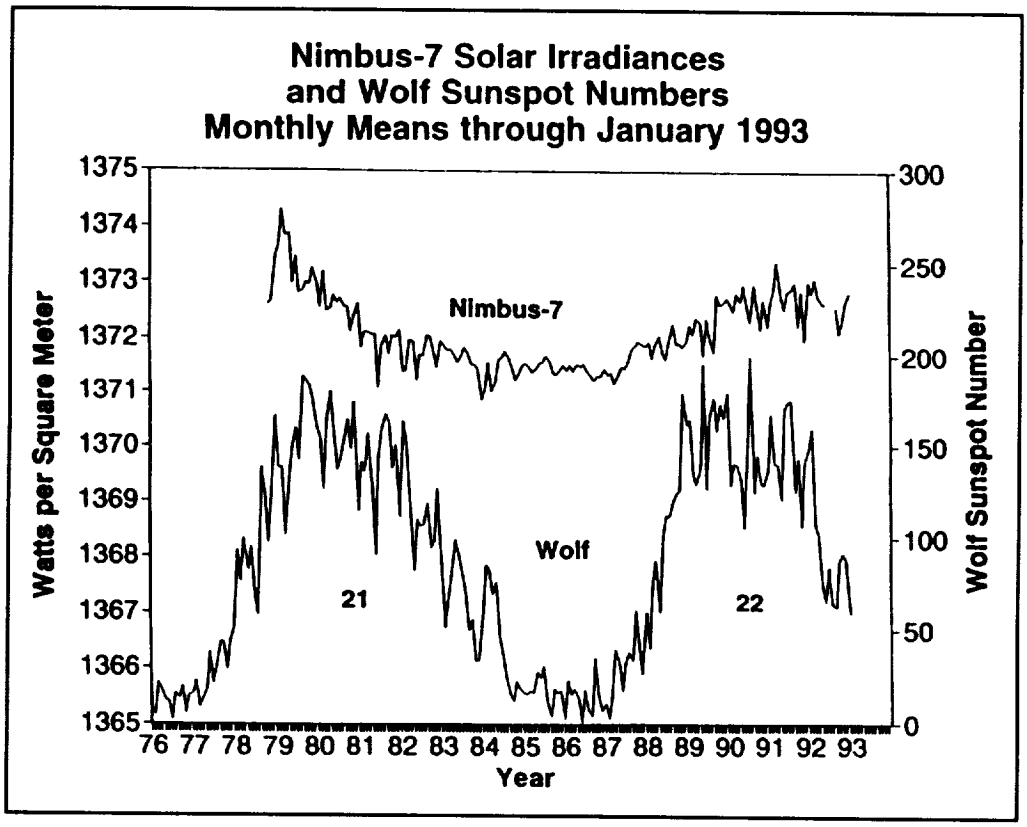

Figure 21. Monthly mean solar irradiances and Wolf sunspot numbers. The Nimbus-7 solar measurements run from November 1978 through January 24, 1993. The Wolf numbers are shown from January 1976 through January 1991.

A summary of the dataset is given in Table 8 and Figure 21. Table 8 considers only the continuous measurement from November 1978 through May 1992. Figure 21 shows the data gap (June 18 to September 1, 1992) as well as the continued measurements through January 24, 1993. Both during the summer of 1992 and after January 24, 1993, the Sun could not be clearly seen by the sensor.

Richard Willson's ACRIM sensor on the Upper Atmosphere Research Satellite (UARS) started taking measurements in October 1991. Given the over 1 year of overlap, it appears that the long-term self-

consistency of the solar irradiance measurements can be maintained at the 0.1 to 0.2 Wm^{-2} level. However, the review in Section 5 shows the importance of having two or more independent measurements at any one time in order to detect possible instrument problems. Otherwise, sensor perturbations might be mistaken for true solar variations.

Table 8
Nimbus-7 Dataset Summary
Period covered November 16, 1978 to May 31, 1992

	Mean Value · (W/m^2)	Uncertainties (W/m^2)		
		Absolute Calibration	Stability	
			Short-Term	Long-Term
Total Period	1372.08 ± 0.82*	±7.0	±0.35	±0.1
1 Cycle (10 Years) 11/16/78-11/16/88	1371.92 ± 0.78*			
Worst Case				±0.4

Range (Max - Min) W/m^2		
	Yearly Means	Monthly Means
Cycle 21	2.01	3.46
Cycle 22	1.31	2.23

*Standard deviation of daily means.

7. REFERENCES

Ardanuy, P. E., H. L. Kyle, and D. Hoyt, 1992: Global Relationships Between the Earth's Radiation Budget, Cloudiness, Volcanic Aerosols, and Surface Temperature, *J. Climate*, **5**, 1120-1139.

Friis-Christensen, E., and K. Lassen, 1991: Length of the Solar Cycle: An Indicator of Solar Activity Closely Associated with Climate, *Science*, **254**, 698-700.

Hickey, J. R., 1973: A Satellite Experiment to Establish the Principal Extraterrestrial Solar Energetic Fluxes and Their Variance in the Extraterrestrial Solar Spectrum, a chapter in *The Extraterrestrial Solar Spectrum*, A. J. Drummond and M. P. Thekaekara, Eds., Pub. by *Inst. of Environ. Sci.*, Mt. Prospect Illinois, p. 135-160.

Hickey, J. R., 1991: Passive Exposure of Earth Radiation Budget Experiment Components LDEF Experiment AO-147: Post-Flight Examinations and Tests, An Article in: LDEF-69 Months in Space, First Post-Retrieval Symposium, NASA Conference publication 3134 (Part 3), 1494-1509.

Hickey, J. R. and A. R. Karoli, 1974: Radiometer Calibrations for the Earth Radiation Budget Experiment, *Appl. Opt.*, **13**, 523-533.

Hickey, J. R., R. G. Frieden, F. J. Griffin, A. S. Cone, R. H. Maschhoff, and J. Gnaidy, 1977: *Proceedings of the Annual Meeting of the American Solar Energy Society*, **1**, 15-1, 15-4.

Hickey, J. R., L. L. Stowe, H. Jacobowitz, P. Pellegrino, R. H. Maschhoff, F. House, and T. H. Vonder Haar, 1980: Initial Solar Irradiance Determination from Nimbus-7 Cavity Radiometer Measurements, *Science*, **208**, pp. 281-283.

Hickey, J. R., B. M. Alton, F. J. Griffin, H. Jacobowitz, P. Pellegrino, and R. H. Maschhoff, 1982: Indications of Solar Variability in the Near UV From the Nimbus-7 ERB Experiment, International Association of Meteorology and Atmospheric Physics (IAMAP), Third Scientific Assembly, Hamburg, FRG, August 17-28, 1981. (The Symposium on the Solar Constant and the Spectral Distribution of Solar Irradiance; Extended abstracts edited by J. London and C. Frohlich; Boulder, Colorado, 1982), pp. 103-109.

Hickey, J. R., 1985: Analysis of Calibration of Nimbus-7 Radiometry, in Advances in Absolute Radiometry," ed. by P. Foukal, pp. 30-33, Cambridge Research and Instrumentation, Inc., Cambridge, MA.

Hickey, J. R., H. L. Kyle, B. M. Alton, and E. M. Major, 1986: ERB Nimbus-7 Solar Measurements, 7 Years, *Extended Abstracts of the Sixth Conference on Atmospheric Radiation*, Williamsburg, VA, May 13-16, 1986 (American Meteorological Society, Boston, Massachusetts), 290-293.

Hickey, J. R., B. M. Alton, H. L. Kyle, and E. R. Major, 1987: Solar Irradiance Measurements by the Nimbus-7 ERB Experiment: An Update of 100 Months, in *Solar Radiative Output Variation, Proceedings of a Workshop of November 9-11, 1987 at NCAR, Boulder, Colorado*, edited by P. Foukal, pp. 189-194, Cambridge Research and Instrumentation, Cambridge, MA.

Hickey, J. R., B. M. Alton, H. L. Kyle, and D. V. Hoyt, 1988: Total Solar Irradiance Measurements by ERB/Nimbus-7: a review of nine years, *Sp. Sci. Rev.*, **48**, 321-342.

Hickey, J. R., R. G. Freiden, and D. J. Brinker, 1991: Report on an H-F Type Cavity Radiometer After Six Years Exposure in Space Aboard the LDEF Satellite, *Metrologia*, **28**, 269-273.

Hickey, J. R., D. J. Brinker, and P. Jenkins, 1992: Studies of Effects on Optical Components and Sensors: LDEF Experiments AO-147 (ERB Components) and S-0014 (APEX), An Article in LDEF-69 Months in Space, Second Post-Retrieval Symposium, NASA Conference Publication 3194 (Part 4), 1375-1388.

Hoyt, D. V., H. L. Kyle, J. R. Hickey, and R. H. Maschhoff, 1992: The Nimbus-7 Total Solar Irradiance: A New Algorithm for its Derivation, *J. Geophys. Res.*, **97**, No. A1, 51-63.

Hoyt, D. V. and H. L. Kyle, 1990: An Alternative Derivation of the Nimbus-7 Total Solar Irradiance Variations, in *Proceedings of the Conference on the Impact of Solar Variability on Climate*, edited by K. Schatten and A. Arking, *NASA Conference Publication, NASA CP-3086*, 293-300.

Jacobowitz, H., H. V. Soule, H. L. Kyle, F. B. House, and the ERB Nimbus-7 Experiment Team, 1984: The Earth Radiation Budget (ERB) Experiment: An Overview, *J. Geophys. Res.*, **89(4)**, pp. 5021-5038.

Lee, III, R. B., B. R. Barkstrom, E. F. Harrison, M. A. Gibson, S. N. Natarajan, W. L. Edmonds, A. T. Mecherikunnel, and H. L. Kyle, 1988: Earth Radiation Budget Satellite Extraterrestrial Solar Constant Measurements: 1986-1987 Increasing Trend, *Adv. Space Res.*, **8(7)**, 11-13.

Lee, III, R. B., M. A. Gibson, N. Shivakumar, R. Wilson, H. L. Kyle, and A. T. Mecherikunnel, 1991: Solar Irradiance Measurements: Minimum Through Maximum Solar Activity, *Metrologia*, **28**, 265-268.

Major, E. R., J. R. Hickey, H. L. Kyle, B. M. Alton, and B. J. Vallette, 1988: Nimbus-7 ERB Solar Analysis Tape (ESAT) User's Guide, NASA RP-1211, NASA/GSFC, Greenbelt, MD, 89 pages.

Predmore, R. E., H. Jacobowitz, and J. R. Hickey, 1982: Exospheric Cleaning of the Earth Radiation Budget Solar Radiometer During Solar Maximum, Paper Presented at *Proceedings of Society of Photo-Optical Inst. Eng. (SPIE)*, (Tech. Symp. East, Arlington, VA, May 3-7, 1982), **338**, pp. 104-113.

Smith, E. A., T. H. Vonder Haar, and J. R. Hickey, 1983: The Nature of the Short Period Fluctuations in Solar Irradiance Received by the Earth, *Climate Change*, **5**, pp. 211-235.

Soule, H., 1983: Nimbus-6 and -7 Earth Radiation Budget (ERB) Sensor Details and Component Tests, NASA TM-83906, NASA/Goddard Space Flight Center, Greenbelt, MD, 73 pages.

Willson, R. C., H. S. Hudson, C. Frohlich, and R. W. Brusa, 1986: Long-Term Downward Trend in Total Solar Irradiance, *Science*, **234**, 1114-1117.

Willson, R. C. and H. S. Hudson, 1988: Solar Luminosity Variations in Solar Cycle 21, *Nature*, **332**, 810-812.

Willson, R. C. and H. S. Hudson, 1991: The Sun's Luminosity Over a Complete Solar Cycle, *Nature*, **351**, 42-44.

APPENDIX A
A BRIEF HISTORY OF CHANNELS 1-9

Analysis of solar channels 1 through 9 has shown that they do respond to the presence of large spot groups on the Sun. This has been observed in both Nimbus-6 and Nimbus-7 ERB solar measurements. However, all of the major long-term trends in their signals are due to instrument-related phenomena and are not directly due to changes in the solar radiation. Immediately after turn on, the behavior of these nine sensors agreed well with their preflight calibration tests. However, changes in the sensors began promptly and have continued throughout the life of the sensors.

The instrument electronics have proven quite stable and the major perturbations arise from changes in the optics, spectral filters, and in the measurement geometry. A major problem for channels 1, 2, and 4-9 has been the variable transmissivities of their outer Suprasil-W windows. The transmissivity variations are larger in the ultraviolet than in the near infrared. Variation over the years in the off-axis position of the Sun during the measurements is also a problem. But channel 1-9 do contain information about short-term (say 30 days) solar irradiance changes in specific spectral bands (Hickey et al., 1982). However, little interannual information appears to be decipherable from their signals. Even the short-term signals are, at times, confused in the present dataset due to the lack of correction for off-axis measurements.

Explicit inflight calibration for solar channels 1-9 does not exist. However, channels 1 through 3 can be directly compared with channel 10c to determine any changes in the calibration. These channels are equipped with an electrical calibration that inserts a precision voltage staircase at the input to the entire signal conditioning stream. While the electronic calibration cannot be used to infer changes in the sensor or optics characteristics, it does monitor the stability of the associated electronic circuits. Analysis of the electronic calibration data has yielded no abnormalities.

A picture of the ERB instruments is shown in Figure A1. The solar channel subassembly appears on the right. Channels 1, 2, 5, and 7 are on the right side, and channels 3, 4, 6, and 8 are on the left side of the subassembly, while channels 9 and 10 are in the middle. In flight, the solar panel faces forward, in the direction of the satellite's motion, and the Sun is observed once per orbit, near the Earth's South Pole, at satellite sunrise. The subassembly was originally designed to rotate 20° to either side in order to track the seasonal changes in the sunrise position relative to the satellite's orbit. However, for protection, during launch and from the initial outgassing from the satellite, a cover door was later added on the right side. Since November 16, 1978, this door has been open as shown. The door decreases the viewing range on the right side by a degree or so.

Since the off-axis angle response function of channel 10c is known, its measurement range was originally thought to extend to about 24.7°. However, on the right, the door reduces this range to 22.2° (see Section 3.3). On the right side the measurement ranges of the other channels, with respect to channel 10 are: 1° less for channels 1, 2, 5, and 7; 1° more for channels 3, 4, 6, and 8; and the same for channel 9. However, the off-axis response functions of channels 1-9 have not been well analyzed. Measurements near the edge of the unrestricted field-of-view only became important near the end of the experiment when the measurement angle to the Sun (the β angle) first approached and then exceeded 20°. This first occurred during the summer of 1991 (refer to Figure C5).

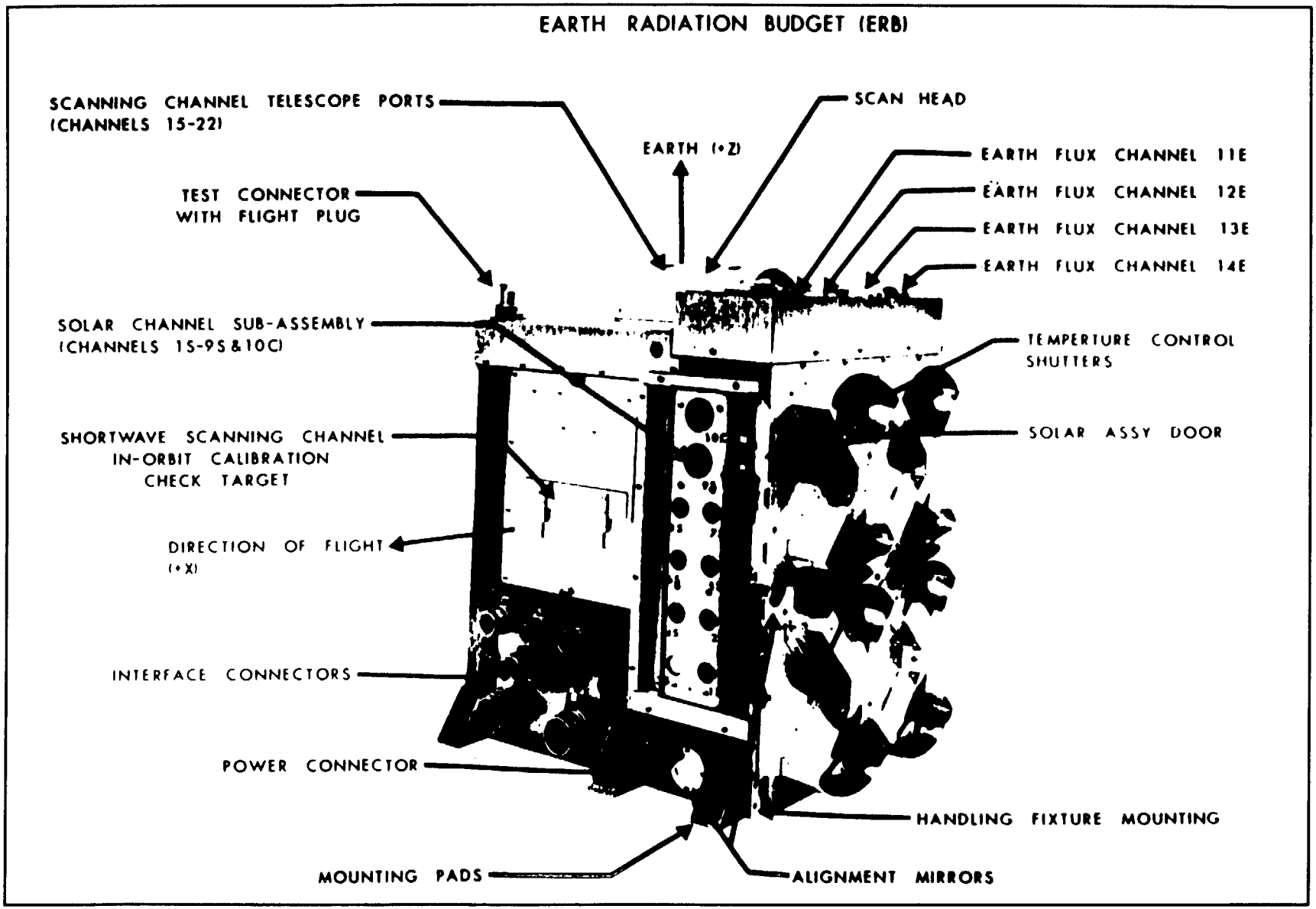

Figure A1. The Nimbus-7 Earth Radiation Budget Instrument. As shown, the solar channel subassembly is on the right, and the Earth-viewing sensors are on the top.

The degradation with time of solar channels 1 through 9 for the first 8 months of flight is depicted in Figure A2, while Figure A3 summarizes the spectral bands to which each channel is sensitive (see also Table 1). The probable cause of the observed behavior shown in Figure A2 has been discussed by Predmore et al. (1982). Channels 1, 2, and 4 to 9 have two Suprasil W windows (Figure A4); an outer one to block energetic particles and an inner one to reduce variations in the net thermal radiation incident on the detector chip (Hickey, 1973; Soule, 1983). Channels 4 through 9 also have spectral filters between these two windows to restrict the wavelength of the transmitted light (Table 1 and Figure A3). Channel 3 is open to space; it has no windows. The rapid degradation of the solar channels after observations started on November 16, 1978, is attributed to transmission loss originating from the growth on the windows of an organic film by photolytic polymerization. The organic contaminants probably came from both prelaunch films on the windows plus outgassing from the instrument and satellite after launch. But the interaction with sunlight was required to cause noticeable transmission loss. The wide pass band (0.2 to 3.8 μm) channels 1 and 2 are identical in construction but channel 1 remained covered except for a very few observations during the first 8 months of operation. During this period, channel 2 degraded but channel 1 did not. Also observe that the darkening occurred chiefly in the ultraviolet. The transmission loss is large at short wavelengths (channels 7-9, 0.2 to 0.46 μm) but small in the near infrared (channel 5, 0.7 to 2.8 μm). The LDEF experiment results verify the large loss of transmissivity in the far UV (see Appendix B).

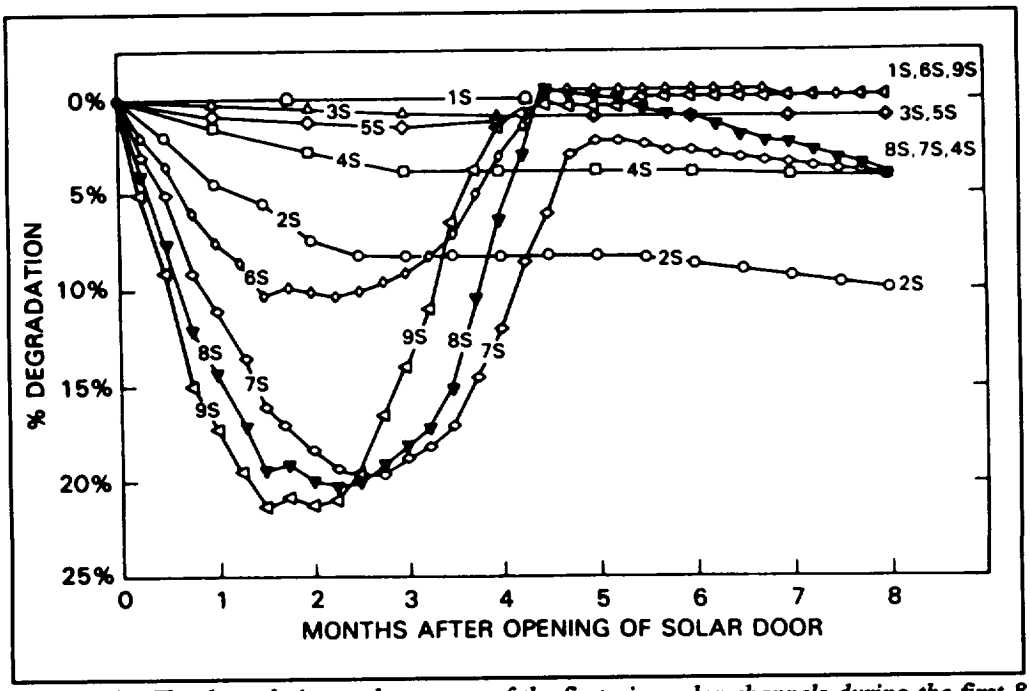

Figure A2. The degradation and recovery of the first nine solar channels during the first 8 months (Jacobowitz et al., 1984).

After degrading rapidly during the first 6 weeks, the shortwave channels 6-9 then began to recover. The satellite was launched near the start of the maximum activity portion of the approximately 11-year long sunspot cycle. Further, the solar telescope was mounted in a forward facing, ram position. This accentuated the sensors' interaction with the rarefied, but chemically active atmospheric gases. The atmosphere, at the Nimbus-7 altitude of 950 km, is much denser at solar maximum than at solar minimum. The chemical composition also changes. At solar minimum, the chief gas at this altitude is helium with some atomic hydrogen. However, at solar maximum the amount of atomic oxygen present increases by over a factor of 100 and becomes a major component. Predmore et al. (1982) assume that

reactions between the atmospheric O, O+, H, and H+ and the organic contaminant film formed gaseous products such as CO, CO_2, and H_2O that evaporated and removed part or all of the film. Note, however, that channels 7 and 8 then started to degrade again while channels 2 to 5, which include longer wavelengths, showed no marked recovery.

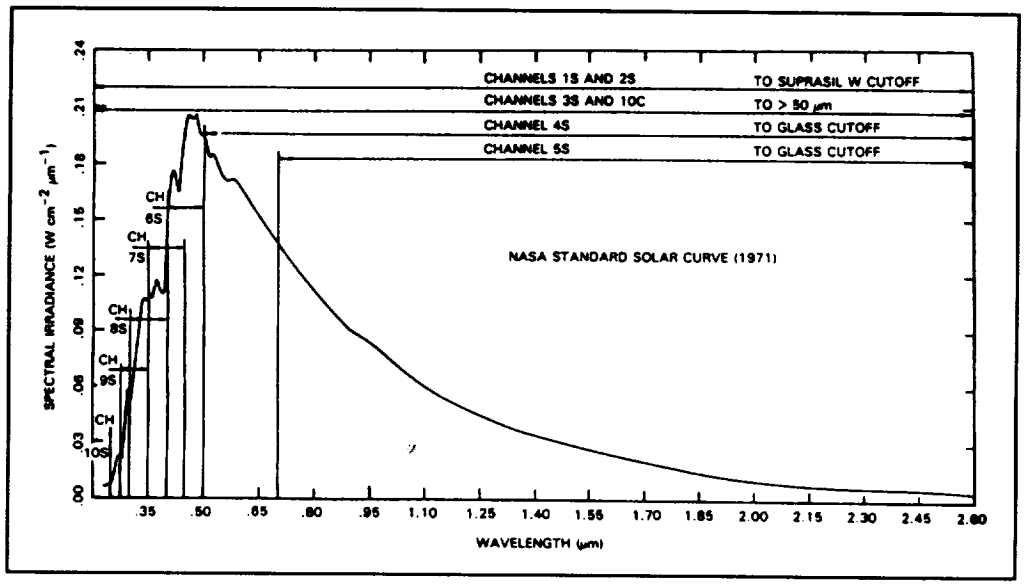

Figure A3. The spectral pass bands for solar channels 1-9 on the Nimbus-6 and -7 ERB instruments. The pass band for channel 10c on the Nimbus-6 ERB is also shown. The NASA standard extraterrestrial solar curve (1971) is also shown.

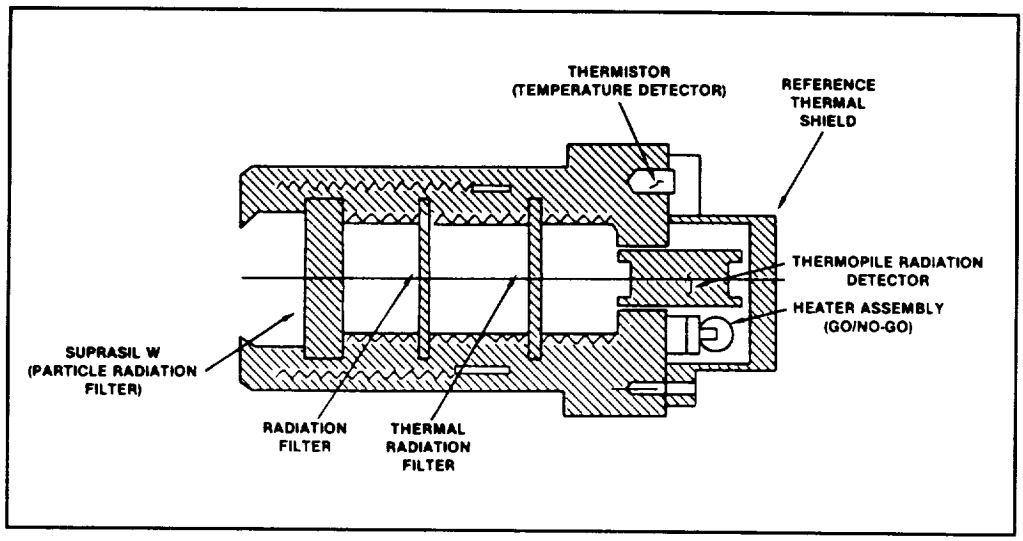

Figure A4. Typical solar channel schematic. The front windows on many of the channels, 1 and 2 for instance, were 2 mm thick, but those for channels 4 and 5 were 4 mm thick. All of the rear window (thermal radiation blockers) were 2 mm thick. Channel 3 had neither windows nor radiation filter.

The long-term behavior of the first 9 solar channels is shown in Figure A5 for the period November 1978 through 1990. The quiet Sun period runs essentially from 1984 through 1987 with a moderate upturn of solar activity in 1988. The Sun was quite active in 1989 and 1990. The various channels show considerable individuality in their behavior, but there is an overall pattern. There is a steady decline in sensor response through 1987, then in 1988 there is a partial recovery for all channels except channels 1 and 7. This recovery can probably be attributed to the increase in atomic oxygen at the spacecraft altitude. But it is not clear why the recovery starts in the spring of 1987 for the shortwave channels 6, 8, and 9 and in the fall for channels 2, 4, and 5 which extend into the near infrared. Note that channel 9, and to some extent channel 6, show signals larger than on the first day. This is probably attributable to either or both shifts in the spectral filters or the development of pinholes in the filters. The steady degradation of channel 7 may be related to the fact that its spectral filter contains lead. A decrease in the transmissivity of the spectral filter is suspected (see Appendix B). The same can be said for channel 8.

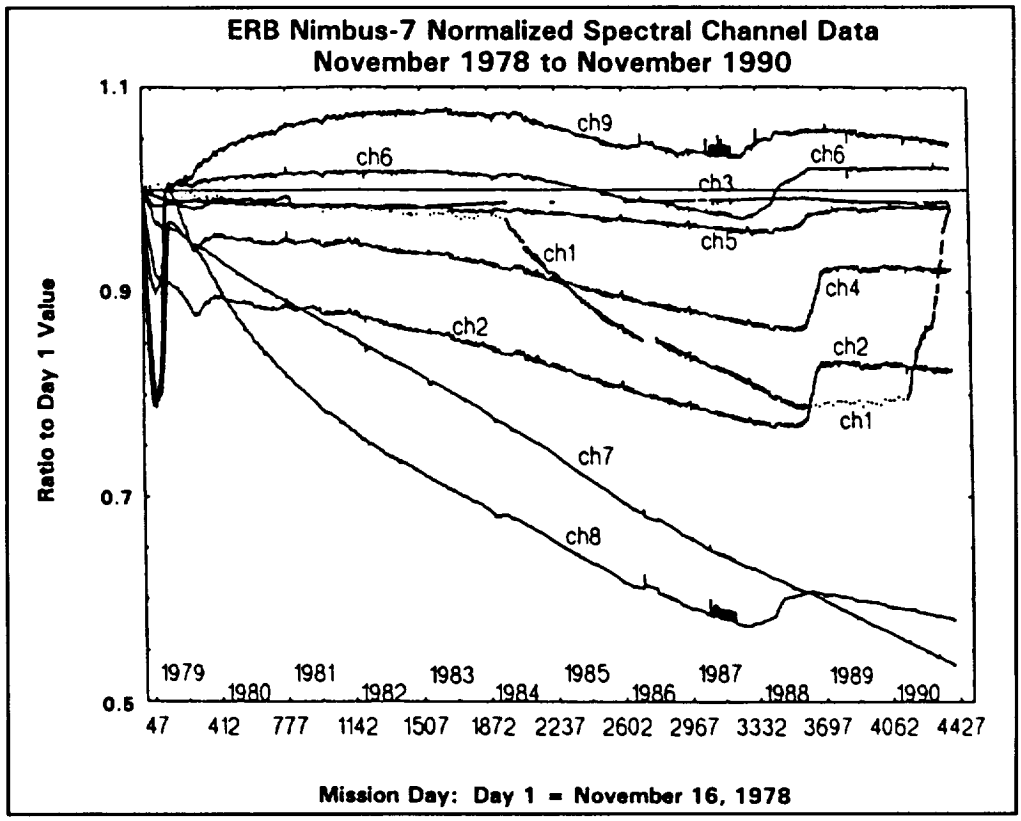

Figure A5. Changes in the responses of solar channels 1 to 9 relative to day 1 (November 16, 1978) for the period November 1978 to 1990.

Predmore et al. (1982) also examined the Nimbus-6 shortwave solar measurements (channels 6-9) from July 1975 through 1979. The Nimbus-6 was launched into a circular orbit with an altitude of 1100 km, during the quite Sun portion of the solar cycle. Slow degradation was noted in all channels through 1977. A pause occurred in 1978; this undoubtedly was due to the slow start of the cleansing process as the solar activity started to increase. Then a fairly rapid recovery occurred in 1979, when the solar activity was high. Channel 6 completely recovered, while channel 9 registered larger signals than in July 1975. Only a partial recovery was observed in channels 7 and 8. The qualitative behavior of these channels appears similar in both Nimbus-6 and -7 experiments. The quantitative differences can chiefly be ascribed to: Nimbus-7 being a dirtier satellite than Nimbus-6, the difference in the solar cycle at launch, and the difference in satellite altitudes.

In Figures A2 and A5, the behavior of channel 1 is governed by the opening and closing of its cover. This cover is so designed that when channel 1 is open, channel 3 is covered and vise versa. In Figure 5, the dotted portions of the curve for channels 1 or 3 indicate that that channel is chiefly closed and is opened only for periodic checks. Channel 1 was opened in the spring of 1984 and remained open, with a break in 1986, until the fall of 1988. Thus, channel 1 was closed just at the time a recovery phase should have started. When it was re-opened in the spring of 1990, a sharp recovery occurred.

Shortly after launch, calibration coefficients were fixed for channels 1-9 and these have been used, unchanged ever since. The temperature sensitivity correction factors are given by

$$S(T) = S_v[1 + A(T - L)] \qquad \textbf{(A1)}$$

where

S_v = Channel sensitivity in a vacuum at 25°C (22°C) for channel 10c only) in counts per watts/m^2 (see Table A1).

A = Temperature sensitivity at 25°C (22°C for channel 10c only) in °C^{-1} (see Table A1).

T = Temperature in °C.

L = Reference temperature: Channels 1 through 9: 25°C, Channel 10c: 22°C.

The channel sensitivity (S_v) was determined from laboratory measurements at an average temperature (L) for the calibrations (Hickey, 1985).

Table A1. Channel Coefficients

Channel	S_v	A
1	1.299	0.0007
2	1.275	0.0008
3	1.214	0.0008
4	1.719	0.0007
5	2.424	0.0006
6	6.931	0.0007
7	9.588	0.0003
8	12.715	-0.0004
9	30.170	-0.0011
10c	1.3013	0.000524

The uncorrected net solar irradiance:

$$R = [V_o - \frac{1}{2}(V_- + V_+)] / S(T) \qquad \textbf{(A2)}$$

where

V_o = Solar channel detector output in counts at t_o, where t_o = time of minimum solar elevation (i.e., when the telescope is pointing most directly at the Sun).

V_- = Solar channel detector output in counts at t_o - 13 minutes.

V_+ = Solar channel detector output in counts at t_o + 13 minutes.

S(T) = Temperature sensitivity correction factor.

Adjustment of channel 10c for reflectance. (Note: This correction is applied to channel 10c only):

$$R_{10c} = U_{10c} * 0.998 \qquad \textbf{(A3)}$$

U_{10c} = Unadjusted channel 10c net solar irradiance.
R_{10c} = Adjusted channel 10c net solar irradiance.

All of the irradiances are then normalized to the mean Earth flux distances. The center time (t_o) of the solar measurements is taken as the center of the local minimum in channel 5 (Figure A6). If this local minimum cannot be found, t_o is set to the time when the southern terminator is crossed. When the channel 10c data were reprocessed, t_o was redetermined as the time of the maximum in the channel 10c counts.

The present irradiance values in the ERB SEFDT archive were determined using these equations. The analysis shown in Figures A1 and A4 were based on the irradiances thus derived. The final channel 10c irradiances are calculated using the information on the SEFDT. This document discusses the new calibration equation used to calculate channel 10c irradiances. Similar equations are not available for channels 1-9. If they existed, such equations would have to account for:

1. Changes in sensitivity S. This depends on:
   - Time dependent changes in the transmissivity of the optics.
   - Changes in S due to changes in the sensor chip or its cover paint.
   - Any changes in the filter pass bands.

2. Correction for off-axis observations.
   - The off-axis angular response function of each channel would have to be determined (see Appendix D).

3. An improved determination of the Earth/Sun distance at the time of the observation.

Although modifications (2) and (3) are fairly straightforward, we know of no way to correct the sensitivity function for channels 4 through 9. Channels 1-3 could be corrected by comparison with channel 10c, but this would merely yield noisier copies of the channel 10c results.

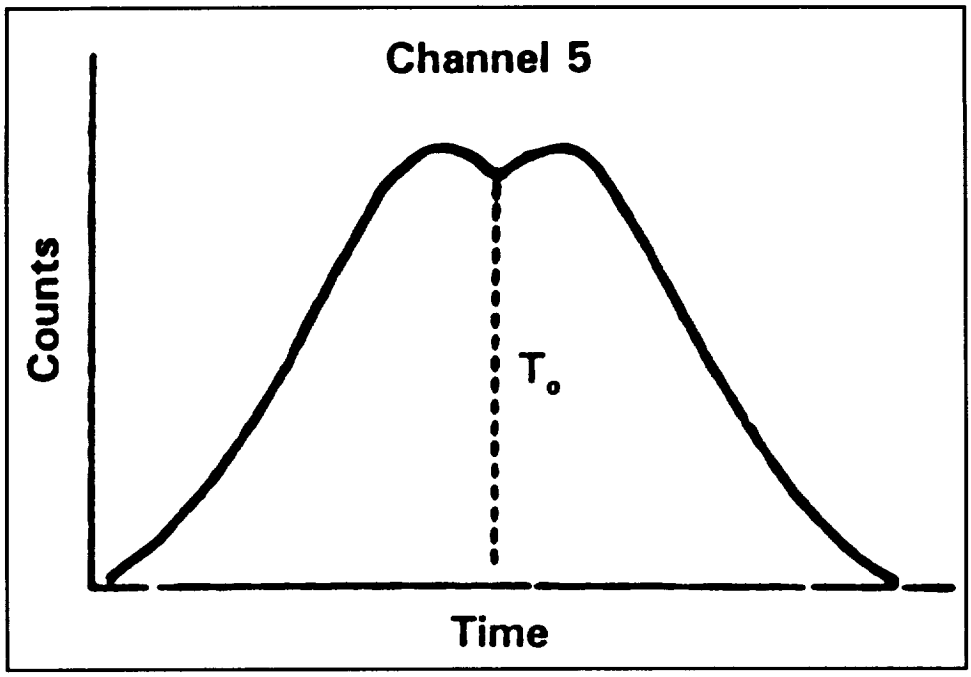

Figure A6. The time of minimum solar elevation, T_o, is associated with the median of the possible smallest count values (n/2) in the central local minimum of channel 5 (i.e., if the smallest count values occur eight times, T_o will be the time associated with the fourth occurrence). If no time of minimum solar elevation was found, T_o was set to the southern terminator time for selection of solar data records.

APPENDIX B
RECOVERED ERB-TYPE SENSORS FROM THE LDEF SATELLITE

The Long Duration Exposure Facility (LDEF) satellite was placed into orbit by the Space Shuttle *Challenger* on April 1, 1984, and retrieved by the *Columbia* on January 12, 1990. The basic purpose of the flight was to expose various equipment and materials to a low Earth orbit environment for a period to see how they were affected. The satellite was placed in a nearly circular orbit of 474 km altitude with an inclination of 28.5° to the Equator. The launch occurred at the start of the quiet Sun period of the solar cycle and the original plan was to recover the satellite after 1 year. In fact, the actual recovery occurred nearly 6 years later. Thus, the materials were affected by the changes in the Earth's upper atmosphere at the start of the excited Sun period in 1989.

Two of the experiments on the LDEF contained Nimbus ERB-related sensors (Hickey, 1991; Hickey et al., 1992). The Passive Exposure Earth Radiation Budget Experiment Components (PEERBEC) experiment included the flight spare sensors from the ERB experiments on the Nimbus-6 and -7 satellites. The 10 solar sensors (Table 1 in Section 1) were mounted in LDEF tray B-8. The Nimbus-7 cavity radiometer, channel 10c, was not included in this group. There was no flight spare channel 10c. A cavity radiometer, qualitatively similar to channel 10c, was part of the Advanced Photovoltaic Experiment (APEX). The cavity sensor in tray E-9 was on the leading (ram) edge of the satellite. The B-8 tray was 30° off the ram direction, but the solar block was tilted to face forward.

The four Earth flux sensors were mounted in tray G-12 looking earthward. The orbital decay to lower altitudes, coupled with the changes in the solar radiation and in the Earth's upper atmosphere during solar maximum caused the LDEF to be exposed to a broader range of space environmental effects than had been anticipated.

The cavity radiometer experienced no measurable degradation during its nearly 6 years in low Earth orbit (Hickey et al., 1991). Initial results show that the electrical properties of the thermopile and heater circuits were unaffected. There was a slight visible change in the painted surface of the cavity, possibly caused by atomic oxygen impingement late in the mission. This apparently has not affected the agreement with ground-based reference standards. Intercomparisons to date indicate agreement of approximately 0.1% but with an uncertainty at this same 0.1% level. Under intense illumination, it could be seen that the interior cavity paint (Z302 specular black paint) exhibited some "puckering." The Z306 baffle paint appeared unaffected. Measurements of the cavity reflectances were also performed using a laser source and a shaped pyroelectric detector. This test was done at the World Radiation Center in Davos, Switzerland in October 1990. Initial results indicated reflectance values of:

250 ± 80 parts per million (ppm) for the APEX/LDEF cavity
270 ± 80 ppm for a new cavity of the same type

It appears that the change in the cavity paint has not affected the performance of the sensor within the level of uncertainties of these tests. Thus, it is possible that the LDEF cavity radiometer was unaffected by its in-orbit history down to the 0.01% level.

The other solar channels did suffer noticeable degradation in the transmissivity of the Suprasil W windows plus changes in some spectral filters. The spectral transmittance of the fused silica windows was measured. A witness sample, from the same boules and of the same thickness as each flight sample was available from the original ERB repository. The transmittance of the 2 mm thick front windows of the matching channels 1 and 2 over the range from 200 to 400 nm is shown in Figure B1. The transmittance

of the witness sample is at the top of the plot. The two LDEF front windows degraded in the UV by close to 11% at 200 nm and lesser amounts out to 330 nm. A 2 mm thick sample was also included in the APEX experiment. This sample, which was contaminated, has suffered a much larger degradation over the whole UV range. The 4-mm-thick front window on channel 5 showed slightly more transmittance loss than did the 2-mm windows on the other channels. Only the 4-mm window in channel 5 could be examined as the one in channel 4 was lost. Since there was no important transmittance loss in the near infrared (wavelengths >0.7 μm), the examined channel 5 was not bothered by this problem. The rear windows also showed some transmittance losses but they were not affected as much as the front windows.

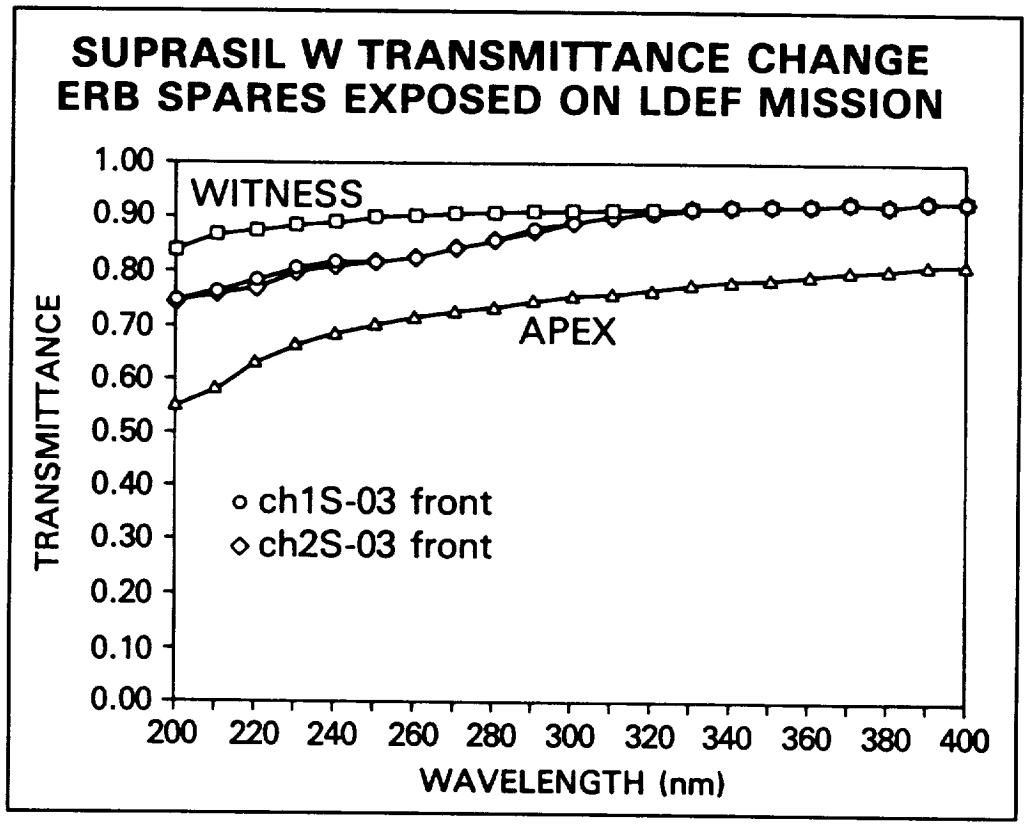

Figure B1. Measured postflight transmittances for the 2-mm thick front windows on ERB channels 1 and 2 in the PEERBEC experiment on the LDEF satellite. The top curve shows the transmittance of a similar window which remained in the laboratory. The bottom curve is from a similar window in the APEX experiment on the LDEF. It received more contamination than did the PEERBEC windows.

The behavior of the spectral filters varied when the spectral transmittances, preflight and postflight, were compared. Filter 6S (0.398 to 0.508 μm) showed very little change, except that the band did broaden slightly. Filter 7S (0.344 to 0.46 μm), on the other hand, exhibited a decay in transmittance and a narrowing of the band. Channels 8 (0.30 to 0.41 μm) and 9 (0.275 to 0.360 μm) also showed a decrease at the wavelengths of maximum transmittance. However, channel 9 also showed a small band shift toward longer wavelengths. The colored glass filters in channels 4 and 5 showed no important preflight to postflight spectral changes. Of course, the results from the LDEF experiment can only be applied qualitatively to the Nimbus-7 ERB.

APPENDIX C
THE CHANNEL 10C TEMPERATURE HISTORY AND THE
NIMBUS-7 ERB OPERATIONS CALENDAR

Although the channel 10c cavity radiometer is reasonably stable, it does respond at a low level to its environment. The sensor temperature appears to be the most important environmental parameter which affects the sensor readings. Figure C1 shows the sensor temperature variations from start of data taking, November 16, 1978, through the loss of Sun on January 25, 1993. The observed temperature variations mirror the major changes in the satellite environment near and inside the ERB instrument; major events in the ERB instrument history are summarized in Table C1. During the first several years, the ERB instrument was turned on and off frequently. Normally the instrument was on for 3 days and off on the fourth day. This caused the 3° to 4°C temperature range shown for the first few years. On September 11, 1983, the ERB was put on a full-time on schedule but this was interrupted during the summer and fall of 1984, in the spring of 1986, and in the spring and summer of 1987. The problems observed during these special operations periods are also discussed in Section 4.4.3.

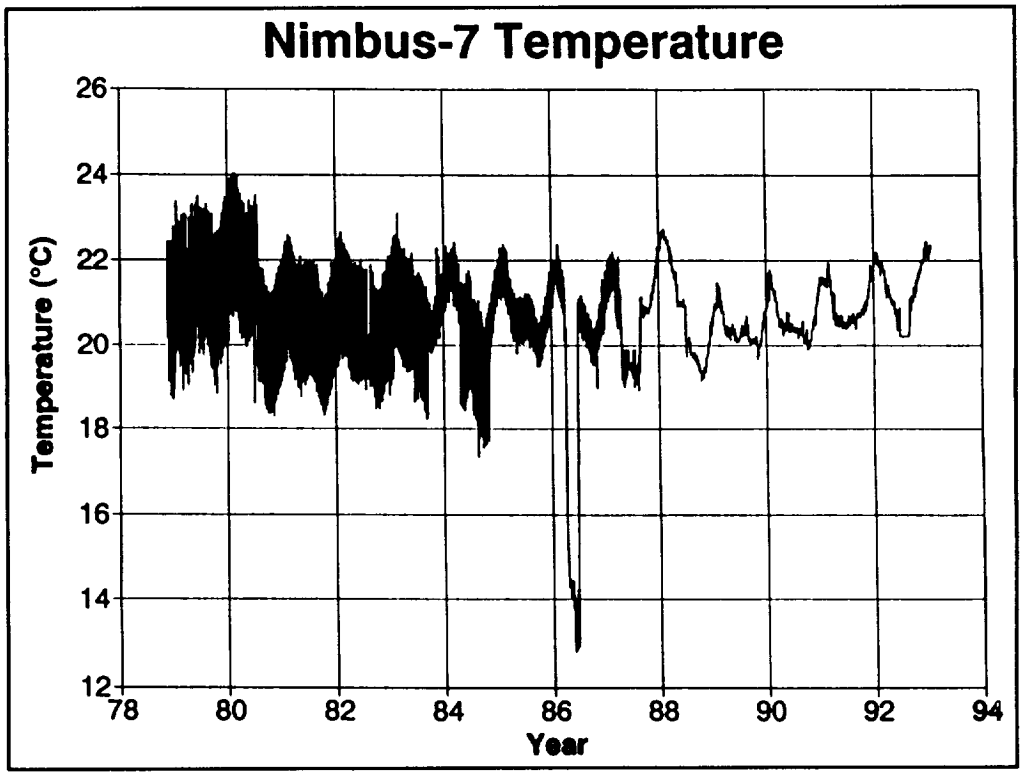

Figure C1. The temperature history of solar channel 10c. The plotted temperatures correspond to measurements that passed all quality checks. Thus since the Sun was out of view in July and August 1992, no temperature data are shown.

Prominent in Figure C1 is the annual temperature cycle which can be associated with the yearly cycle in the Earth to Sun distance. Due to the eccentricity of the Earth's orbit, the solar irradiance incident on the front of the ERB instrument is 6.7% larger in early January than in early July. This apparently causes, in most years, the sensor temperature to be about 1.5°C higher in January than in July. The January peak is absent in 1979. This is undoubtedly due to variations in the ERB scanner's operating schedule for the period December 10 through April 13, 1979 (see Table C1). Note the approximately

1.5°C drop in the temperature of the solar sensor in July 1980 when the scanner motor was permanently turned off.

Table C1. Major ERB Events

Date	Event
November 16, 1978	Initial turn on. ERB in 3-day-on/1-day-off power sharing schedule with other Nimbus-7 experiments. From time to time, the schedule varied somewhat.
December 10, 1978 through April 13, 1979	ERB scanning activity is curtailed because it interfered with the short-lived LIMS experiment which studied trace gases in the stratosphere. 12/10 to 12/30/78 — Scanning on 2-day-on/2-day-off schedule; WFOV and solar on 3-day-on/1-day-off schedule 12/30 to 3/9/79 — Further curtailment; no scanning near the north pole, nor in the northern hemisphere at night 3/10 to 3/31/79 — global scanning, 2-day-on/2-day-off schedule 4/1/ to 4/13 — ERB on 1-day-on/1-day-off mode but no scanning
April 14, 1979	ERB and scanner returns to 3-day-on/1-day-off schedule, but with occasional variations
June 22, 1980	Scanner chopper wheel stops. This terminates useful scanner measurements. Efforts to restart the chopper continued through July 18. The noise in channel 10c decreased noticeably after July 18.
September 11, 1983	ERB put on full-time on schedule
April 18, 1984	ERB returns to 3-day-on/1-day-off schedule
October 28, 1984	ERB back on full-time on schedule
April 9 to June 23, 1986	No Earth flux measurements, but ERB was on for 20 minutes on most orbits for solar measurements. This allowed the CZCS experiment additional power for its end-of-life program
April 22 to August 20, 1987	Earth flux measurements taken only on alternate days to conserve power. On the off days, ERB was on for 30 minutes per orbit to make solar measurements; however, these measurements were noisy
August 24, 1987	ERB back on full-time on schedule
September 24-28, 1989	ERB sensor data blanked out by a temporary electronics problem possibly caused by a cosmic ray. Normal data transmission recommenced on the afternoon of September 28.
January 4-11, 1992	The ERB solar telescope refused to move from $\gamma = 14°$ to 15° in order to track the Sun, but it would move in the other direction. Several tests were made and finally on January 11, the telescope moved to $\gamma = 15°$. The telescope has moved normally since that time.

Table C1. Major ERB Events	
Date	Event
January 15-23, 1992	Some of the ERB sensor data became meaningless, then it all became saturated. Data alternated between meaningless signals and saturation. This was probably caused by energetic particles damaging the electronic circuits. Normal operation resumed on January 23.
June 17-September 2, 1992	The Sun was not clearly visible during this period. The solar telescope can move only over the range, $\gamma = \pm 20°$. The precession of the orbit over the years combined with the seasonal progression of the Sun relative to the satellite moved the Sun out of the unrestricted field of view of channel 10c during this period.
January 25, 1993	The continued precession of the orbit again moved the Sun out of the unrestricted field of view of channel 10c.
February 9, 1993	ERB electronics turned off.

The other instruments on the Nimbus-7 affected the ERB solar measurements chiefly by imposing a power-sharing operations mode. Measurements were lost when it was the ERB's turn to be turned off. In addition, after turn on, it required a few hours for the sensor to warm up to normal operating temperatures. The calibration equation 1 does not properly treat measurements made during this warming period and, hence, some additional measurements are rejected as noisy. Smith et al. (1983) suggested that a modified calibration equation might be developed which would properly handle much of the presently rejected data. A nonlinear temperature correction to the calibration coefficient (k_{cal} in Eq.(1)) was proposed. This proposal was never evaluated in detail. However, the special operations period in the spring of 1986 forced a partial re-evaluation of the problem. During this period, the ERB was turned on for only 20 minutes per orbit so that a solar measurement could be taken. Little temperature change occurred during these 20 minutes so that a bias offset could be used in conjunction with Eq.(1) to evaluate the measurements (Section 4.4.3).

A lesser power problem occurred in the spring and summer of 1987, when the ERB went into a 1-day-on/1-day-off mode of operation. On the off-days, there was sufficient power to turn on the ERB for 20 or 30 minutes per orbit for solar measurements. On these days, the sensor always appeared to be in a rapidly warming or cooling phase, thus, the present calibration procedure yields a noisy product which is not used. Fortunately, good measurements were obtained during the alternate full-time-on days. Noisy products also occur for short periods at the beginning and end of the 1986 special operations period and after turn-on on January 23, 1992 (see Table C1).

The Scanning Multichannel Microwave Radiometer (SMMR) was situated directly over the ERB instruments. Its operation schedule is also mirrored in the ERB channel 10c temperature record. However, the direct SMMR-driven temperature variations did not noticeably affect the quality of the ERB solar measurements. They are discussed here as background information.

Expanded ERB temperature records for 1984, 1987, and 1988 are given, respectively, in Figures C2 to C4. In the spring and fall of 1984, the ERB was on full-time, but from April 18 through October 27 it was on a 3-day-on/1-day-off schedule. In the May to September period, the increased Earth-to-Sun distance results in a decreased irradiance on the solar panels from which the satellite draws its power. Thus, at this time, power rationing among the several Nimbus-7 experiments is most needed. Over time, various instruments were turned off and this allowed the ERB to stay on longer. The SMMR normally ran on a 1-day-on/1-day-off schedule. The day-to-day heating and cooling of the SMMR accounts for the

approximately 1°C jitter in the temperature of the ERB solar sensor at the start and end of the year. It also accounts for part of the 3°C temperature variations observed during the ERB power sharing period. During normal power sharing, the SMMR would be on during the second ERB on-day and again on the ERB off-day.

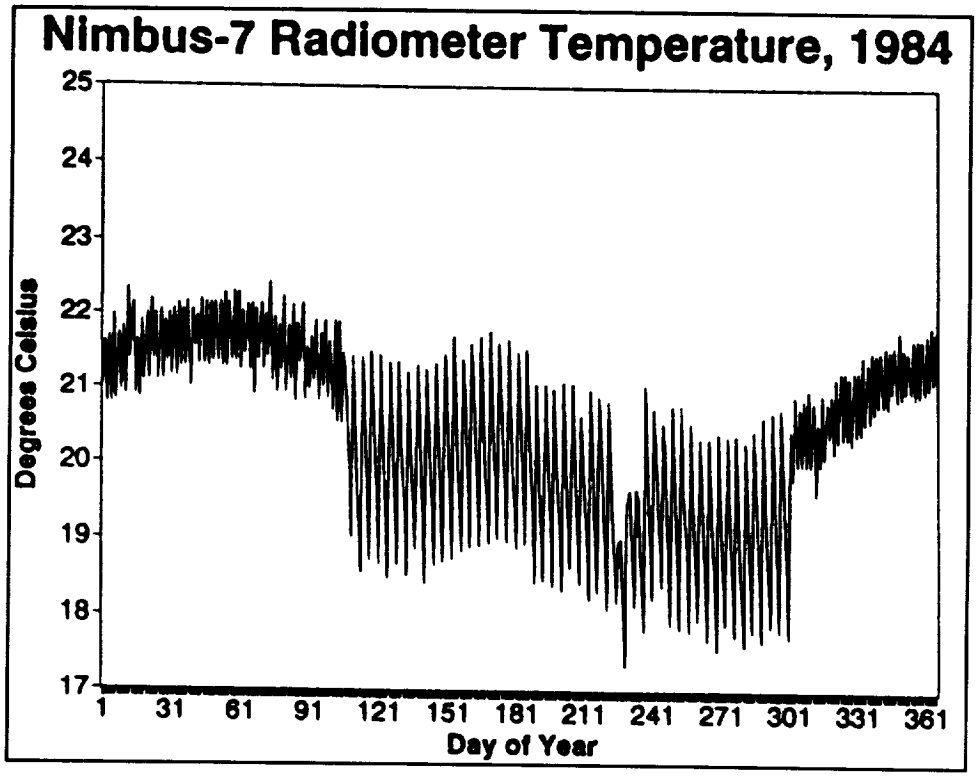

Figure C2. Channel 10c temperatures for the year 1984. The 3°C temperature variations in the center show the heating and cooling of the sensor due to the 3-day-on/1-day-off operating schedule in mid-year. The 1-day-on/1-day-off schedule of the neighboring SMMR instrument cause the 1°C variations at the beginning and end of the year.

The graph for 1987, Figure C3, shows the ERB special operations period in the middle of the year. The temperatures during the rejected 30 minutes on per orbit days were 16° to 17°C and are not plotted on either Figures C1 or C3. Due to a suspected, developing mechanical fault, the SMMR stopped scanning and went into a nonscanning "stare" mode on August 21. This reduced the power demand and allowed both SMMR and ERB to remain on full time. This also removed the 1°C day-to-day temperature jitter at the ERB solar sensor.

The history for 1988 is shown in Figure C4. In mid-spring, one of the remaining SMMR channels was turned off and this caused the ERB channel 10c temperature to drop by about 0.6°C. Early in July the SMMR was turned all the way off and this produced another 1.0°C drop in the channel 10c temperature.

The satellite environment had a strong affect on the ERB solar measurement program. Some 18% of the time useful data products were not produced. No measurements were made for about 13% of the time while about 5% of the measurements were made when the sensor was not in thermal equilibrium. It is probable that the calibration equation could be modified to handle some of these nonequilibrium measurements, but it is not clear that the additional effort would be scientifically rewarding. Both the ERB scanner (see also Section 4.2) and the nearby SMMR experiment did slightly perturb the temperature

of the solar sensor as did variations in the Earth-to-Sun distance. But none of these small perturbations noticeably affected the measurement accuracy. On the other hand, the multiple experiments on the Nimbus-7 resulted in power rationing. This in turn caused the Nimbus ERB to be frequently turned off and on. This caused missed measurement opportunities followed by some noisy measurements taken while the sensor warmed to normal operating temperatures.

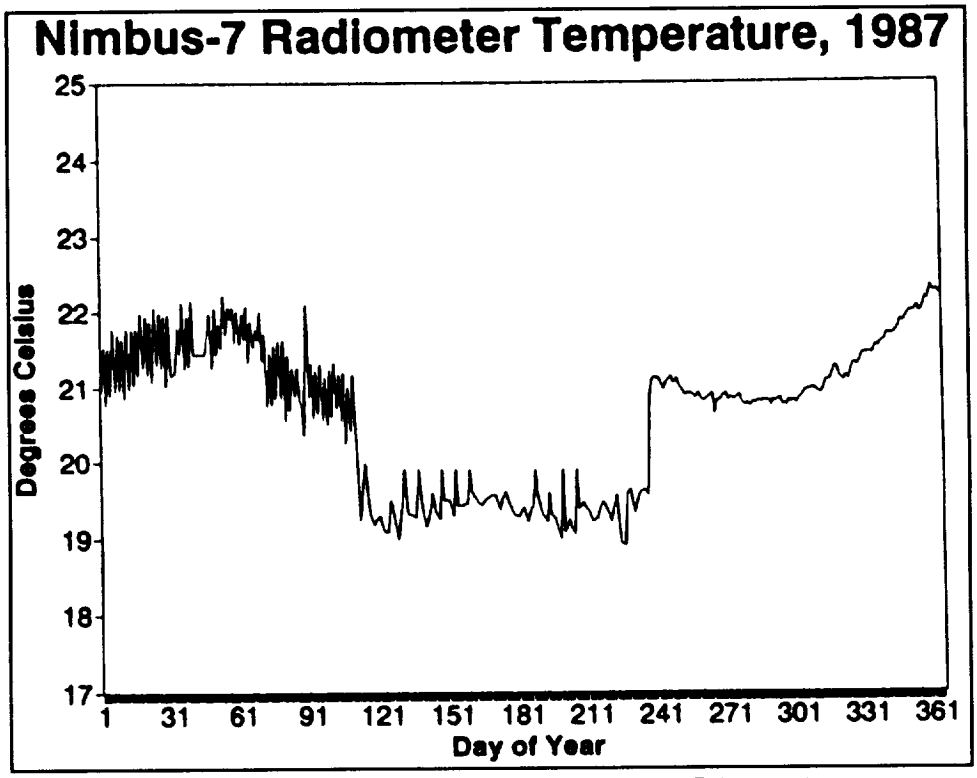

C3. Channel 10c temperature variations in 1987 (see text).

Both the sensor and its electronics have proven quite robust. In the later years, two electronic and one mechanical problems are listed in Table C1, but these were all short-lived, and left no apparent after affects. The electronics problems were probably caused by energetic particles damaging solid-state components in the electronic circuits. In both September 1989 and January 1992, the instrument was then turned off for a day or so and this apparently allowed the damaged component to heal itself. The sticking of the telescope in January 1992 was apparently caused by some unknown object or particle interfering with the cog wheel drive which moved the telescope. This problem was also short-lived.

The telescope can, however, only track the Sun for about 22° on either side of the orbit plane. The telescope itself can only move $\pm 20°$. The telescope pointing angle, the γ-angle, is illustrated in Figure 2 in Section 3.1. However, measurements can be made for Sun angles as large as 22° (see Section 3.3). A time history (1982 to 1985) of the orbit to Sun angle, the β-angle, is given in Figure C5. Both a seasonal cycle and a slow, long-term orbital precession are clearly shown. The two motions combined to move the Sun out of the sensor's field of view during the summer of 1992 and during the major portion of 1993. The last viewing opportunity occurs in the fall of 1993.

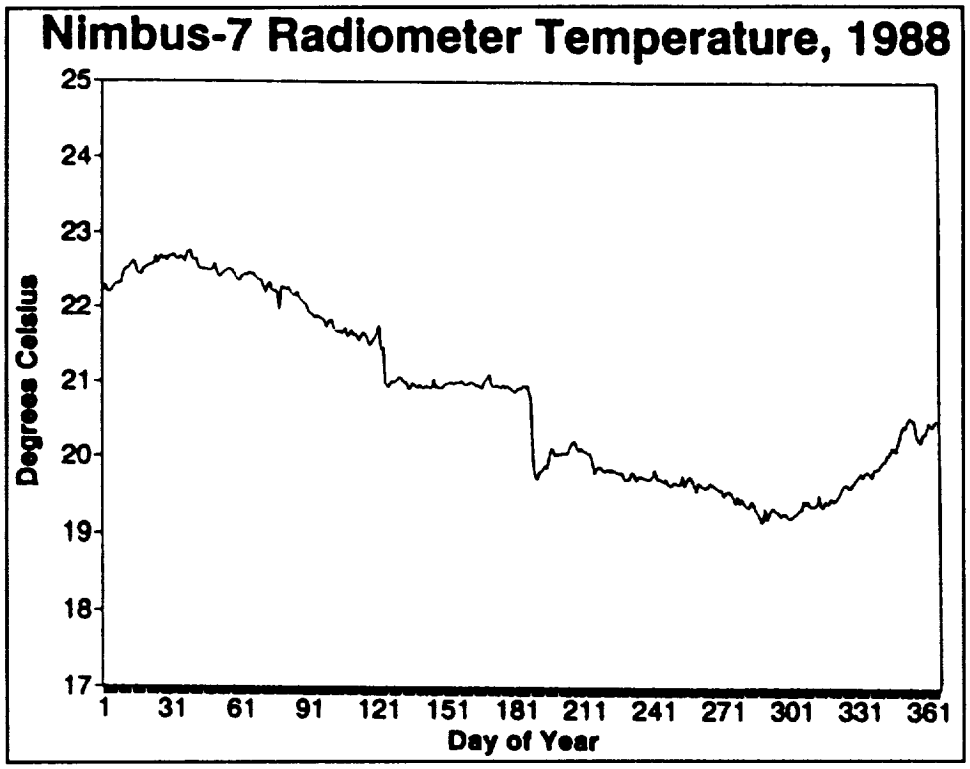

Figure C4. Channel 10c temperature variations in 1988 (see text).

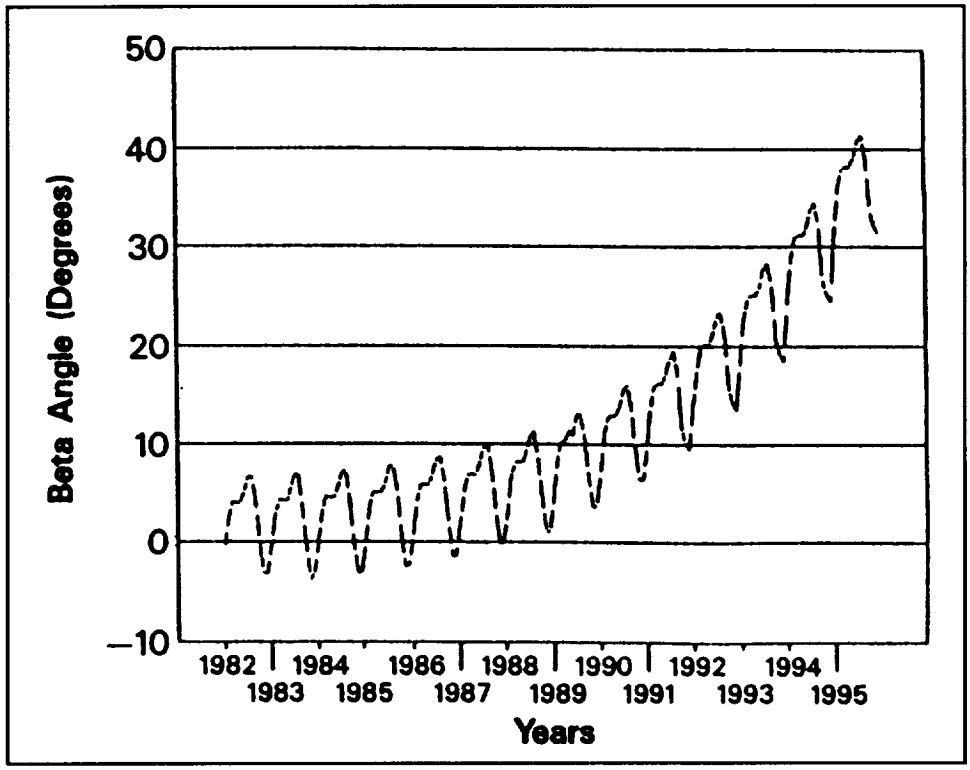

Figure C5. The angle from the Nimbus-7 orbit plane to the Sun, 1982 to 1995. This angle is called the β-angle, and varies both seasonally and because of the slow year-to-year precession of the orbit with respect to the ecliptic plane.

APPENDIX D
THE GAMMA-ANGLE TEST

D.1 The γ-Angle Shaft Angle Encoder

As demonstrated in Section 3, the γ-angle scale has evidently shifted 1° since November 1978. The solar telescope moves in calibrated 0.5° steps in a plane perpendicular to the nadir axis of the spacecraft. A given command moves the telescope 1° (two 0.5° steps). The actual γ-angle readout comes from a shaft angle encoder geared to the telescope axis. The encoder contains a multitrack disk that rotates relative to a stationary cage containing spring-loaded pins. The encoder signal describes the position of the disk and thus the telescope axis relative to the pins. The as-built unit rotated with close-to-zero torque (friction), however, for periods greater than 1 year the lubricant will evaporate in a vacuum resulting in an increased friction. This has the potential for dragging the pin cage along with the disk for a small angular distance when the telescope axis rotates during a γ-angle change command. The cage is held in position by a spring load against a shoulder, but it has no hard stop to prevent motion when friction is abnormally high. Wires, which connect the pins to the γ-angle monitor, also provide a small restraining force to the cage. These wires have a small amount of slack, but they will prevent the cage from moving more than a small angular distance from its original position. The longer the telescope remains in the same position, the greater the sticking should become. The largest sticking and hence the greatest chance of slippage should therefore occur in the late spring when the γ-angle is changed for the first time after having remained fixed for about 3 months (see Figure 3).

Nimbus Operations judges the success of a move command on the observed change in the γ-angle readout. On numerous occasions, no readout change has been observed on the first command and a second command has been sent to obtain the desired readout change. On some of these occasions the pins and their cage might have actually moved with the disk and telescope. In such a case, no relative motion would be indicated by the encoder. While the telescope is commanded to move in two ½° steps at a time, it is possible that the cage could make a single ½° step. If all else were equal, the pins would be just as likely to move to the left as to the right and over a period of time the average displacement would be zero. Figure 4, however, indicates that there is a preferential drift of the γ-angle zero position towards $-\gamma$.

D.2 Sensor Response Functions During Solar Transits

This appendix gives some additional details concerning the response functions of the solar sensors as the Sun passes through their fields-of-view once each orbit. It concentrates on channel 10c which has been by far the most useful of the 10 solar sensors. However, we will also discuss briefly the response functions of the other 9 channels, but details will only be given for channels 5 and 10c. Channel 10c is a cavity radiometer with a precession aperture and an approximate cosine response (see Section 3). However, channels 1 through 9 are flat plate radiometers with field-of-view limiters (Jacobowitz et al., 1984). The inner walls of the field-of-view limiters are anodized to reduce reflectivity. Nevertheless, there remains some reflectivity, particularly in the near-infrared. Thus, channels 1 through 9 normally have a saddle-type response with a local minimum when the Sun is at or near the center of the field-of-view.

As the Sun passes across its unrestricted field-of-view, channel 10c has a response function which is closely approximated by cos(a) where (a) is the off-center angle in the transit direction (see Figure D1). The sensor response is digitized to prevent the introduction of unknown biases during data storage and transmission activities, and this introduces the steps into the observed response function. The Nimbus

system allowed ±2048 digitization bits and the solar sensors were originally set so that their on-Sun readings were in the range (1,700 to 1,900 counts). For channel 10c, the quantized step height from one count value to the next is approximately 0.7 W/m² (see Hoyt et al., 1992).

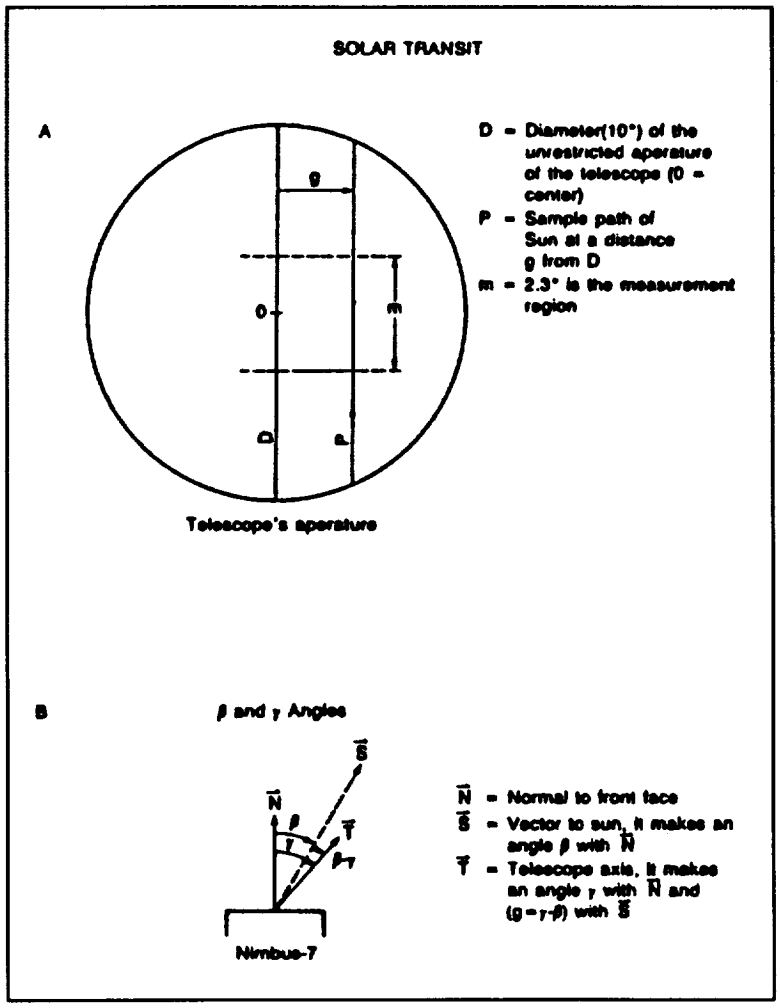

Figure D1. The geometry of the solar measurement is illustrated in (a) and (b). The transit of the Sun across the telescope is diagrammed in (a). The transit cord, P, is an angular distance (g) from diameter D. Only the maximum 40 contiguous measurements, Region m, are used in the calculation. The measured solar and telescope angles, β and γ, respectively, are shown in (b). As planned, the off-axis angle was support to be g=(γ-β); however, an error developed in the measured γ-angle (see text). This is the same as Figure 2.

The response function remains a cosine independent of whether the Sun passes directly through the center of the field-of-view or passes near the edge of the field-of-view. This is illustrated in Figure D2. The sensor aperture is 10° in diameter; thus, it is 5° from the center to the edge of the aperture. As indicated in Table D1, the Sun passed near the center of the field-of-view (g=-0.1°) on orbit 65,902 but was always near the edge (g=-4.2°) on orbit 65,913. The angle g (Figure D1) measures the closest approach to the center. During the γ-angle tests, the response functions are measured both in the transition direction (angle a) and the perpendicular (angle g) direction. Table D1 indicates that in the g direction the maximum response is not at the center (g=0) but close to g=-2.4° (see Section 3). This is the chief

reason why the maximum on orbit 65,902 is smaller than on the other two orbits. Note that raw counts are plotted in Figure D2 while in Table D1 the counts are normalized by R^2, the square of the Earth/Sun distance. The normalization is required for increased accuracy in the calculations.

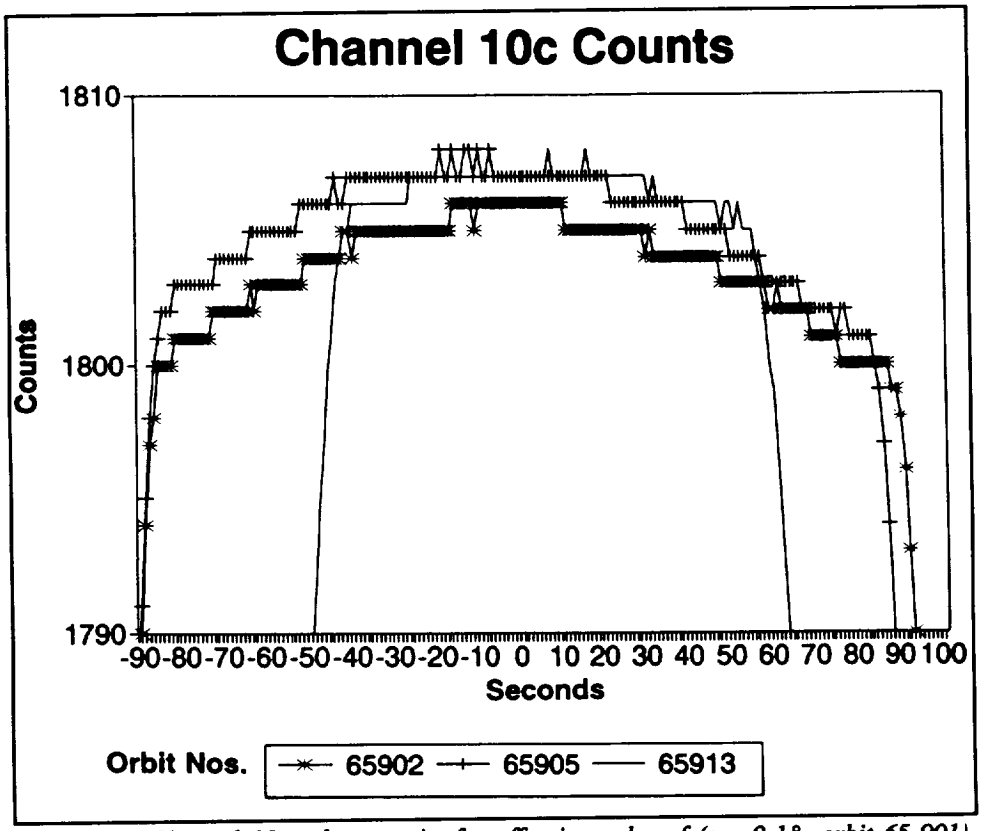

Figure D2. Channel 10c solar transits for off-axis angles of (g=-0.1°, orbit 65,901), (g=-1.2°, orbit 65,905), and (g=-4.2°, orbit 65,913).

Channels 1 through 9 have bowl-shaped response functions. Table D1 and Figure D3 indicate the channel 5 response curves in the perpendicular a-angle and g-angle directions. During the calibration procedure, the sensor was pointed directly at the source (Sun). Thus, the proper reading in Figure D2 comes from the local minimum on orbit 65,902 (g=-0.1°). The spectral channels are bothered by off-center readings even more than channel 10c. The γ-angle tests contain information that could be used to develop detailed response functions for these channels also. This has not been done because these channels suffer from other unresolved problems. The chief problem is a lack of in-flight calibration procedures for the spectral channels. Thus, the available measurements for channels 1 through 9 need both calibration adjustments and off-center measurement corrections. Lacking these corrections, these channels tell us little about the Sun's history during the past 14 years.

D.3 The γ-Angle Tests

The accuracy of the solar telescope γ-angle readings was checked by six inflight tests. As illustrated in Figure D1, the γ-angle gives the direction the solar telescope is pointing relative to the front face of the instrument. A γ-angle encoder on the instrument records the γ-angle (Section D.1) and this is then inserted in the data stream. These tests also established the response of the solar sensors as a function of the off-axis angle (g). The angle (g) describes how close the Sun comes to the center of the sensor field of view during a given solar observation (see Figure D1). During the tests, the γ-angle was moved

through a series of positions in order to observe the variation in the solar signal as the Sun as viewed near the center, near the edge, and out of the sensors unobstructed field of view. The tests showed that the encoder slipped by 1° between November 1978 and December 1989 (see Section 3). They also showed that channel 10c's maximum response occurred at g=-2.4° rather than at g=0° as expected.

Table D1. Channel 5 and 10 γ-Angle Response
November 1991 Test

		Channel 5		Channel 10c	
Off-Center Angle g (°)	Orbit	R^2T Counts	$(R^2T/R_oT_o^2-1)$ x 1,000	R^2T Counts	$(R^2T/R_oT_o^2-1)$ x 1,000
3.8	65,885	1647.87	5.3	1751.30	-10.02
2.8	65,895	1647.30	4.9	1758.04	-6.21
1.0	65,901	1641.08	1.1	1766.25	-1.57
-0.1	65,902	1639.26	0.0	1769.03	0.0
-1.2	65,905	1644.78	3.4	1770.31	0.72
-2.2	65,908	1649.50	6.2	1770.96	1.09
-3.2	65,911	1651.29	7.3	1770.78	0.99
-4.2	65,913	1651.18	7.3	1769.73	0.40

T is the mean "on-Sun" counts value.
R is the Earth to Sun distance in astronomical units.
T_o represents the g=0 (centered Sun) counts value; we use the g=-0.1 value to calculate the ratios.
The solar irradiance remained nearly constant during the November 1991 test (see Table D2).

Two and sometimes three types of information were obtained from each test. These were: the sensor response function in the γ-angle direction, how long the Sun was in view for given values of (γ and β), and the approximate γ angle where the sensor just failed to see the Sun. As built, the off-axis angle in the γ direction was

$$g = \gamma - \beta \tag{D1}$$

where β is the satellite/Sun angle (Figure D1). The experiments showed that now

$$g = \gamma_r - \beta - 1 \tag{D2}$$

or that the γ-angle scale had slipped and that now

$$\gamma = \gamma_r - 1 \tag{D3}$$

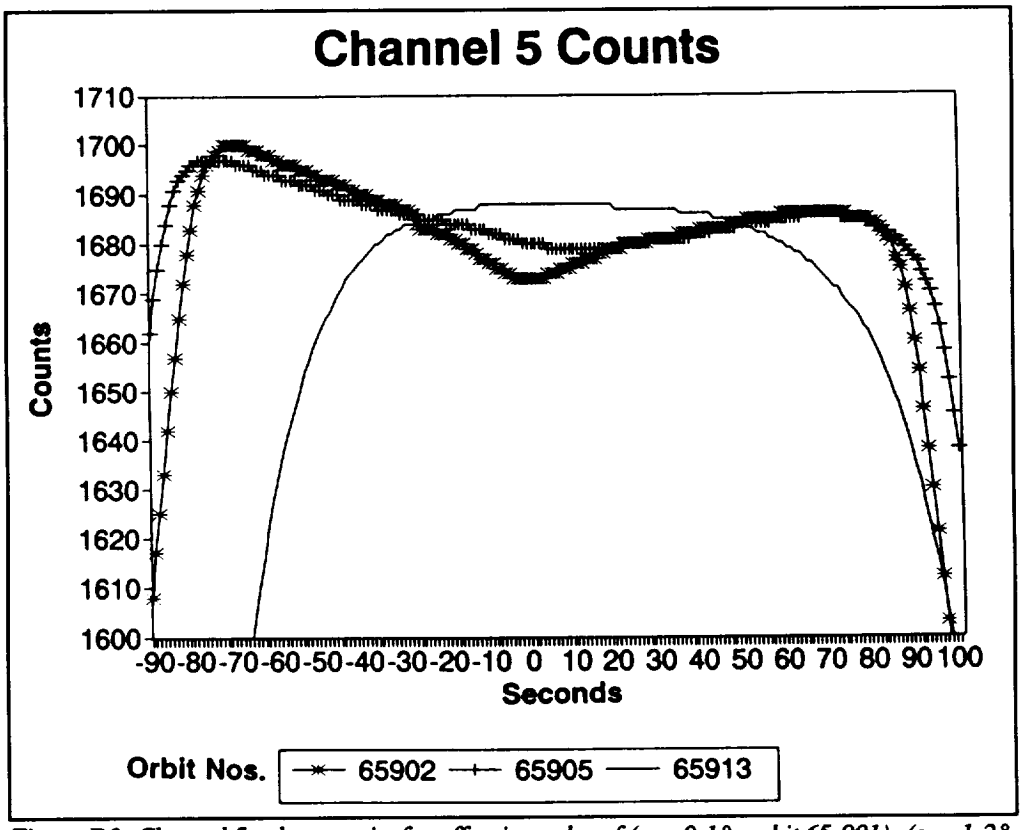

Figure D3. Channel 5 solar transits for off-axis angles of (g=-0.1°, orbit 65,901), (g=-1.2°, orbit 65,905), and (g=-4.2°, orbit 65,913).

where γ_r is the γ-angle read by the shaft encoder (see Section D.1). The sensor's γ-angle response function is defined as

$$f(g) = I(g)/I_s \tag{D4}$$

where I(g) is the measured signal for the angle (g). $I=R^2 * T$, where T is the measurement in counts and R is the Earth to Sun distance.
I_s is the maximum response for a fixed input. Experimentally $I_s=I(-2.4°)$ for channel 10c.

During the in-orbit tests, the Sun varied a little during the tests. This variation could be estimated since readings for a fixed γ-angle were taken at the beginning, middle, and end of each test. Once it was determined that

$$f(g) \cong \cos(g + 2.4°) \text{ for } g \leq 0 \tag{D5}$$

The true solar signal could be tracked to within 0.03% or better during each test. Each test required one or more days. During the tests, the γ-angle is held fixed for two 104-minute orbits and then moved to a new position. The unobstructed field of view is 10° across. During a given test, the γ-angle range varied from 4° to 12°. Thus, some tests check only a few degrees on either side of the center of the field

of view while the November 1991 test took out-of-field readings on either side of the center. The telescope could be commanded to move only in multiples of 1° steps. Thus, a test spanning 12° took about three days with some positions checked twice.

The results of the six tests are summarized in the tables. Table D2 gives the time of each test and the solar counts, I_s, used in calculating the response function for each test. In the calibration of channel 10c measurements (Eq.1, Section 2.3), the response function is assumed to be cos (g + 2.4°). Table D3 gives the individual measurements of the accuracy of this assumed response function. Table D4 gives the "Sun in-view times," (Eq.3 in Section 3) in seconds.

$$\Delta t = No.\ of\ readings\ [T \geq (T_{MAX} - 10)] \qquad \text{(D6)}$$

There is one reading per second.

Spacecraft yaw causes the sensor/Sun (β) angle to vary slightly from orbit to orbit. Thus, the off-axis angle g (Eq.D1) often does not change in exact 1° steps during the tests. Because of signal noise and uncertainties in the experiment, some measured response function values are slightly greater than 1 in Table D3. Finally the Δt in Eq.(D6) slightly overestimates the true "Sun in-view" time. Note that in Figure 10, Δt is plotted against (γ_r-β) to illustrate the change in the γ-angle between 1978 and 1989. In Table D4, Δt is compared to g the true off-axis angle.

Table D2. The γ-Angle Tests

Test Data		Solar Signal Used to Calculate f(g)	
Year	Days of Year	Orbits	$I_s = R^2T_s$ (counts)[b]
1978	320-322	327-328	1771.14
		329-338	1772.14
		350-353[a]	1771.39
1989	352-355	56,297-342	1771.5
1990	87-89	57,686-89	1771.52
		57,690-713	1771.62
		57,714-721	1771.82
1990	247-249	59,904-6	1771.0
		59,907-24	1770.60
		59,924-29	1770.80
1991	44-46	62,143-48	1772.1
		62,153-70	1772.5
1991	315-318	65,880-925	1770.90

[a]In the first test, the telescope was inadvertently left in a test position for 2 days.
[b]One count is similar to 0.7 W/m^2.

Table D3. Accuracy of Present Shape Factor f = cosG
G = g + 2.4° (assume same sign convention for $\gamma_r + \beta$)
$[(R^2T)/I_S - \cos G] * 10^3$

		$g = \gamma_r - \beta$	$g = \gamma_r - \beta - 1$					
g	G	11/78	12/89	03/90	09/90	02/91	11/91	
-6.6	-4.2[a]		-210.18					OUT OF CLEAR FOV
-6.5	-4.1[a]					-183.67		
-6.4	-4.0[a]			-170.09				
-6.3	-3.9[a]					-180.05		
-6.2	-3.8[a]			-137.10				
-6.0	-3.6[a]						-112.73 -103.91	
-5.7	-3.3[a]		-60.19					
-5.6	-3.2[a]		-41.34 -36.34					
-5.5	-3.1[a]					-43.80 -42.78		
-5.3	-2.9[a]			-23.22 -25.99				
-5.0	-2.6						-3.008 -1.941	CLEAR FOV
-4.7	-2.3				-0.053			
-4.6	-2.2		+0.091 +0.150		-0.234	-0.228		
-4.5	-2.1					-0.051		
-4.3	-1.9			-0.240 -0.201				
-4.2	-1.8						-0.167	
-4.0	-1.6						-0.265	
-3.7	-1.3		+0.020 -0.064 -0.081		-0.228			
-3.6	-1.2		-0.238		-0.091 -0.199 -0.086			
-3.5	-1.1		-0.211			-0.024 -0.004		
-3.4	-1.0		+0.130					
-3.3	-0.9			-0.029 -0.255 -0.023 -0.023 -0.447				
-3.2	-0.8						+0.030 -0.111 +0.075	

Table D3. Accuracy of Present Shape Factor f = cosG
G = g + 2.4° (assume same sign convention for $\gamma_r + \beta$)
$[(R^2T)/I_S - \cos G] * 10^3$

		$g = \gamma_r - \beta$	$g = \gamma_r - \beta - 1$					
g	G	11/78	12/89	03/90	09/90	02/91	11/91	
-3.0	-0.6						-0.047	
-2.8	-0.4				-0.026			
-2.7	-0.3		-0.026		+0.014			
-2.6	-0.2		-0.067		+0.294	-0.028 +0.006		
-2.5	-0.1					+0.007 -0.055 -0.027		
-2.4	0.0			-0.023				Normalization Point
-2.3	+0.1			+0.018		-0.083		CLEAR
-2.2	+0.2						+0.040	FOV
-2.1	+0.3	+0.0002 -0.0274						
-2.0	+0.4						+0.024	
-1.9	+0.5		+0.128 -0.052					
-1.8	+0.6				+0.055			
-1.7	+0.7		-0.010 +0.035		+0.024 -0.089 -0.129			
-1.6	+0.8		+0.244		+0.001	-0.083 -0.134		
-1.5	+0.9				+0.044 -0.040 -0.074	-0.102 +0.044 -0.018		
-1.4	+1.0				-0.011 -0.068	-0.090		
-1.3	+1.1			-0.318 -0.279 -0.324 -0.279 -0.346 -0.307 -0.267 -0.222		-0.013	+0.049 +0.083	
-1.2	+1.2			-0.221			-0.114 -0.266 -0.289	
-1.1	+1.3						-0.189	
-1.0	+1.4						+0.282 -0.085	
-0.9	+1.5	-0.058						

Table D3. Accuracy of Present Shape Factor f = cosG
G = g + 2.4° (assume same sign convention for $\gamma_r + \beta$)
$[(R^2T)/I_S - \cos G] * 10^3$

		$g = \gamma_r - \beta$	$g = \gamma_r - \beta - 1$				
g	G	11/78	12/89	03/90	09/90	02/91	11/91
-0.6	+1.8		-0.670 -0.156			+0.059 +0.008 -0.031	
-0.5	+1.9					-0.409 -0.438	
-0.4	+2.0			-0.943	-0.718		
-0.3	+2.1	-0.283 -0.108		-0.848			
-0.2	+2.2			-1.131			
-0.1	+2.3						-0.250
0.0	+2.4						-0.241
+0.1	+2.5	+0.025	-0.324 -0.403 -0.380				
+0.2	+2.6	+0.025 +0.059					
+0.3	+2.7		-0.566 -0.600				
+0.4	+2.8				-0.585 -0.540 -0.845	-0.420	
+0.5	+2.9			-1.722		-0.530	
+0.6	+3.0				-0.764		
+0.7	+3.1			-1.189 -0.907 -1.206 -1.624	-0.632		-0.942
+0.8	+3.2						-0.824 0.925
+1.0	+3.4						
+1.3	+3.7	-0.726 -0.624	-1.347 -1.065				-0.866
+1.6	+4.0				-3.145		
+1.7	+4.1			-1.561 -1.742			
+1.8	+4.2						-1.877
+1.9	+4.3						-1.968
+2.1	+4.5		-2.077				
+2.2	+4.6	-1.395 -1.306	-2.040				
+2.3	+4.7	-0.781 -1.112 -1.095					

Table D3. Accuracy of Present Shape Factor f = cosG
G = g + 2.4° (assume same sign convention for $\gamma_r + \beta$)
$[(R^2T)/I_S - \cos G] * 10^3$

		$g = \gamma_r - \beta$	$g = \gamma_r - \beta - 1$					
g	G	11/78	12/89	03/90	09/90	02/91	11/91	
+2.4	+4.8		-2.110					
+2.7	+5.1			-2.685 -2.515			2.744	
+2.8	+5.2						-3.146	
+3.1	+5.5		-2.921 -3.022					
+3.3	+5.7		-3.094					
+3.7	+6.1			-3.928 -3.953				
+3.8	+6.2						-5.219 -5.383	
+4.1	+6.5		-4.179					
+4.2	+6.6		-3.968					
+4.8	+7.2						-5.074 -5.148	
+5.8	+8.2[a]						-91.97	OUT OF CLEAR FOV
+6.0	+8.4[a]						-88.94	

[a]Sun partially shaded.

Table D4. Sun In-View Time (seconds)						
	$g = \gamma_r - \beta$	$g = \gamma_r - \beta - 1$				
g	11/78	12/89	03/90	09/90	02/91	11/91
-6.6		25.5				
-6.5					24.0	
-6.4			27.5			
-6.3					23.5	
-6.2			23.0			
-6.0				33.0 24.5		
-5.7		28.0				
-5.6		26.5 27.0				
-5.5					26.0 27.0	
-5.3			28.0 29.5			
-5.0						42.3 45.5
-4.7				71.0		
-4.6		85.33 83.0		75.0	80.5	
-4.5					85.0	
-4.3			93.83 95.0			
-4.2						106.67
-4.0						112.83
-3.7		125.0 125.0 120.0		125.17		
-3.6		125.0		125.5 125.5 128.33		
-3.5		130.0			134.0 134.67	
-3.4		132.0				
-3.3			139.80 138.33 139.33 141.17 140.5			
-3.2						140.0 139.0 142.0
-3.0						144.6
-2.8				153.0		
-2.7		151.33		156.67		

Table D4. Sun In-View Time (seconds)						
	$g = \gamma_r - \beta$	$g = \gamma_r - \beta - 1$				
g	11/78	12/89	03/90	09/90	02/91	11/91
-2.6		151.67		157.0	156.67 159.83	
-2.5					159.5 159.5 141.67 162.0	
-2.4			158.3			
-2.3			160.7		160.3	
-2.2						164.0
-2.1	157.0 158.67					
-2.0						164.67
-1.9		168.0 165.33				
-1.8				175.5		
-1.7		167.33 168.33		179.25 187.0 172.67		
-1.6				176.33	175.0 174.17	
-1.5				181.67 182.17 177.67	175.3 173.5 173.5	
-1.4				179.33	175.0	
-1.3			177.63 177.63 178.0 177.0 180.7 179.7 175.83 175.0	181.83	160.0	
-1.2			179.3			175.5 176.3
-1.0						174.5
-0.9	170.67					
-0.6		175.83 175.67			183.50 184.33 183.0	
-0.5					183.33 184.67	
-0.4			185.0	182.0		
-0.3	175.92 179.0		186.3			
-0.2			184.2			
-0.1						180.3

Table D4. Sun In-View Time (seconds)						
	$g = \gamma_r - \beta$	$g = \gamma_r - \beta - 1$				
g	11/78	12/89	03/90	09/90	02/91	11/91
0.0						
+0.1	178.33	177.5 177.33 177.67				
+0.2	176.5 176.5					
+0.3		179.5 178.34				
+0.4				187.8 187.3 186.3	185.33	
+0.5			184.0		184.67	
+0.6				184.83		
+0.7			183.67 184.0 184.0 183.3	186.3		179.3
+0.8						181.0 179.3
+1.0						179.67
+1.3	172.67 175.67	175.17 176.58				
+1.6				184.25		
+1.7			177.3 177.0			
+1.8						171.33
+1.9						171.92
+2.1		168.17				
+2.2	168.25 166.0					
+2.3	165.0 166.92 165.75	164.5				
+2.4		163.67				
+2.7			158.5 160.3			156.25
+2.8						155.33
+3.1		148.25 146.0				
+3.3		143.67				
+3.7			136.3 137.7			
+3.8						106.67 110.00
+4.1		112.65				

Table D4. Sun In-View Time (seconds)						
	$g = \gamma_r - \beta$	$g = \gamma_r - \beta - 1$				
g	11/78	12/89	03/90	09/90	02/91	11/91
+4.2		113.17				
+4.8						64.0
+6.0						26.0

APPENDIX E
CRITERIA FOR REJECTING DATA AS NOISY

In the final processing, the orbit and daily means were subjected to both subjective and objective screening. First a visual inspection of the data was made and values that were out-of-line were rejected from further processing. Normally only a small amount of data were rejected by this method; however, during 1987 this inspection accounted for most of the rejected data. During the special operation period, the ERB instrument was on full-time 1 day and just 30 minutes per orbit on the next. The calibration algorithm did not properly treat the 30-minute measurements and therefore, the data were rejected by inspection (see Section 4.4.3 and Figure 13). Short problem periods also appeared when the ERB instrument moved from one major operation period to another. This includes the beginning and end of the 1986 special operations period. Similarly, the data are suspect just after the January 23, 1992 turn on (see Table C1). In these cases, the instrument was going through an extended warming or cooling phase and the calculated irradiances were suspect. Nonthermal problems occurred when the Sun was not in the normal measurement region of the Channel 10c field of view. This occurred at times during the γ-angle tests (Appendix D) and in 1992 and 1993 when the Sun slowly drifted into or out of the unrestricted sensor field of view (see Section 3.3 and Figure 9). The data from these periods, which were rejected by inspection, are included with the missing data in Table E1. Thus, some of the "missing data" are available for study, but not considered useful.

The objective screen rejected orbits when the standard deviations from the orbital mean was greater than three counts. These were termed bad measurements. It also rejected those orbits that were more than two standard deviations from the daily means. over 2,000 orbits were rejected by this later criteria. Most of these were associated with nonthermal equilibrium conditions. Table E1 lists the total, missing, bad, useful, and used orbits for each year from November 16, 1978 through January 24, 1993.

Table E1. Summary of Useful, Bad, or Missing Orbits (1978 to 1993)

Year	First	Last	Total	Missing	Bad	Useful	Used	Percent
1978	323	949	627	168	4	455	439	70.02
1979	950	5994	5045	1677	44	3324	3197	63.37
1980	5995	11052	5058	1385	21	3652	3513	69.45
1981	11053	16097	5045	1292	27	3726	3586	71.08
1982	16098	21142	5045	1322	13	3710	3572	70.80
1983	21143	26188	5046	916	10	4120	3980	78.87
1984	26189	31247	5059	719	9	4331	4209	83.20
1985	31248	36293	5046	27	1	5018	4861	96.33
1986	36294	41338	5045	415	0	4630	4489	88.98
1987	41339	46384	5046	1165	2	3879	3749	74.30
1988	46385	51444	5060	17	10	5033	4909	97.02
1989	51445	56490	5046	83	7	4956	4809	95.30
1990	56491	61536	5046	8	9	5029	4885	96.81
1991	61537	66584	5048	29	18	5001	4833	95.74
1992	66585	71646	5062	992	159	3911	3665	72.40
1993	71647	72075	429	33	86	310	283	66.00
Totals			71753	10248	420	61085	58979	82.20

First = first orbit number in dataset for year even if data are missing
Last = last orbit number in dataset for year
Total = total number of orbits in year
Missing = orbits that are missing (no measurement or visually rejected measurement; 14.28% of the orbits)
Bad = orbits that are bad, meaning the on-Sun counts have a standard deviation ≥ 3 counts (0.58% of the orbits)
Useful = number of orbits that may provide some useful measure of the solar irradiance. Some of these values are dropped in later analyses if they are more than 2 standard deviations away from the daily means (85.13% of the orbits)
Percent = percent of total orbits that are at present used
Used = number of orbits actually used in the final calculations of daily means (82.20% of the orbits); some 2106 values or 3.45% of the number called "useful" are discarded as being more than 2 standard deviations from the daily mean
Totals = summation of the values in the columns

REPORT DOCUMENTATION PAGE

Form Approved
OMB No. 0704-0188

1. AGENCY USE ONLY *(Leave blank)*	2. REPORT DATE	3. REPORT TYPE AND DATES COVERED
	September 1993	Reference Publication

4. TITLE AND SUBTITLE
Nimbus-7 Earth Radiation Budget Calibration History--Part I: The Solar Channels

5. FUNDING NUMBERS
665-10-70
NAS5-31331

6. AUTHOR(S)
H. Lee Kyle, Douglas V. Hoyt, John R. Hickey, Robert H. Maschhoff, and Brenda J. Vallette

7. PERFORMING ORGANIZATION NAME(S) AND ADDRESS (ES)
Goddard Space Flight Center
Greenbelt, Maryland 20771

8. PEFORMING ORGANIZATION REPORT NUMBER
93B00110

9. SPONSORING / MONITORING ADGENCY NAME(S) AND ADDRESS (ES)
National Aeronautics and Space Administration
Washington, DC 20546-0001

10. SPONSORING / MONITORING ADGENCY REPORT NUMBER
NASA RP-1316

11. SUPPLEMENTARY NOTES
Kyle, Goddard Space Flight Center, Greenbelt, Maryland; Hoyt and Vallette, Research and Data Systems Corporation, Greenbelt, Maryland; Hickey, The Eppley Laboratories, Newport, Rhode Island; Maschhoff, Gulton Industries, Albuquerque, New Mexico

12a. DISTRIBUTION / AVAILABILITY STATMENT
Unclassified - Unlimited
Subject Category 92

12b. DISTRIBUTION CODE

13. ABSTRACT *(Maximum 200 words)*

The Earth Radiation Budget (ERB) experiment on the Nimbus-7 satellite measured the total solar irradiance plus broadband spectral components on a nearly daily basis from November 16, 1978, until June 16, 1992. Months of additional observations were taken in late 1992 and in 1993. The emphasis in this paper is on the electrically self-calibrating cavity radiometer, channel 10c, which recorded accurate total solar irradiance measurements over the whole period. The spectral channels did not have inflight calibration adjustment capabilities. These channels can, with some additional corrections, be used for short- term studies (one or two solar rotations--27 to 60 days), but not for long-term trend analysis. For channel 10c, changing radiometer pointing, the zero offsets, the stability of the gain, the temperature sensitivity, and the influences of other platform instruments are all examined and their effects on the measurements considered. Only the question of relative accuracy (not absolute) is examined. The final channel 10c product is also compared with solar measurements made by independent experiments on other satellites. The Nimbus experiment showed that the mean solar energy was about 0.1 percent (1.4 W/m^2) higher in the excited Sun years of 1979 and 1991 than in the quiet Sun years of 1985 and 1986. The error analyusis indicated that the measured long-term trends may be as accurate as ±0.005 percent. The worse-case error estimate is ±0.03 percent.

14. SUBJECT TERMS
Solar constant measurements; solar spectral observations; sensor characterization; calibration

15. NUMBER OF PAGES
82

16. PRICE CODE

17. SECURITY CLASSIFICATION OF REPORT	18. SECURITY CLASSIFICATION OF THIS PAGE	19. SECURITY CLASSIFICATION OF ABSTRACT	20. LIMITATION OF ABSTRACT
Unclassified	Unclassified	Unclassified	UL